Ground Response Analysis of Selected Sites in Hawassa Area

Addis Ababa University

Addis Ababa, Ethiopia

November, 2017

Addis Ababa University

Addis Ababa Institute of Technology

School of Civil and Environmental Engineering

GROUND RESPONSE ANALYSIS OF SELECTED SITES IN HAWASSA AREA

November, 2017

A thesis submitted to the School of Graduate Studies of Addis Ababa University in Partial fulfillment of the Degree of Master of Science in Geotechnical Engineering.

ABSTRACT

Hawassa, a lakeside city in southern Ethiopia found at the heart of the East African Rift system, has been frequented with a series of minor to strong earthquakes reaching up to a magnitude of 7. A recent minor earthquake caused structural distresses in the city that tempts one to hypothesize that this may be principally attributed to the young lacustrine deposit typical of the city. Primary data from refraction and resistivity tests and secondary data from available geotechnical reports were collected from different locations of the city so as to model respective soil profiles. Due to lack of measured strong ground motion records in the area, input motions were selected from PEER database using relevant filtering criteria and scaled according to the local seismic hazard. The selected ground motions are used in a one-dimensional ground response analysis software, DEEPSOIL, and responses at the surface and at various depths are obtained. A typical geotechnical profile across the city consists of a thick silty sand soil with a thin horizon of welded-tuff at a shallow depth. The results obtained from the study show that ground motions are greatly influenced by local site soils across the selected locations, with amplifications much exceeding the prediction of design spectra specified by current codes. This led to the proposal of a design spectrum that fitted the analysis outputs from 56 cases.

TABLE OF CONTENTS

List of Tables v

List of Figures vi

CHAPTER ONE

1. Introduction.....1

1.1. Background and Motivation 1

1.2. Objectives of Research 2

1.3. Scope of the Study.....2

1.4. Organization 3

CHAPTER TWO

2. Geology and Seismicity of Hawassa Area.....4

2.1. Location and Topography.....4

2.2. Regional Geology 5

2.3. Local Geology and Geomorphology 6

2.4. Seismicity of the Area 7

2.4.1. Ethiopian Building Code Standard, (EBCS 1995).....7

2.4.2. Global Seismic Hazard Assessment Program (GSHAP).....8

2.4.3. Ethiopian Standards based on Euro Norms, ES EN 1998:2015 11

CHAPTER THREE

3. Relevant Literature Review 15

3.1. Soil Response under Cyclic Loading.....15

3.2. Ground Response Analysis.....20

3.2.1. Introduction.....20

3.2.2. One-Dimensional Ground Response Analysis.....22

3.2.3. Linear Approach 22

3.2.4. Equivalent Linear (EQL) Approach.....23

3.2.5. Non-Linear Approach 24

CHAPTER FOUR

4. Acquisition and Processing of Input Data 26

4.1. General Workflow of the Study 26

4.2. Input Motions 27

4.2.1. Definition of Target Spectrum 28

4.2.2. Magnitude Range 30

4.2.3. Duration Range 31

4.2.4. Time Series Scaling 31

4.2.5. Shear-wave velocity of uppermost 30m ($V_{S,30}$) 34

4.2.6. Additional Records 36

4.3. Data from Geotechnical Investigation 39

4.3.1. SPT-V_S Correlation 42

4.3.2. Statistical Extrapolation 47

4.4. Data from Geophysical Investigation 49

4.4.1. General Background 49

4.4.2. Seismic Refraction Survey 50

4.4.2.1. Theoretical Formulation 50

4.4.2.2. Conducting Seismic Refraction Survey 53

4.4.2.3. Data Processing 60

4.4.2.4. Output 61

4.4.2.5. V_P-V_S Conversion and Extrapolation 63

4.4.3. Electrical Resistivity 67

4.4.3.1. Theoretical Background 67

4.4.3.2. Output 70

CHAPTER FIVE

5. Analysis and Discussion 73

5.1. Equivalent Linear Analysis Procedure 73

5.2. Consideration of Ignimbrite 75

5.3. Analysis Results....77
5.3.1. Summary of Profiles....77
5.3.1.1. Summary of PGA Profiles....77
5.3.1.2. Summary of Displacement Profiles....79
5.3.1.3. Summary of Strain Profiles....80
5.3.2. Response Spectral Analysis....81
5.3.3. Comparison with Code Specified Design Spectra....84
5.3.3.1. Site-specific Comparisons....84
5.3.3.2. Absolute Mean Response Spectrum....86
5.3.3.3. Proposed Design Spectrum....87
5.3.4. Effect of the Ignimbrite Layer....91
5.3.5. Effect of Half-space Selection....91

CHAPTER SIX

6. CONCLUSIONS AND RECOMMENDATIONS....94
6.1. Conclusions....94
6.2. Recommendations....95

REFERENCES....96

APPENDIX

LIST OF TABLES

Table 2.1 Bedrock Acceleration Ratio, α_0 (EBCS 1995) 8

Table 2.2 Bedrock Acceleration Ratio, α_0 (ES EN 1998:2015) 11

Table 2.3 A summary of PGA values for selected cities in Ethiopia (ES EN 1998:2015) 14

Table 4.1 Values of the parameters describing the recommended Type 1 elastic response spectra (ES EN 1998:2015) 29

Table 4.2 Selected Ground Motions from PEER database 35

Table 4.3 Summary of additional motions typically used for analysis, from Haile (1996) 37

Table 4.4 A summary of relevant geotechnical reports for buildings in Hawassa 40

Table 4.5 SPT-V_S correlations developed by Ohta and Gotto (1978) 44

Table 4.6 SPT-V_S correlations recommended by Wair et al. (2012) 44

Table 4.7 Summary of SPT correction and correlation for: (a) Profile 1 | Progress International Hotel, BH9, (b) Profile 2 | Industrial Park, BH B35C, (c) Profile 3 | Nib International Bank, BH1, and (d) SPEDM, BH3 45

Table 4.8 Extrapolated shear-wave velocities of the four selected geotechnical profiles 48

Table 4.9 Selected 1-D P-wave profiles and their correlation to S-waves 65

Table 4.10 Extrapolated shear-wave velocities of the four profiles generated from refraction survey 66

Table 5.1 Welded-tuff parameters used in soil models from geophysical methods 76

LIST OF FIGURES

Figure 2.1. Map of Hawassa (Google Earth) 4

Figure 2.2. Geological Map of Hawassa Area, an extract from Geological Map of Sodo-Hawassa Area, Japan International Cooperation Agency (JICA 2012) 6

Figure 2.3 Seismic Hazard Map of Ethiopia (EBCS 1995) 8

Figure 2.4. Seismic Hazard Map of: (a) Ethiopia, and (b) the Main Ethiopian Rift (Giardini et al. 1999) 10

Figure 2.5. Seismic Hazard Map along the Horn of Africa (ES EN 1998:2015) 12

Figure 2.6. Seismic Hazard Map of Ethiopia (ES EN 1998:2015) 13

Figure 3.1 A Kelvin-Voigt Mechanical Model of a thin solid element 15

Figure 3.2 A typical stress-strain loop of soils under cyclic loading. After Stewart et al. (2013) 16

Figure 3.3 Curves of: (a) normalized modulus reduction, and (b) material damping proposed by Seed et al. (1986) as replotted by Darendeli (2001) 18

Figure 3.4 Curves of: (a) shear modulus reduction (b) material damping proposed by Vucetic and Dobry (1991) as replotted by Darendeli (2001) 19

Figure 3.5 Shear modulus and damping curves with: (i) varied confining pressure, and (ii) varied plasticity index (Darendeli 2001) 19

Figure 4.1 A generalized flowchart showing parameters and inputs required for GRA 26

Figure 4.2 Plot of Type 1 design spectra for ground types A to E (5% damping) for Hawassa city 30

Figure 4.3 A plot of three empirical predictive models for significant duration: Abrahamson and Silva (1996), Kempton and Stewart (2006) and Bommer et al. (2009). (Taken from Bommer et al. 2009) 31

Figure 4.4 Conditional Mean Spectrum based target with 11 selected and scaled motion | Illustration of two approaches of scaling (a) Approach 1, using a range of periods (0.01-10 sec). (b) Approach 2, using a single matching period at 2.0 sec. After Stewart et al. (2014). 32

Figure 4.5 – Scaled time histories of Whittier Narrows 1987 (a), Loma Prieta 1989 (b) and Parkfield 2004 (c) earthquakes 36

Figure 4.6 Imperial Valley Earthquake (1940) ElCentro Record: (a) deconvolved, Haile (1996) and (b) scaled to Hawassa's PGA of 0.11g.....37

Figure 4.7 Kern County Earthquake (1952) Taft Record: (a) deconvolved, Haile (1996), and (b) scaled to Hawassa's PGA of 0.11g 38

Figure 4.8 Tokachi-oki Earthquake (1968) Hachinohe Record: (a) deconvolved, Haile (1996) and (b) scaled to Hawassa's PGA of 0.11g 38

Figure 4.9 Hyogoken-nanbu Earthquake (1995) Kobe JMA Record: (a) deconvolved, Haile (1996) and (b) scaled to Hawassa's PGA of 0.11g 39

Figure 4.10 Rough demarcation of the city based on geotechnical investigation 42

Figure 4.11 Schematic of seismic refraction survey. After Redpath (1973) 51

Figure 4.12 Incident and refracted waves propagating through two mediums of different stiffness. After Everett (2013).....51

Figure 4.13 A simple, two-layer case with plane, parallel boundaries and corresponding time-distance curve. After Redpath (1973) 52

Figure 4.14 Distribution of selected sites for in-situ tests (Google Earth) 55

Figure 4.15 Site 1: Amora Gedel Park Site.....55

Figure 4.16 Site 2: Industrial park Site 56

Figure 4.17 Site 3: Hawassa University, College of Agriculture Site 57

Figure 4.18 Site 4: Meskel Adebabay Site.....57

Figure 4.19 (a) Strike plate and (b) Hammer used as energy source 58

Figure 4.20 (a) Geophones, and (b) Spreading the geophones at intervals 59

Figure 4.21 Seismograph 60

Figure 4.22 Tomographic plots showing P-wave profile of: (a) Site 1, (b) Site 2, (c) Site 3 and (d) Site 4.....63

Figure 4.23 Poisson's ratio for: (a) 10% non-plastic silt content, and (b) 15% non-plastic silt content in Tyoura sand (Suwal and Kuwano 2012).....64

Figure 4.24 Current injection into a wholespace of uniform resistivity, ρ. After Everett (2013) 68

Figure 4.25 Schlumberger configuration 69

Figure 4.26 Terrameter 69

Figure 4.27 Tomographic plots showing P-wave profile of: (a) Site 1, (b) Site 2 [1 of 2], (c) Site 3 and (d) Site 4 72

Figure 5.1. Multiple-layered system of different amplitudes, thicknesses, densities, shear moduli and damping ratio. After Kottke & Rathje 2009 74

Figure 5.2 PGA profiles of the four sites modeled from geotechnical investigation reports 77

Figure 5.3 PGA profiles of the four sites modeled from refraction and resistivity surveys 78

Figure 5.4 Peak displacement profiles of the four sites modeled from geotechnical investigation reports 79

Figure 5.5 Peak Displacement profiles of the four sites modeled from refraction and resistivity surveys 79

Figure 5.6 Strain profiles of the four sites modeled from geotechnical investigation reports 80

Figure 5.7 Strain profiles of the four sites modeled from refraction and resistivity surveys 80

Figure 5.8 A summary of response spectra at the ground surface for the four selected profiles: (a) Profiles 1 and 3 from geotechnical investigation reports, and (b) Profiles 2 and 4 from refraction and resistivity surveys 82

Figure 5.9. Mean response spectra of geotechnical and geophysical output for each Profile 83

Figure 5.10. Observed resonance at Amora-Gedel Park site 84

Figure 5.11 Comparison of some analysis outputs against building codes 85

Figure 5.12 Comparison of the absolute mean against design spectra of building codes 86

Figure 5.13 Response of Pseudo-velocity (a), and displacement (b), of the absolute mean 87

Figure 5.14 Proposed design spectrum fitted to the absolute mean 88

Figure 5.15 Comparisons between the proposed design spectrum and design spectra of two site classes for ES EN 1998:2015 (a), and NEHRP 2015 (b) 89

Figure 5.16 Selected design spectra that were found to be closest to the proposed design spectrum 90

Figure 5.17 Spectral curves at the ground surface for Profile 4: (a) with ignimbrite, and (b) without ignimbrite 91

Figure 5.18 Comparison of: (a) analysis performed on Profile 4 done for elastic and rigid half-space, and (b) the mean spectral ordinates 93

CHAPTER ONE

INTRODUCTION

1.1 Background and Motivation

Hawassa is a lakeside growing metropolis in the south of Ethiopia with a continually rising status as Ethiopia's southern capital. It is a city that finds itself located inside the Great East African Rift Valley, a region characterized by significant seismic activity. The rapid growth of population in the city, extensive infrastructure and high-rise building development, coupled with the inadequate seismic exploration of the area call for detailed studies of the area for seismic vulnerability.

On January 24, 2016 an earthquake of magnitude 4.3 hit Hawassa and was also felt in the nearby towns such as Shashemene, Alaba Kulitu and Yirgalem. According to a report from the Ethiopian News Agency, "no serious damage was encountered except for some cracks in some buildings". The Ethiopian Observer reported a statement by the Mayor of City, Tedros Gelil, who told the media that "about 100 students sustained minor injuries and that no significant damage to infrastructures occurred". The fact that such a minor earthquake was observably responsible for several structural distresses in the city led to the hypothesis that this could potentially be attributed to the thick lacustrine deposit over which the city rests, among other possible factors.

The effect of local soil conditions on modifying the three important characteristics of ground motion - amplitude, frequency content and duration- has been known for quite some time now (Borcherdt 1970, 1996; Nozu 2003; Hashash et al. 2010). In a bid to estimate different responses at the surface, ground response analyses (GRA) are conducted, which yield surface time-histories and response spectra. Different techniques are available for performing site response analysis, the most popular one being the equivalent-linear (EQL) approach (Kramer 1996). In comparison with non-linear approaches, the EQL approach requires straightforward soil properties, while it gives reasonably accurate estimates until a certain strain threshold (Kaklamanos 2013). Different one-dimensional (1D) ground response analyses programs are made available for performing GRA following the development of the pioneering program "SHAKE" (Schnabel et

al. 1972). SHAKE solved the equation of motion in the frequency domain by applying the concept of complex modulus through the use of Fourier expansion. Although SHAKE dealt with nonlinear problem using an equivalent linear approach, other programs called “truly nonlinear methods” surfaced in 1980s and 1990s (Yoshida 2015). More recently, DEEPSOIL, a one-dimensional site response analysis program that can perform both equivalent linear and non-linear site response models was developed at the University of Illinois, Urbana-Champaign (Hashash et al. 2016). In addition to having powerful computing capabilities, DEEPSOIL has a graphical user-interface that is easy to use and understand.

1.2 Objectives of Research

The main objective of this research is to conduct ground response analysis at representative sites in Hawassa area. In doing so, the research aims to achieve the following particular objectives:

i. obtain dynamic soil properties at selected sites; and model different soil profiles for performing site response analysis;

ii. investigate if the amplification potential of the sites in the area is significant;

iii. construct average response spectra for the city and ultimately propose design spectra should the pertinent design spectra from building codes be found inadequate.

1.3 Scope of the study

The study, as its primary focus, involves conducting ground response analysis of the soil in the area. This indicates the need for city-wide soil characterization and seismic microzonation. However, such a large scale study will prove expensive and non-feasible given the time constraint. This is due to the challenge posed to obtain some of the required primary input data at required locations and depths. Instead, available geotechnical investigation reports are compiled and refraction and resistivity surveys are conducted at selected sites for this thesis. In spite of this, some of the data were still incomplete and had to be estimated using justifiable means.

Furthermore, as is the case with most related researches in this area, finding earthquake time-histories in Ethiopia pertaining to this research is not possible. Hence, the paper will be limited to using time-histories of known earthquakes that occurred globally which are adjusted to local conditions. A one-dimensional, equivalent-linear ground response analysis is conducted without resorting to nonlinear methods and multidimensional analysis techniques. This is due to the reasonably flat terrain of the area and the fairly uniform soil formation.

1.4 Organization

This thesis is organized into six chapters. Chapter 2 deals with the description of the study area, including general information on location and topography, and focusing on overview of the geology, geomorphology and seismicity. In Chapter 3, theoretical background on behavior of cyclically-loaded soils and one-dimensional ground response approaches is presented. Furthermore, notable works in this regard are provided. In Chapter 4, data acquisition and processing is treated. Acquired secondary data to be used as input for GRA are summarized, corrected, correlated and extrapolated. A brief overview of the theoretical background and simplified procedures of the geophysical methods are also presented in this chapter, followed by presentation of the data. These inputs are used for analysis and their results are discussed in Chapter 5. The last chapter provides a summary, conclusions and recommendations.

CHAPTER TWO

GEOLOGY AND SEISMICITY OF HAWASSA AREA

2.1 Location and Topography

Hawassa is a fast-growing city founded on the eastern side of Lake Hawassa. Located at 440000m-447500mE and 773400m-784700mN (Figure 2.1), it is among the most populous cities in Ethiopia. The city is situated 285km south of the national capital, Addis Ababa and is currently the seat of the Southern Nations, Nationalities and Peoples' regional government.

Hawassa's terrain can be described as more or less flat. The lowest altitude of the region is situated at the lake, leveling at 1686m. Two hills are found in the central-western (Mt. Tabor) and southern (Mt. Alamura) parts of the city, with the latter having a peak altitude of approximately 2015m. The city's level rises negligibly going south, with less than 1% of gradient from the city's northern edge up to the bottom of the southern mountain.

Figure 2.1. Map of Hawassa (Google Earth)

Found at the heart of the Main Ethiopian Rift (MER) specifically and the East African Rift System (EARS) in a broader sense, Hawassa is frequently visited by a series of minor to strong earthquakes that can reach a magnitude of 7. With recent statistical estimates indicating a population of more than 300,000 and significant rise in economic activities, earthquake will prove to be a serious hazard for the city. The need for proper consideration of earthquake hazard in the city's development plan is further corroborated by the appreciable damages caused by recent low-magnitude events in the city.

2.2 Regional Geology

East Africa presents a uniquely special geological feature in that it contains a triple tectonic plate junction, connecting major rifts from the Red Sea, the Gulf of Aden and one extending deep into the continent to form the EARS (Williams 2016). EARS has the MER in the north, continuing in the south-west direction to Kenya, Tanzania and Mozambique, forming the biggest continental rift in the world. Another branch, diverting from around Lake Turkana, runs almost North-South cutting across Kenya and entering deep into Tanzania. Two plates –the Somalian and Nubian plates – are separated by the MER that extends in NE-SW direction. It is believed to have developed within the epochs from Oligocene to Holocene. The Wonji Fault Belt (WFT), a system of tensional faults that run along the axis of MER formed at the rift floor, is understood to have been formed in Pleistocene (JICA 2012). Ziway, Langano, Abiyata, Shala, Hawassa, Abaya and Chamo lakes are found within the rift.

The Hawassa area finds itself surrounded by steep caldera walls. The floor of the caldera, upon which the city rests, is typified by Holocene sediments containing pyroclastics and welded tuffs. This caldera borders another caldera, the Corbetti caldera, forming a complex nested form of calderas together. The Corbetti caldera is believed to have witnessed its recent volcanic activity about 20,000 years ago (Acocella et al. 2002; JICA 2012). Corbetti has now been identified to have significant geothermal energy potential.

2.3 Local Geology and Geomorphology

High variability characterizes the geomorphology of the area. This is attributed to repeated volcanic, tectonic and deposition processes (Nida and Bizuye 2014). The region, hence, is principally covered by pyroclastic-lacustrine deposits as shown in the geological map of the area given in Figure 2.2.

The present lakes have originated from an ancestral lake of much larger size in the early stages of the Quaternary, resulting in significant lacustrine sediments. Several borehole logs have shown that these sediments can be found intercalated with Pliocene to Pleistocene ignimbrite, showing the presence of volcanic eruption at the time of deposition. These sediments, mainly represented by sand and silt, can be observed in Figure 2.2 to have covered the majority of the region (Nida and Bizuye 2014). The major engineering geological rock units in the region are rhyolites. Bounded by caldera walls, a tectonic depression about 50km wide hosts Hawassa town and Hawassa Lake in the east. The pyroclastic-lacustrine deposits have resulted in a flat terrain, although two hills reside in the south west and southern sides (Mt. Tabor and Mt Alamura).

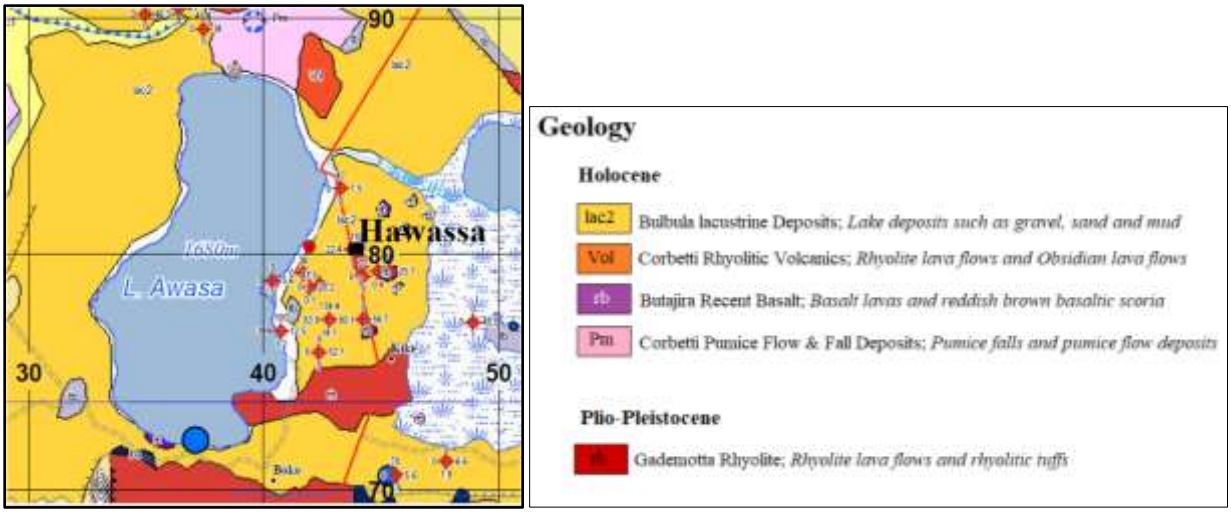

Figure 2.2. Geological Map of Hawassa Area, an extract from Geological Map of Sodo-Hawassa Area, Japan International Cooperation Agency (JICA 2012)

2.4 Seismicity of the Area

Extensional tectonics is the predominant activity for earthquake occurrence in Ethiopia and the surrounding region. Even though such tectonic activities are not as severe as other most known types of tectonic activities elsewhere in the world, significant seismic hazard involving earthquake magnitudes up to 7 are anticipated in the MER region. Historically, little has been studied regarding earthquake hazard in the region up until the pioneering compilation by Gouin (1976). Two documented earthquakes of 1906, with magnitudes of 6.6 and 6.8, are believed to be the strongest documented records within the rift in the past several decades. Although USGS made a global catalogue available since the early 1970s, organized reports of earthquakes within the rift surfaced since 1983 (Malek 2014).

Since the study of local seismic hazard is an important step in Ground Response Analysis, this section will provide seismic hazard assessment review of some depth. In addition to provisions of local building codes, likely PGA values to be experienced in the area have also been referred to from other alternatives.

2.4.1 Ethiopian Building Code Standard, (EBC 1995)

Volume 8 of the Ethiopian Building Code Standard of 1995 (EBCS 1995) was the ultimate design basis for earthquake design in the country until 2015. This particular volume of the code is popular even among engineers of seismic-prone regions of East Africa, outside Ethiopia. However, the code is found severely lacking as far as proper consideration of site-soil effects is concerned. In addition, the risks of adapting a 100-year return period instead of the customary 475-year return period accepted worldwide have been pointed out (Worku 2011; 2014). Despite the recent revision in 2015, the 1995 version continues to be used largely in the local construction industry.

According to the seismic hazard map of Ethiopia in the 1995 code, the country is subdivided into four seismic zones on the basis of peak ground acceleration (PGA), with bedrock acceleration ratio (α_0) for each zone given as follows.

Table 2.1. Bedrock Acceleration Ratio, α_o (EBCS 1995)

Zone	4	3	2	1
α_0	0.10	0.07	0.05	0.03

The respective seismic hazard map of the country is shown in Figure 2.3.

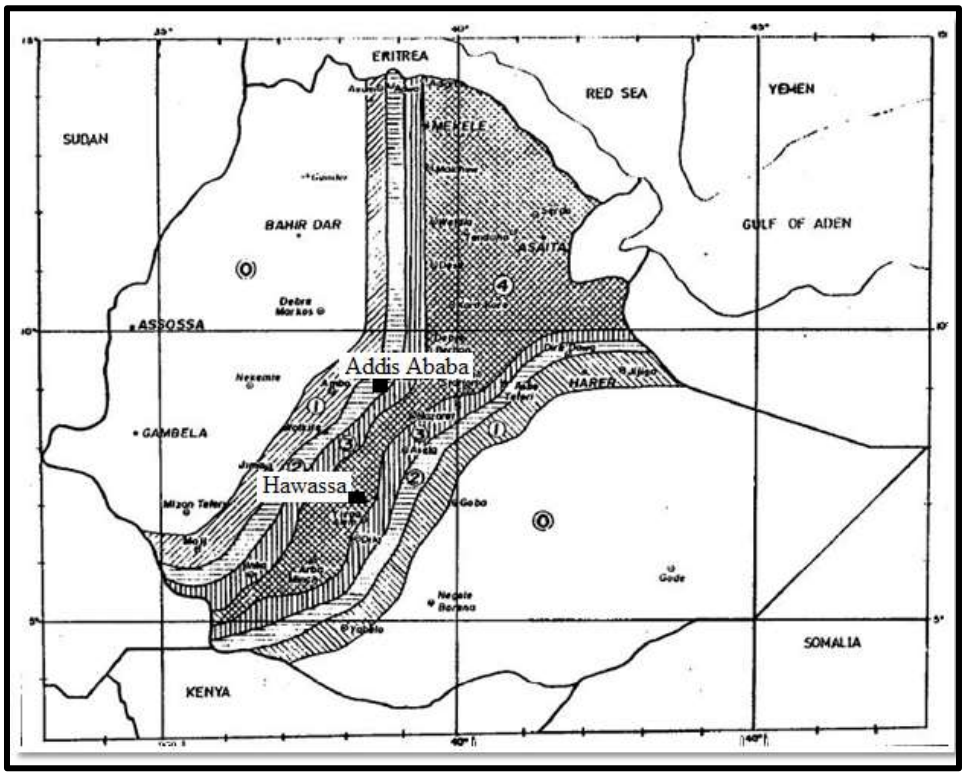

Figure 2.3 Seismic Hazard Map of Ethiopia (EBCS 1995)

Located at $07^0$04'N and $38^0$31'E (EBCS 1995), Hawassa is found in Zone 4 as can be read from the map, with a design bedrock acceleration of 0.1g. The code also provides a tabular listing for selected towns, consistent with what can be read from the map.

2.4.2 Global Seismic Hazard Assessment Program (GSHAP)

The Global Seismic Hazard Assessment Program (GSHAP) was launched following a proposal made by the International Lithosphere Program as part of an international demonstration project. The United Nations (UN) accepted the proposal under the International Decade for Natural

Disaster Reduction (IDNDR), which was aimed principally at mitigating seismic related risks. In addition, the GSHAP made it its primary goal to ensure that national agencies be able to assess seismic hazard in a regionally coordinated fashion and with the most advanced methods. The program was expected to fill a critical gap cited by many countries in their attempt to properly assess the seismic hazard of their respective territories (Giardini and Basham 1993). The GSHAP was a particularly powerful program in that:

- it conducted hazard assessment through the coordination of international and national (local) teams;
- it had promoted the establishment of a homogenous criteria on the scientific methodologies for the seismic hazard evaluation; and
- it employed the most advanced methodologies available at the time.

The GSHAP had been endorsed by international scientific agencies such as the International Council for Science (ICSU), the International Union of Geodesy and Geophysics (IUGG), the International Union of Geological Sciences (IUGS) and the International Association of Seismology and Physical of Earth's Interior (IASPEI). Having principally targeted developing countries, the GSHAP coordinated with the aforementioned agencies (others also included) in assembling appropriate regional databases on historical and instrumental seismicity, strong motion and micro-seismic data (Giardini and Basham 1993).

Locally, the GSHAP coordinated with the Institute of Geophysics, Space Science and Astronomy (IGSSA) and respective seismic hazard of the region was assessed. Under the framework of GSHAP, cooperation of nine countries in the eastern and southern Africa (Eritrea, Ethiopia, Uganda, Kenya, Tanzania, Malawi, Zambia, Zimbabwe and South Africa) was fostered. This led to the eventual establishment of the Eastern and Southern Africa Regional Seismology Working Group (ESARWG); later a recognized component of IASPEI's Committee for Developing Countries (Midzi et al. 1999).

The seismic hazard map of Ethiopia and the MER is presented in Figure 2.4 as plotted using available tools and the GSHAP database. The Global Seismic Hazard Map depicts the seismic hazard as Peak Ground Acceleration (PGA) with 10% probability of exceedence in 50 years, corresponding to a return period of 475-years as depicted in Figure 2.4.

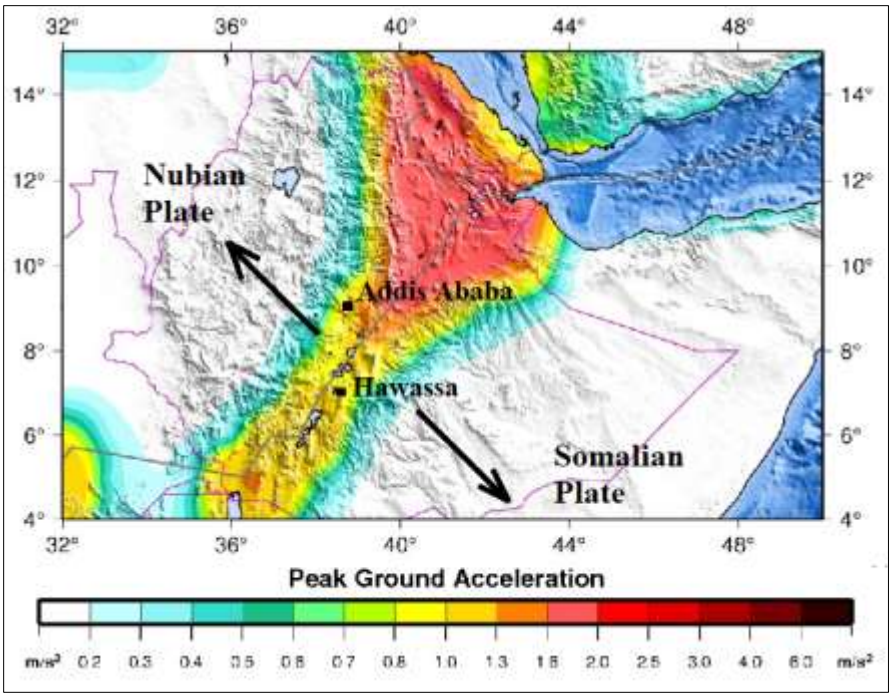

(a)

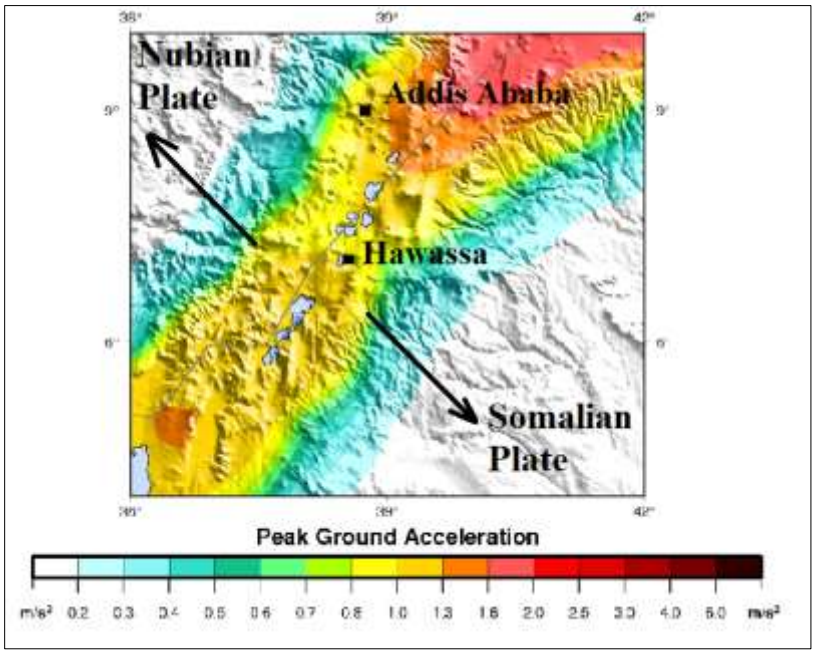

(b)

Figure 2.4. Seismic Hazard Map of: (a) Ethiopia, and (b) the Main Ethiopian Rift (Giardini et al. 1999)

It can be noted that the seismic risk is maximum along the plate boundary of EARS that crosses Ethiopia with estimated peaks having a PGA range of 0.2-0.25g in the north-eastern part of the country, where the triple junction is located in Afar Region. Hawassa city is found right next to Hawassa Lake, in the dark yellow region of 0.1-0.13g PGA. With the assumption that PGA increases as one nears the Nubia-Somalia plate boundary, Hawassa can be estimated to have a PGA of 0.11g.

2.4.3 The New Ethiopian Seismic Code based on Euro Norms, ES EN 1998:2015

The revised building code of Ethiopia (ES EN 1998:2015), recently introduced based on Euro Norms, made notable improvements in seismic provisions. In addition to including additional site classes, it has also adopted a 475-year design earthquake return-period for buildings, instead of 100-year return-period. The hazard, like in the case of its predecessors, is expressed in terms of a single value of effective peak ground acceleration in rock called "design ground acceleration". The volume provides a five-zone division of seismic hazard in the country as follows.

Table 2.2. Bedrock Acceleration Ratio, α_o (ES EN 1998:2015)

Zone	5	4	3	2	1	0
$\alpha_0 = \frac{a_g}{g}$	0.2	0.15	0.10	0.07	0.04	0

The volume provides two seismic hazard maps; one for the Horn of Africa (Figure 2.5); and the other one covering Ethiopia (Figure 2.6). It also provides a long list of towns with their respective seismic zonation.

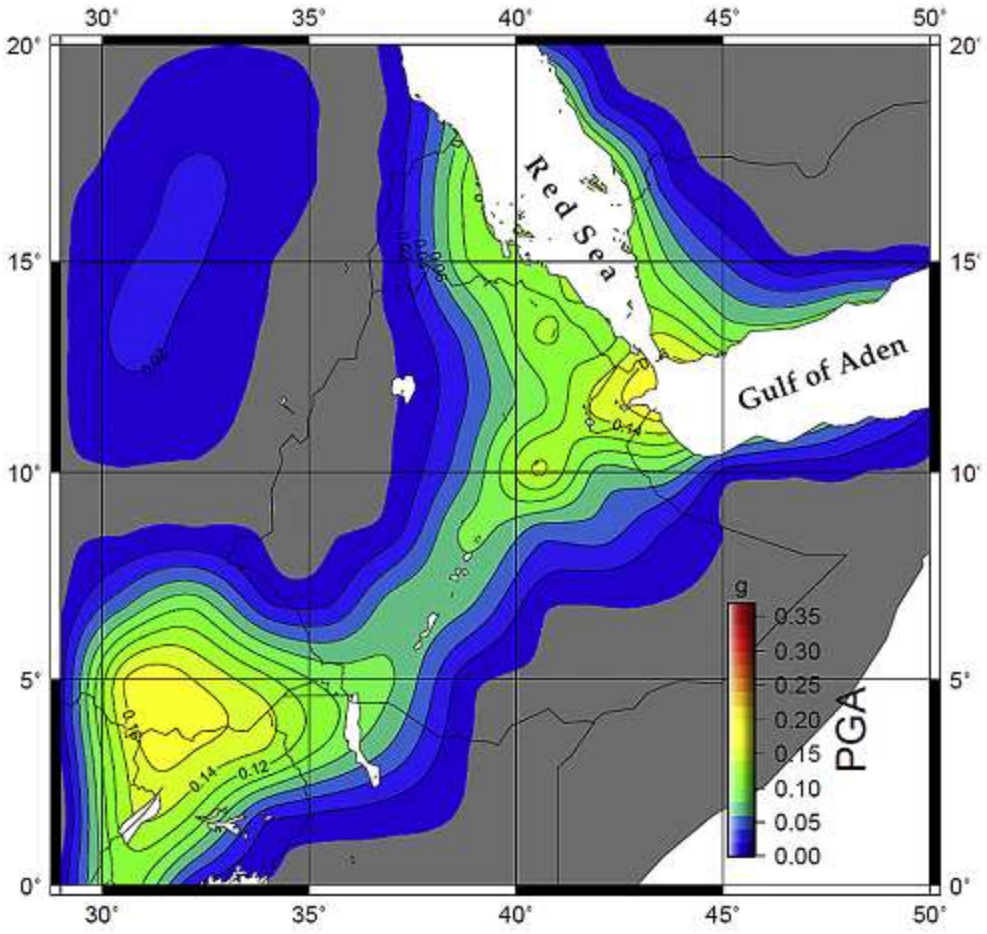

Figure 2.5. Seismic Hazard Map of the Horn of Africa (ES EN 1998:2015)

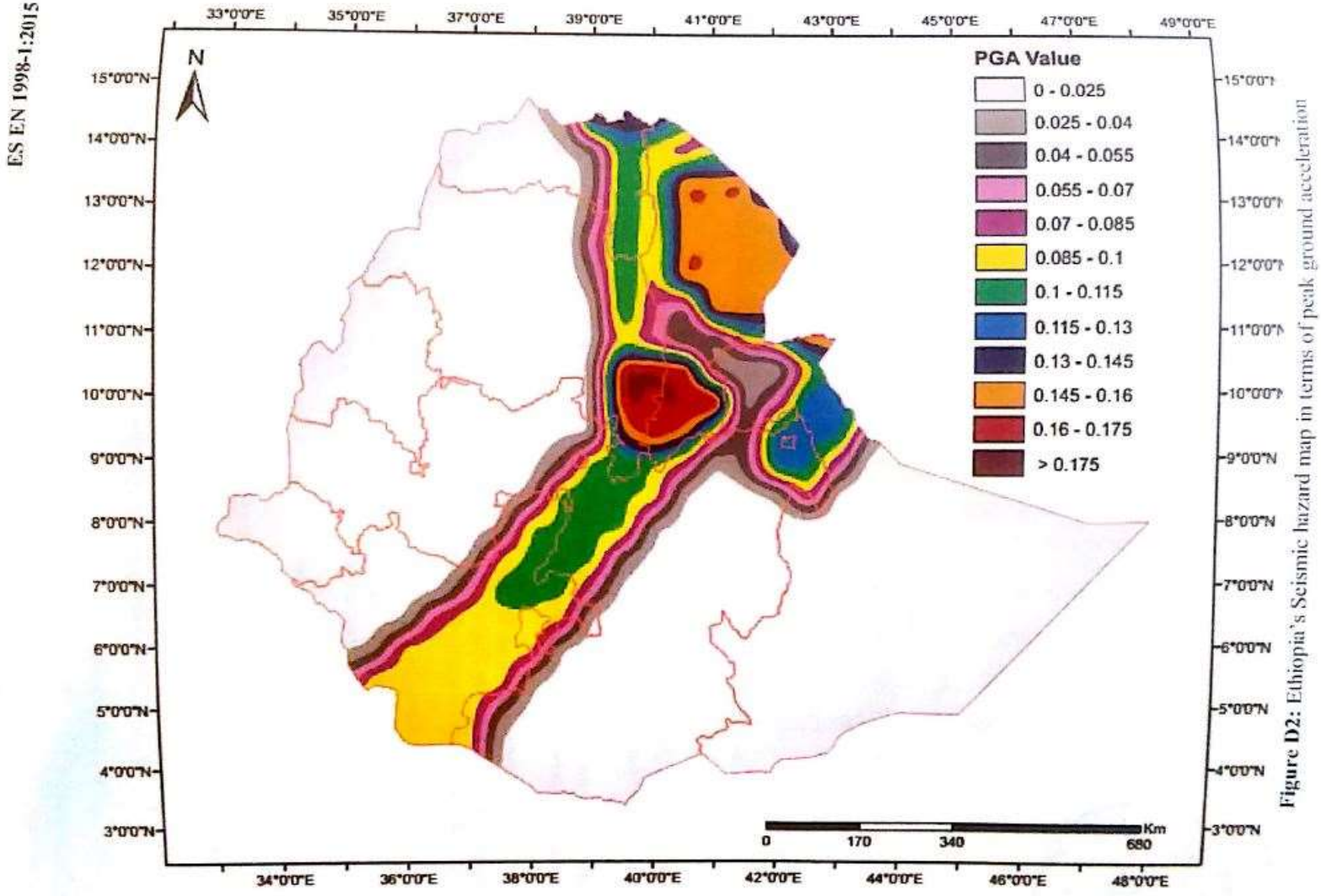

Figure 2.6. Seismic Hazard Map of Ethiopia (ES EN 1998:2015)

Despite the code's significant improvement on the existing seismic provision, it is not without its own visible pitfalls. For instance, one can easily identify discrepancies between design PGA values presented in the hazard maps and those in the tabular listing. Hawassa city is one such a location, where one can read 0.1g on the hazard map, while it falls under Zone 4 with a PGA of 0.15g for the 475-year return period in the table. Note the contradiction that the former value of 0.1g is just the same as the one specified in the older code for a return period of 100 years. The document does not provide any explanation for this discrepancy. Table 2.3 shows PGA values as presented in the hazard map and in the table for selected cities, showing obvious discrepancies. The PGA of Hawassa city in the table is almost twice the value shown in the map.

Table 2.3. A summary of PGA values for selected cities in Ethiopia (ES EN 1998:2015)

Cities	**GPS**		**Range of PGA's | (Map of Ethiopia) (g)**	**PGA Value| (Tabular Listing)**
Addis Ababa	8.9806^0N	38.7578^0E	0.07-0.085	[Z3] - 0.10
Dire Dawa	9.6009^0N	41.8501^0E	0.07-0.085	[Z3] - 0.10
Mekele	13.4936^0N	39.4657^0E	0.1-0.115	[Z4] - 0.15
Adama	8.5263^0N	39.2583^0E	0.1-0.115	[Z4] - 0.15
Dese	11.1270^0N	39.6363^0E	At the interface of 0.085-0.1 and 0.1-0.115	[Z3] – 0.10
Hawassa*	7.0504^0N	38.4955^0E	At the interface of 0.085-0.1 and 0.1-0.115	[Z4] – 0.15

*There is further conflict with Hawassa's PGA as it can be read from the hazard map of Horn of Africa that the city is found in an area of PGA of about 0.08g, implying that the city has even lesser PGA than what could be read from the hazard map of the country and the tabular listing.

Hoping that these clear discrepancies will be ironed out soon, the seismic hazard assessment from the GSHAP is employed in the subsequent sections of this study.

CHAPTER THREE

RELEVANT LITERATURE REVIEW

3.1 Soil Response under Cyclic Loading

Unlike the majority of materials that obey Hooke's law of elasticity for ranges of strains, soil neither behaves linearly nor elastically. Numerous studies over the past five decades have shown that the stiffness of soil is affected by cyclic strain, mean principal stress, void ratio, over-consolidation ratio (Hardin and Drenvich 1972) and plasticity index (Vucetic and Dobry 1991). Unified formulas have also been attempted (Ishibashi and Zhang 1993) to express dynamic stiffness and energy dissipation in terms of the aforementioned parameters.

It is a common practice to model soils as viscoelastic solids (Kelvin-Voigt solids), where the stress-strain relationship of such solid is given by the relation in Equation 3.1. A thin Kelvin-Voigt solid element is shown in Figure 3.1 where the total resistance to shearing deformation is a combined effect of an elastic component (a spring) and a viscous component (a dashpot).

$$\tau = G\gamma + \eta \frac{\partial \gamma}{\partial t} \tag{3.1}$$

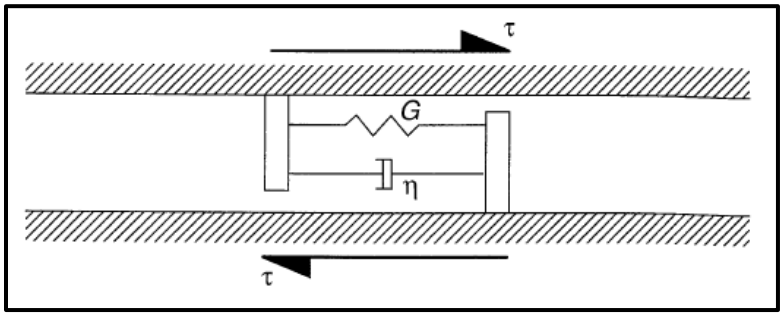

Figure 3.1 A Kelvin-Voigt Mechanical Model of a thin solid element

Subjecting a soil sample with cycles of constant amplitudes, stress-strain curves similar to the depiction in Figure 3.2 is observed. A curve, known as a backbone curve can be used to connect the tips of these loops of various strains. A tangent, with a slope known as tangent shear modulus (G_{tan}), can describe the stiffness of the soil during the loading process.

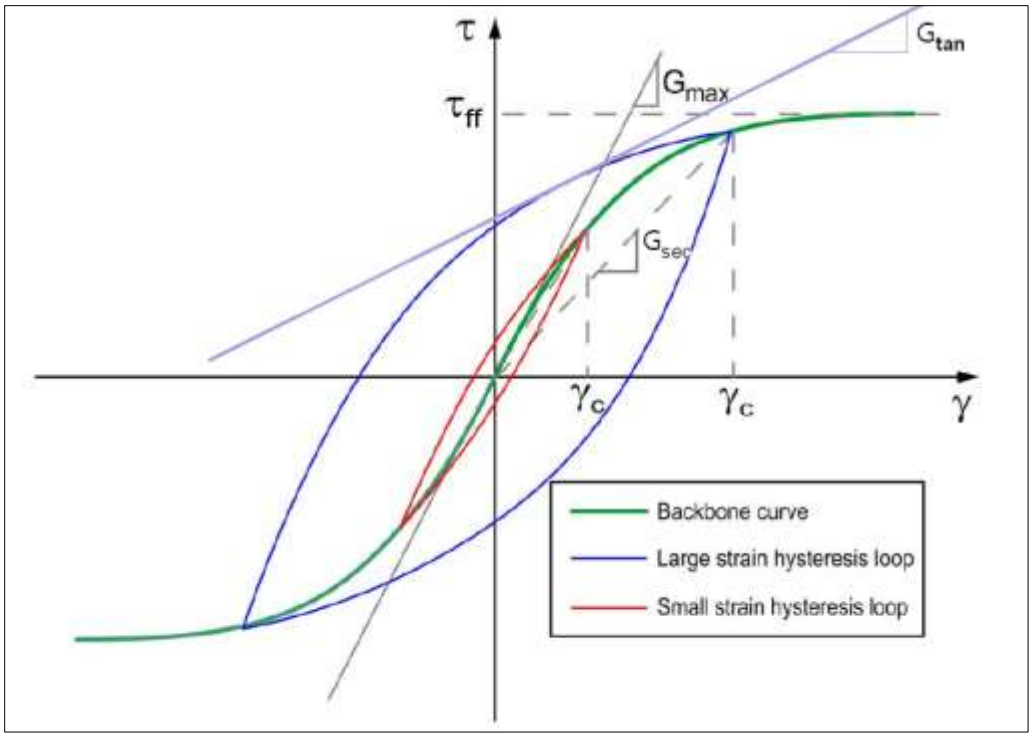

Figure 3.2 A typical stress-strain loop of soils under cyclic loading. After Stewart et al. (2013)

As G_{tan} varies throughout a cycle of loading, an average approximation called secant shear modulus is often used. The slope of the tangent, which entails a ratio between incremental shear stress and strain, describes the shear modulus; hence the secant shear modulus (G_{sec}) can be described as a ratio between shear stress and shear strain amplitudes (Kramer 1996) as

$$G_{\text{sec}} = \frac{\tau_c}{\gamma_c} \tag{3.2}$$

As G_{sec} is the shear modulus where the increments of shear stress and strain are related to the origin, it describes the general inclination of the loop. It has been observed that with further increments of shear stress and strain, slippage between soil grains is inevitable; and this consequently results in weakening of soil structure and decrease of stiffness (Srbulov 2008). This phenomenon is directly portrayed in the stress-strain plot, whereby the hysteretic loops are observed to lean further and further toward the horizontal axis. Connecting the tips of the hysteresis loops yields what is known as a backbone curve as shown in Figure 3.2.

At very small strain levels, where soil, like any other material, can be treated as a linear-elastic material, the stiffness (or the slope of the tangent) is maximum and is denoted by G_{max}. As most

seismic geophysical tests cause such minimal strains, their measurement outputs can be used to compute G_{max} (Kramer 1996).

$$G_{\max} = \rho \cdot v_s^2 \tag{3.3}$$

Equation (3.3) relates the maximum shear modulus to a measured shear-wave velocity and density of a soil formation. G_{max} is a very important parameter as stiffness values are customarily presented normalized in reference to this maximum value.

The second parameter to describe the loop is its breadth. From a solution of a viscously-damped single degree of freedom system, a plot relating exerted net force and displacement can be constructed. The plot shows linear relationship between net force and displacement for zero damping, and elliptical relationship (a hysteresis loop) for non-zero damping. It can be shown that the energy dissipated is given by the area inside the hysteresis loop, and the strain energy stored at maximum displacement is only a function of stiffness. Consequently the damping ratio boils down to the following simple equation. (Details of the formulation can be found in Kramer (1996), Appendix B).

$$\xi = \frac{W_D}{4\pi W_S} \tag{3.4}$$

where ξ is the damping ratio, W_D is the dissipated energy and W_S is the stored strain energy.

Notable researches

Several research works have been conducted in the final decades of the 20th century in regards to finding relations between normalized shear modulus and damping on one hand, and shear strain on the other, for different types of soils (Darendeli 2001). Seed and Idriss (1970) pioneered the proposition of curves for cohesionless soils and this was later re-analyzed by Seed et al. (1986) as shown in Figure 3.3.

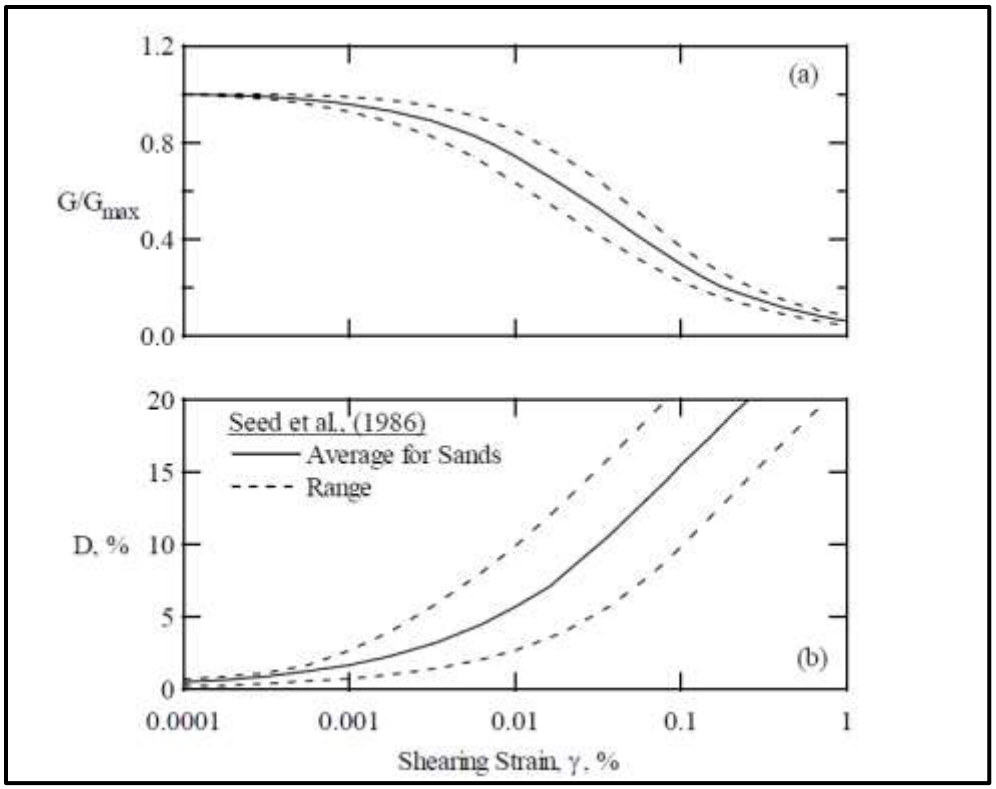

Figure 3.3 Curves of: (a) normalized modulus reduction, and (b) material damping proposed by Seed et al. (1986) as replotted by Darendeli (2001)

The ranges in Figure 3.3 take into account variability in characteristics of the granular particles, non-linear soil behavior and effect of confining pressure (Darendeli 2001). The curves have been found consistent with measured results of Idriss'(1990) and Darendeli's (2001) studies. Idriss (1990) also proposed a generic damping curve for all soil types. Additional studies that took into account the effect of plasticity of soils were conducted, a notable contribution being that of Vucetic and Doby (1991), who provided different curves for shear modulus and damping at different plasticity index values.

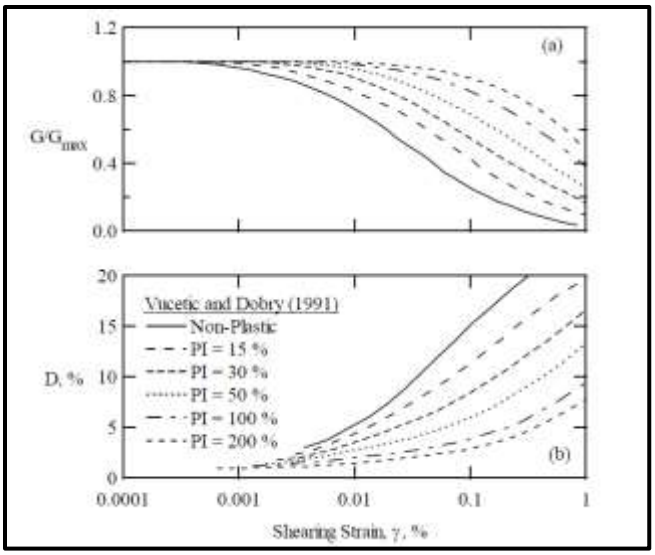

Figure 3.4 Curves of: (a) shear modulus reduction (b) material damping proposed by Vucetic and Dobry (1991) as replotted by Darendeli (2001)

Further studies from Darendeli (2001) showed that soil behaviors vary, albeit with different extent, with plasticity index (PI), mean effective confining pressure (σ_m), over consolidation ratio (OCR) and number of loading cycles (N). His output yielded the curves in Figure 3.5.

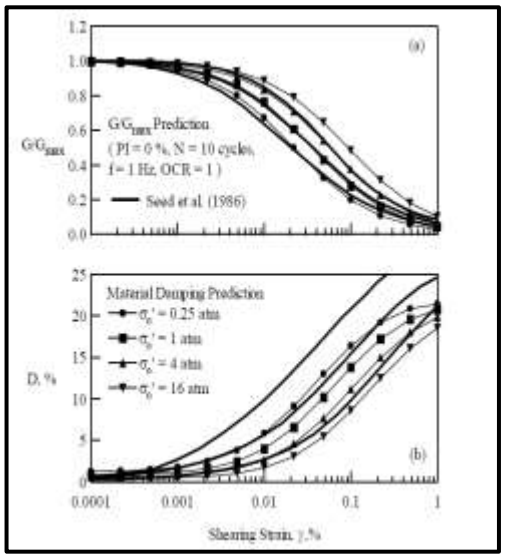

(i)

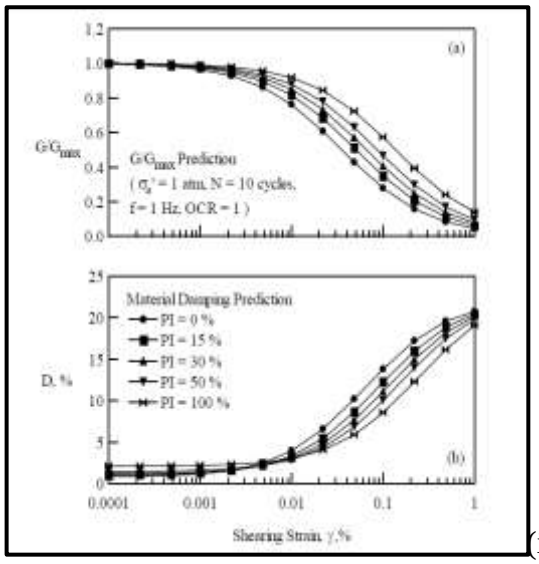

(ii)

Figure 3.5 Shear modulus and damping curves with: (i) varied confining pressure, and (ii) varied plasticity index (Darendeli 2001)

3.2 Ground Response Analysis

3.2.1 Introduction

Ground Response Analysis is a site-specific analysis used to predict ground motions at the surface. It has a variety of applications, most notable ones being the evaluation of liquefaction hazards and the development of design response spectra (Kramer 1996). Its site-specific nature gives it added benefits, relative to the use of predictions from empirical ground motion prediction equations (GMPEs). One of the most important outputs from GRA is the level of amplification/deamplification of peak ground acceleration (PGA) as a selected input motion propagates through a profile of interest.

Determining response of a soil deposit to a bedrock motion is the principal objective of a ground response analysis. Although the term ground response analysis is one that should, ideally, comprise all aspects of earthquake simulation (from rupture mechanism to ground response at the surface), the complexities that come with analyzing fault rupture mechanisms force the scope to be limited to the aforementioned principal objective. The effect of soil conditions on modifying ground shaking has been known for quite a while. However, with the advent of strong-motion instruments taking place only recently, quantitative description of local site effect is made possible (Kramer 1996).

Earlier observations of site effects go as far back as the early 19^{th} century. The observations were described purely qualitatively, noting that more damage could be seen on buildings on soils as compared to those founded on rocks. More recently, Borcherdt's (1970) ground motion measurements showed the clear amplification among records from underlain by a layer of younger bay mud and those on nearby bedrock. Further studies on the 1989 Loma Prieta Earthquake suggested that soil amplification was one of the major contributors in causing damage to vulnerable structures (Borcherdt 1996). During the 2000 Tottoriken-seibu earthquake, the installation of seismographs on the ground surface and at deep depths helped produce contours of peak acceleration that clearly demonstrated amplification at the ground level. Furthermore, four acceleration records near Sakaiminato during the earthquake provided clearer evidence. The four stations were within a fairly close distance with each other, however the two stations that were on a thick surface deposit recorded accelerations of greater magnitude

compared to those located in a mountain area (Nozu 2003 as cited by Yoshida 2015). Ground response analysis, is hence necessary to quantify and simulate the behavior of ground during earthquakes.

The non-linear behavior of soils at very small strains, and the soil particle-water complications make the problem of ground analysis more difficult as compared with those of structural analysis. “SHAKE”, a computer program developed in 1972, aimed at tackling this problem using an equivalent linear method. Although SHAKE dealt with the nonlinear problem using an equivalent-linear approach, other programs dubbed as “truly nonlinear methods” were later introduced in the 1980s and 1990s (Yoshida 2015). Although most of these programs attempted to overcome the major limitation of SHAKE, some of them require specialized programming knowledge and are not easily understood. The past decade witnessed the development of powerful GRA performing packages such as DEEPSOIL, a program capable of performing both equivalent linear and non-linear analysis which is comparatively easy to use with its user-friendly Windows interface.

In addition to estimating site-related amplification potential, Ground Response Analysis is also used to evaluate the dynamic stresses and strains in the evaluation of liquefaction hazard. The very tendency that cohesionless soils have to densify under static and dynamic loading, results in the build-up of excess pore water pressure provided that the soils are saturated. Under rapid loading, where the water does not have enough time to ooze out and hence is in an undrained condition, the densification results in the increment of excess pore water pressure which in turn results in the decrease of effective pressure. The 1964 Niigata earthquake is a prime example of this phenomenon and has helped intensify the effort to understand and quantitatively explain the phenomenon. Japan National Committee on Earthquake reported, “… a peculiar phenomenon during the earthquake was the settlement and tilting of many reinforced concrete buildings,” where it attributed the phenomenon to the unusual ground conditions, as the coastal portion of the Niigata Plain is alluvial and consists of marine sediments.

Ground response analyses can be conducted in one, two or three dimensions, depending on the geometric characteristics of the physical condition they are to model. For terrains that are nearly horizontal or gently sloping, one-dimensional (1D) modeling is applied. However, irregularity of some practical situations makes the assumptions of 1D GRA inapplicable, necessitating the use

of 2D or even 3D analyses (Kramer 1996). When soil conditions vary in different dimensions, or for structures such as retaining walls, tunnels and earth dams, multi-dimensional analyses are more suited. Hawassa's flat topography and uniform geological and geomorphological setup make the use 1D GRA appropriate in this study.

3.2.2 One-Dimensional Ground Response Analysis

One-dimensional GRA is a widely used ground motion prediction model that gives reasonable estimates considering three basic assumptions: (1) soil layers are horizontal and extend infinitely; (2) the ground and bedrock surface are horizontal; and (3) incident waves from earthquake motions propagate vertically (Kramer 1996; Phanikanth and Choudhury 2011).

Depending on the choice of soil stress-strain models, three broad approaches are currently available in GRA: Linear, Equivalent Linear and Non-Linear approaches.

3.2.2.1 Linear Approach

Although sparingly employed in actual problems, the linear approach provides simple solutions based on derivations from elasticity. The term linear is used as a consequence of the application of superposition in the evaluation of the combined response of the individual harmonics. In addition to this, the soil is assumed to behave as a Kelvin-Voigt solid with a constant maximum shear modulus and a constant minimum damping ratio. The solutions for GRA in the linear approach are mainly expressed in terms of transfer functions. A transfer function is a ratio of displacement, acceleration or velocity amplitudes at any two points within a soil layer. Defining a proper boundary condition for shear stress or strain (say at the free surface), one can derive mathematical formulations for different cases of soils and bedrock conditions. (Details are presented in Kramer (1996))

The general approach can be summarized in the following steps (Kramer 1996).

1. The base motion is described as a Fourier series, after transforming the time function of the loading to a function of frequency. This is done by approximating the base motion as a sum of a series of harmonic loads of different amplitude, frequency and phase angles. The exponential form of the series can be expressed as,

$$Q(t) = \sum_{n=-\infty}^{\infty} q_n^* e^{i\omega_n t} \tag{3.5}$$

where $Q(t)$ is the loading, $q_n^* n$ is the Fourier coefficient (the * indicates that the coefficient is complex). For fast computational purposes, this bedrock motion is then transformed to the frequency domain using Fast Fourier Transform algorithm. The Fast Fourier Transform is a very efficient numerical procedure that requires the total number of discrete acceleration values to be 2^n.

2. Each term of the Fourier coefficients is multiplied by the respective transfer functions at each frequency ω_n as shown in Equation 3.6 and added by virtue of principle of superposition to give the Fourier series of the output (e.g. ground surface) motion. Hence the total response will be

$$u_n(t) = \sum_{n=-\infty}^{\infty} H(\omega_n) q_n^* e^{i\omega_n t} \tag{3.6}$$

where $H(\omega_n)$ are transfer functions at respective frequencies

3. The output motion is then transformed back to the time domain by obtaining the inverse Fourier transform of the output motion.

The linear approach is limited to applications involving very small strains like machine foundation analysis. It is seldom used in ground response analysis for earthquake excitation.

3.2.2.2 Equivalent Linear (EQL) Approach

It can be observed that the basic assumptions made in the linear approach (taking a constant value of *G* and ξ) only apply when the induced strain is very small. The EQL approach is also in effect linear in the sense that the principle of superposition is applied. However, this approach employs an iterative technique to approximate the non-linear behavior of soils. It was described under Section 3.1 that a single secant modulus, G_{sec}, and an equivalent linear damping ratio ξ can be used to approximate a stress-strain hysteretic loop. These parameters are strain dependent, as shear modulus degrades and damping (which is related to the breadth of the stress-strain loop) increases with increasing strain. The Equivalent-Linear approach, unlike the linear approach,

where a single value of G and ξ are used for a soil layer, iterates between strain, and G and ξ several times so as to simulate the non-linearity. Hence, an important input needed here is the modulus degradation and damping curves of the soil as functions of strain. Using these curves, the following iterative procedure is employed (Kramer 1996).

1. An initial, low-strain is value is assumed, and G and ξ values are read from the modulus degradation and damping curves, respectively.
2. Ground Response analysis is performed and shear-strain time-history is obtained.
3. The maximum shear strain from the time-history is selected. To account for the difference between the short-duration earthquake PGA in reality and the long-duration harmonic loading in the Fourier series, a reduction factor of 65% is customarily used to obtain an effective strain.
4. With this effective strain, new values of G and ξ are read from the modulus reduction and damping curves, and the iteration continues until difference between two successive iterations is reasonably small.

3.2.2.3 Non-Linear Approach

The Equivalent Linear Approach is quite popular among engineers because not only does it give reasonable results for many practical problems, but it does so in a computationally convenient manner. Despite these benefits, one should, however, note that the approach is a mere approximation of the non-linear soil behavior and that the two soil properties (G and ξ) are not truly time-invariant. A true non-linear approach should represent soil stress-strain behavior by actually following the path of the loop. By using numerical integration in small time steps in analyzing the non-linear response, this approach makes it possible to use various constitutive models. The loops need to be represented by curves that can be easily handled in the analysis process. Hyperbolic models with some modifications are commonly implemented in non-linear one dimensional GRA programs. The non-linear approach has the following advantages over EQL:

1. it accounts for the stiffness degradation over the duration of the loading, and hence the stress-strain behavior is more realistically modeled;

2. it can be formulated in terms of effective stresses and hence it can take into account the development of pore water pressure;
3. it gives better estimates when the degree of nonlinearity is large, i.e. where induced strains are high, non-linear approach provides a more reasonable results.

Studies have shown that predictions made by EQL and non-linear site response models are practically similar until a peak strain threshold of around 0.4-0.5% (Kaklamanos 2013; Udaka (1983) as cited by Haile (1996)). Beyond these values, the studies have shown that EQL models show significant bias and are no longer accurate.

Despite its clear advantages over the EQL analyses, non-linear methods have their own shortcomings. The constitutive models that non-linear methods require contain parameters that are not well established and call for a substantial and advanced field and laboratory testing program (Kramer 1996). These parameters are poorly documented and understood; the effect of parametric variability on analysis outputs is unclear; and the benefits of non-linear site response analyses over EQL are unquantified and uncertain, further limiting their implementation into practice (Stewart and Kwok 2008).

CHAPTER FOUR

ACQUISITION AND PROCESSING OF INPUT DATA

4.1 General Workflow of the Study

The study on GRA conducted in this research can be represented by the flowchart given in Figure 4.1.

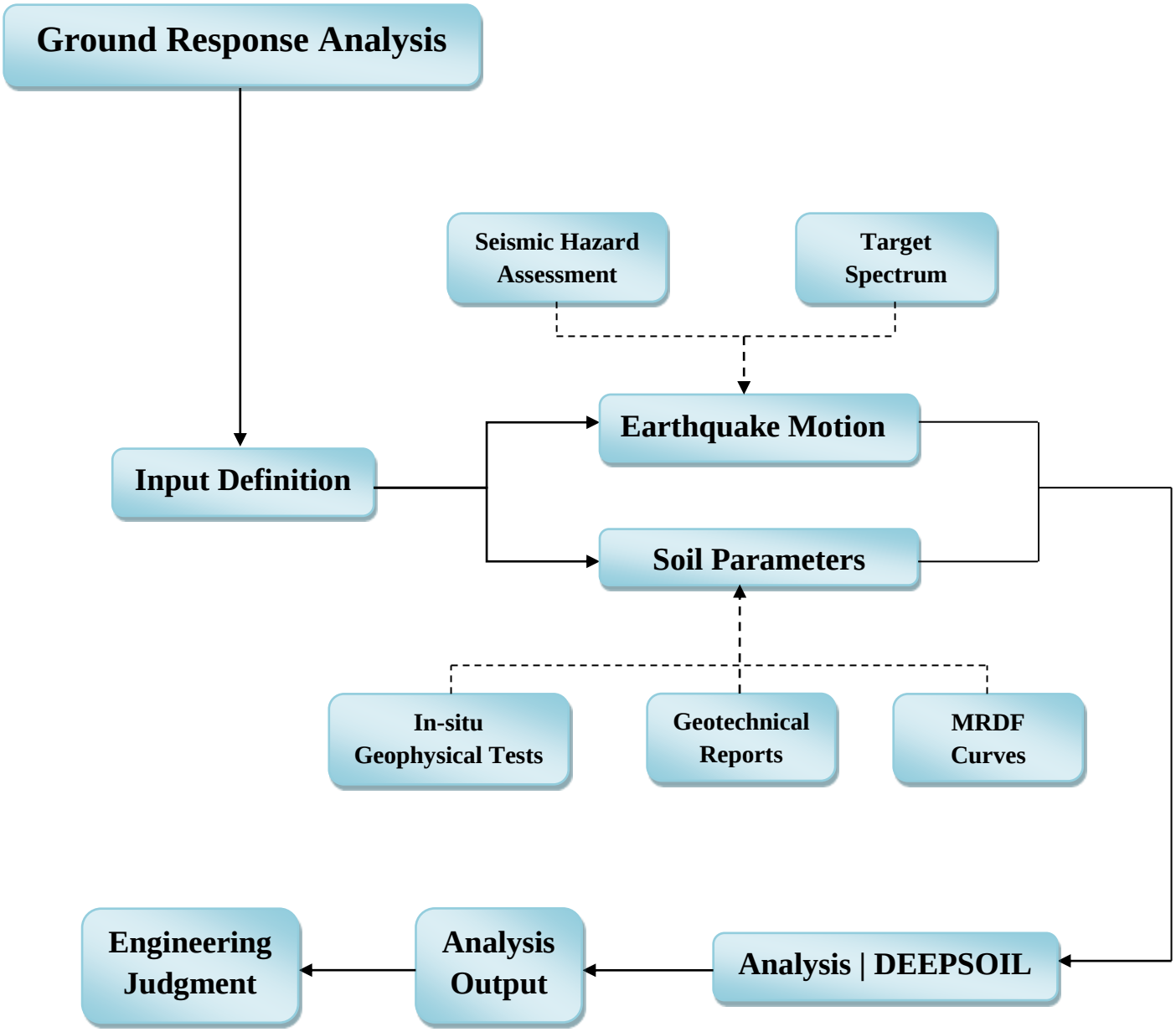

Figure 4.1 A generalized flowchart showing parameters and inputs required for GRA

The flowchart in Figure 4.1 clearly states the parameters required to conduct a complete GRA. It is convenient to categorize these parameters into three:

1. Geotechnical Data – This refers to the characterization of the properties for the soil profile under consideration. Shear-wave velocity and density profiles are the fundamental parameters needed in DEEPSOIL for site characterization. In this regard, available geotechnical reports for structures built in the city were collected. The collected geotechnical reports, which essentially consist of SPT profiles, were correlated to the desired shear-wave velocity profiles. In addition, geophysical methods were attempted in a bid to measure and corroborate the actual field parameters.
2. Input earthquake motion – This category involves the selection of appropriate input motions for use in the GRA. Filtering criteria were employed so as to select best fitting earthquakes for the study area. Furthermore, popular earthquakes with unique attributes were selected.
3. Dynamic Soil Properties – Proper definition of the stress-strain relationship of the soil layers falls under this category. This enables to establish two important dynamic properties of the soil: modulus reduction and energy dissipation potential as functions of strain.

4.2 Input Motions

Selection of input motions is a very important process in any Ground Response Analysis. It involves selecting appropriate input-motion time histories from a pool of available records by applying proper filtering criteria. Due to unavailability of strong ground motion records in Ethiopia, records from the Pacific Earthquake Engineering Research Center (PEER) database (http://peer.berkeley.edu) are used in this research. Additionally, commonly used popular motions for GRA are also used. The steps one needs to follow to properly select input motions are discussed in the following sub-sections.

4.2.1 Definition of Target Spectrum

Target spectrum refers to the response, expressed in form of pseudo-acceleration spectra, for the reference site condition because of ground shaking. In this context, reference site conditions refer to the conditions of the ground below the geotechnical layer that is being analyzed in GRA. As it is customary to terminate site explorations upon reaching a rock formation, reference site conditions are often represented by rock conditions.

The process of setting up a target spectrum begins with defining the earthquake hazard of the region. ES EN 1998:2015 defines design ground acceleration to correspond to a reference return period of 475 years (10% probability of being exceeded in 50 years). Following the discussion in Section 2.4, the target spectra will be drawn using a PGA of 0.11g extracted from GSHAP.

According to the ES EN 1998:2015, the elastic response spectrum $S_e(T)$ is defined by the following expressions,

$$
\begin{aligned}
&0 \le T \le T_B \ : \ S_e(T) = a_g \cdot S \cdot \left[1 + \frac{T}{T_B} \cdot (\eta \cdot 2.5 - 1) \right] \\
&T_B \le T \le T_C \ : \ S_e(T) = a_g \cdot S \cdot \eta \cdot 2.5 \\
&T_C \le T \le T_D : \ S_e(T) = a_g \cdot S \cdot \eta \cdot 2.5 \left[\frac{T_C}{T} \right] \\
&T_D \le T \le 4s \ : \ S_e(T) = a_g \cdot S \cdot \eta \cdot 2.5 \left[\frac{T_C T_D}{T^2} \right]
\end{aligned}
\tag{4.1}
$$

where,

$S_e(T)$ is the elastic response spectrum;

T is the vibration period of a linear single-degree-of-freedom system;

a_g is the design ground acceleration on type A ground;

T_B is the lower limit of the period of the constant spectral acceleration branch;

T_C is the upper limit of the period of the constant spectral acceleration branch;

T_D is the value defining the beginning of the constant displacement response range of the spectrum;

S is the site soil factor;

η is the damping correction factor with a reference value of η =1 for 5% viscous damping.

ES EN 1998:2015 provides the choice of two types of spectra: Type 1 and Type 2. Type 2 design spectrum is used for sites that experience earthquakes below a surface-wave magnitude of 5.5. Previous work done by Kebede and van Eck (1997) has placed the main Ethiopian rift (of which Hawassa is part of) under Zone 2 with upper and lower bound magnitudes being 4 and 7, respectively. For this reason Type 1 spectrum was used. Using the parameters listed in Table 4.1, design spectra of the five ground types for 5% damping can be plotted as shown in Figure 4.2.

Table 4.1 Values of the parameters describing the recommended Type 1 elastic response spectra (ES EN 1998:2015)

Ground type	***S***	***T_B(s)***	***T_C(s)***	***T_D(s)***
A	1.0	0.15	0.4	2.0
B	1.2	0.15	0.5	2.0
C	1.15	0.2	0.6	2.0
D	1.35	0.2	0.8	2.0
E	1.4	0.15	0.5	2.0

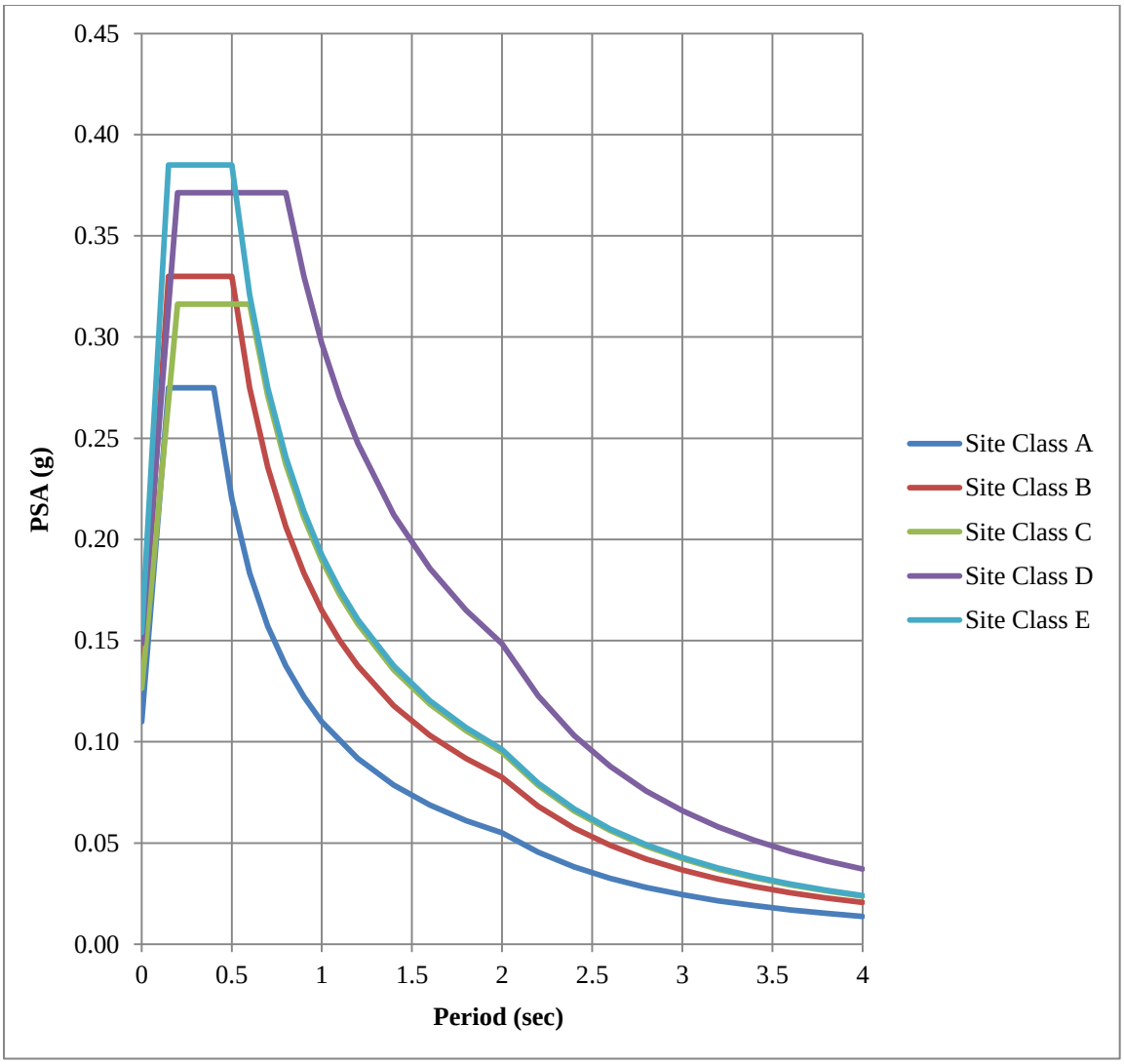

Figure 4.2 Plot of Type 1 design spectra for ground types A to E (5% damping) for Hawassa city

For the target spectrum in the input motion selection, that of site class A has been selected as an input to represent reference rock conditions.

4.2.2 Magnitude Range

In their PSHA for the Horn of Africa, Kebede and van Eck (1997) delineated the region into eight distinct seismic source zones having similar seismotectonic features. Zone 2 comprises the southernmost rifts of Ethiopia and the Main Ethiopian rift (MER) in which Hawassa is located. A region dominated by normal faulting from surface geology, a lower bound magnitude M_0 of 4.0

and an upper bound magnitude M_{max} of 7.0 with error 0.2 were proposed. This range has directly been used in the filtering process.

4.2.3 Duration Range

One can find several definitions for strong ground motion (significant) duration, although all of them can be grouped under three generic categories: bracketed, uniform and significant. Several empirical predictive equations for a number of definitions have been produced over the years. Bommer et al. (2009) developed relations that can be used to estimate ground-motion durations of shallow crustal earthquakes of magnitude between M_w 4.8 and 7.9 at distances of up to 100 km from the source (Figure 4.3), and their proposed relation has been used in determining the range of strong motion duration needed to filter ground motions.

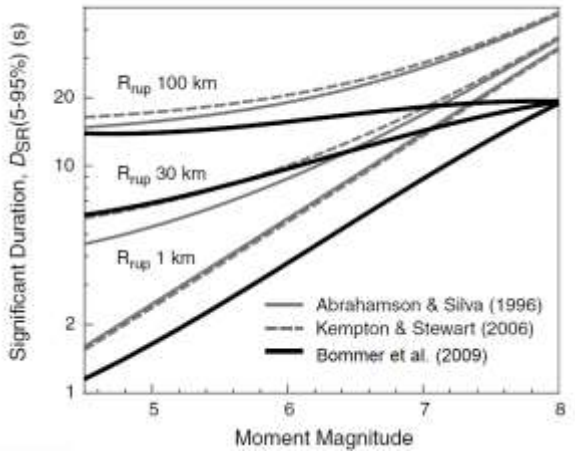

Figure 4.3 A plot of three empirical predictive models for significant duration: Abrahamson and Silva (1996), Kempton and Stewart (2006) and Bommer et al. (2009). (Taken from Bommer et al. 2009)

From the curve by Bommer et al. (2009), an estimated magnitude ceiling occurring at a rupture of 100km yields a maximum duration of approximately 16 seconds. Accordingly, 16 seconds was used as an upper bound for filtering using duration range.

4.2.4 Time Series Scaling

Time series scaling should not be confused with classical ground acceleration amplitude scaling. Scaling here refers to the process of matching ground motion intensities with target spectra up to

the most achievable accuracy. In other words, it sets as its objective, the selection of a record suite that is generally compatible with amplitude and frequency content of the target spectrum (Stewart et al. 2014). Two approaches were considered for scaling.

Approach 1 –matching target over a period range

- Here, it is desired to match spectral ordinates of ground motions to the target spectrum over a defined period range. The period range of structures expected to be subjected to the ground motion is matched with the target spectrum (Figure 4.4 (a)).

Approach 2 – matching target at a single period.

- Ground motions that have been screened through the previous steps are further filtered in such a way that their spectral acceleration at a particular, desired period matches the target spectrum at that particular period as shown in Figure 4.4 (b). This is to be employed if response analysis of a particular structure with known period is required to be analyzed.

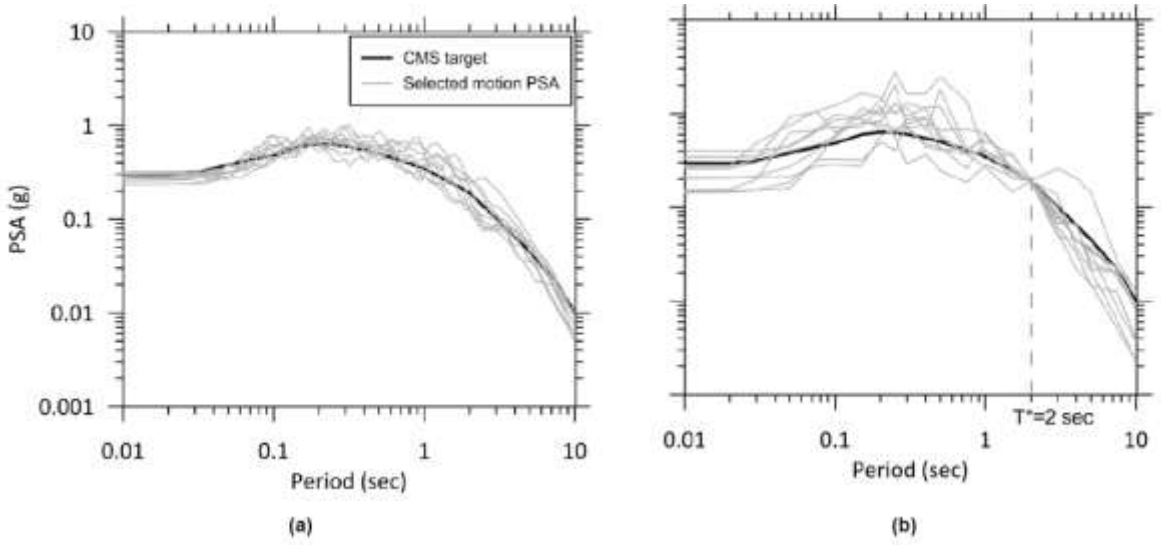

Figure 4.4 Conditional Mean Spectrum based target with 11 selected and scaled motion | Illustration of two approaches of scaling (a) Approach 1, using a range of periods (0.01-10 sec). (b) Approach 2, using a single matching period at 2.0 sec. After Stewart et al. (2014).

The main objective of the thesis is to conduct ground response analysis of representative sites in the city. This dictates the consideration of the ground response for different types of buildings and hence, a range of periods.

ES EN 1998:2015 provides a reasonable approximation to estimate a fundamental period of a structure as follows,

$$T_1 = C_t H^{\frac{3}{4}} \tag{4.2}$$

where T_1 is the fundamental period in seconds, C_t is a coefficient (0.085 for steel frames and 0.075 for concrete frames) and H the height of the building. Hawassa's notable buildings are mostly short-medium height, with the majority of them falling within the range of G+2 to G+9. Considering the rate of growth of the city and anticipating higher buildings to come in the future, a sufficiently high enough (G+20) upper bound was selected. Roughly assigning building heights of 9m and 72m respectively, a period range 0.389 sec and 1.854 sec can be computed. In this filtering, the ranges were extended slightly to 0.2-2.0 seconds.

Once the period range is identified, additional factors that account for deviation come into play. Lanzo et al. (2015) forwarded two parameters in this regard, F_s – a constant scaling factor and D_{rms} – a deviation parameter that indicates the matching extent between the spectral shapes of records and the target spectrum:

$$D_{rms} = \frac{1}{N}\sqrt{\sum_{i=1}^{N}\left(\frac{SA_0(T_i)}{PGA_0}\right) - \frac{SA_s(T_i)^2}{PGA_s}} \tag{4.3}$$

where N is the number of periods at which the spectral shape is specified, $SA_0(T_i)$ is the spectral acceleration from the selected record at period T_i, $SA_s(T_i)$ is the target spectral acceleration at the same period and PGA_0 and PGA_s are peak ground acceleration of the considered record and the zero-period anchor point of the target spectrum, respectively (Lanzo et al. 2015). Best fits of accelerograms are characterized by a low value of D_{rms} and a scaling factor F_s close to unity.

The PEER database gives the user the option to decide the minimum, as well as the maximum initial scaling factors so that those records falling outside of the range will be filtered out. Although it is customary to select scale factors in GRA from 0.25 to 4.0, in this particular selection, a manageable range of scaling factors was selected to be between 0.6 and 1.4.

An additional advantage that the PEER database gives to the user is the freedom to assign weights to a certain discreet periods. Three periods, 0.2, 1.1 and 2.0 sec were chosen to represent short, medium and long periods (in Hawassa's context) and a weight of 1, 1 and 0.5 was assigned to each respectively. The rationale behind this is that the longer periods should not influence the selection greatly as there are no buildings of that height in Hawassa currently, or are not anticipated in the near future. They have been taken into consideration, but with a reduced influence.

4.2.5 Shear-wave velocity of uppermost 30m ($V_{S,30}$)

The final filtering criterion that can be used with the available information is that of the upper 30m soil formation. This range should be a reasonable limit, and not be made too restrictive and limit candidate motions too much. In addition to this, Stewart et al. (2014) strongly recommend that for GRA, the V_S of the underlying half space be compatible with the reference site condition as defined in the target spectrum. Accordingly, a shear wave velocity range of 800-1500 m/s was selected to represent a reference rock condition.

In addition to the aforementioned filtering criteria the following points have also been considered.

- Tectonic Regime: shallow crustal earthquakes represent earthquakes in the MER (Kebede and van Eck 1997). Considering the unavailability of records in the country, the research had to rely on records from locations with similar tectonic regime. Strong motion records from different regimes, such the subduction-dominated faults in the far-east have been filtered out. In addition to this, locations believed to have been frequented with earthquakes from deep sources have also been screened out. Accordingly, records from western United States were found more appropriate and thus considered.
- Lanzo et al. (2015) also applied additional criteria which are put to practice in this research. According to their research, avoiding multiple records from a single earthquake event, and avoiding the use of both horizontal components from the same earthquake can be taken as good rule of thumb in selecting motions for GRA.

Having used the aforementioned criteria, three ground motion records were selected as presented in Table 4.2.

Table 4.2 Selected Ground Motions from PEER database

RSN	Scale Factor	5-95% Duration (sec)	Earthquake Name	Year	Station Name	Magnitude	V_{S30}(m/s)
680	0.9479	6.2	"Whittier Narrows-01"	1987	"Pasadena – CIT Kresge Lab"	5.99	969.07
797	0.9416	14.2	"Loma Prieta"	1989	"SF – Rincon Hill"	6.93	873.1
4083	0.5737*	8.8	"Parkfield-02_CA"	2004	"PARKFIELD – Turkey Flat #1 (0M)"	6.0	906.96

*Although the scale factor of Parkfield event is slightly lower than 0.6, it has been selected anyway so as not to select multiple records from a single event. Multiple records from Loma Prieta event passed the filter, however only one got selected.

It is important to note here under which conditions ground motions will be given. Output of a single record contains nine separate files, comprised of one vertical and two horizontal components for acceleration, velocity and displacement time histories. The downloaded trace files are unscaled (amplitude scaling), processed (where baseline corrections have been applied) and as-recorded (unrotated) displacement, velocity and acceleration time history files.

The downloaded acceleration time-histories have been scaled to Hawassa's PGA of 0.11g and are presented in Figure 4.5. Details of each earthquake are presented in Appendix B.

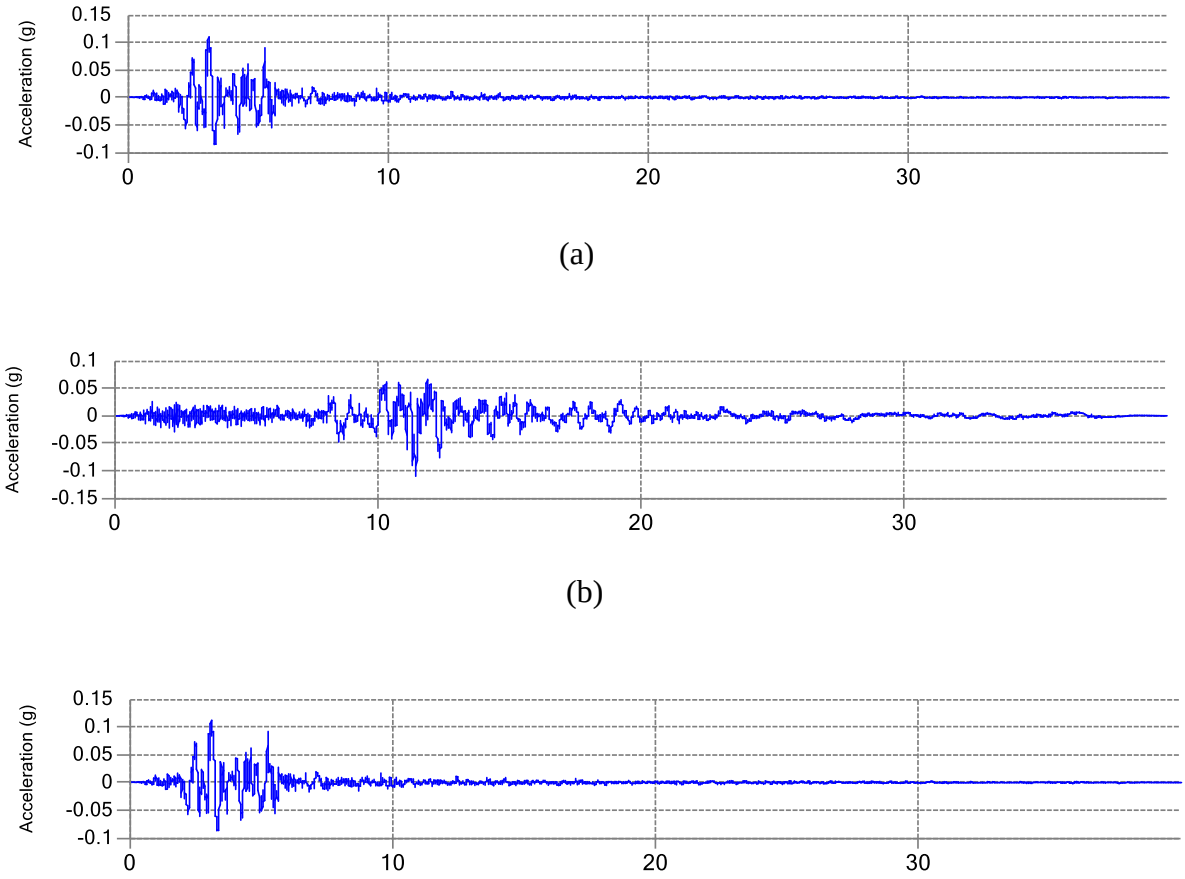

Figure 4.5 – Scaled time histories of Whittier Narrows 1987 (a), Loma Prieta 1989 (b) and Parkfield 2004 (c) earthquakes

4.2.7 Additional Records

Although the procedures employed in the previous subsections tried to select out those records that were believed to be as appropriate for Hawassa as can be made possible, additional records with other selection parameters have also been used.

It is a well-established fact that three parameters are used to describe earthquake: amplitude, frequency content and duration. Having this in mind, many studies customarily propose the use of the following four acceleration records (Table 4.3) with distinct behaviors in regards to these parameters. The deconvolved (processed in such a way that site effect is removed,) time-histories are presented in Figures 4.6-4.9 (Haile 1996).

Table 4.3 Summary of additional motions typically used for response analysis, from Haile (1996)

	5-95% Duration (sec)	Earthquake Name	Year	Station Name	Magnitude
1	23.6	"Imperial Valley"	1940	"ElCentro record"	6.7
2	32.8	"Kern County"	1952	"Taft record"	7.7
3	44	"Tokachi-oki"	1968	"Hachinohe record"	7.9
4	9.8	"Hygoken-nanbu"	1995	"Kobe JMA record"	7.2

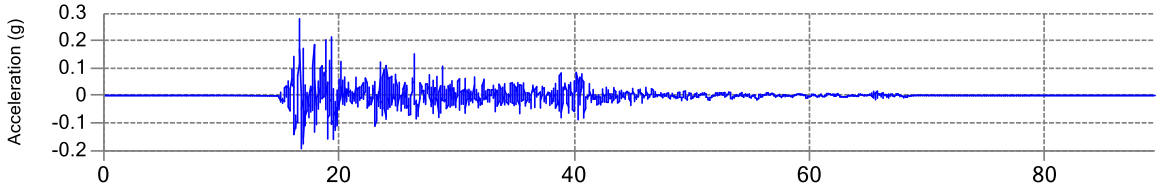

(a)

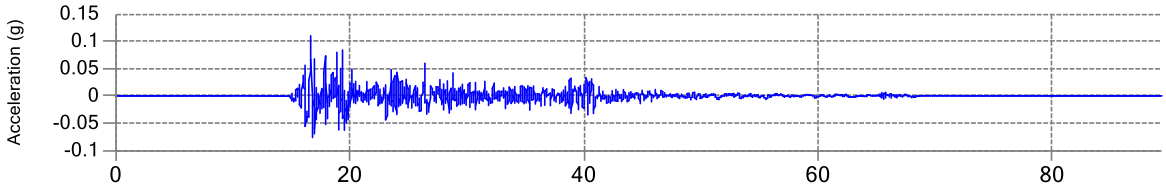

(b)

Figure 4.6 Imperial Valley Earthquake (1940) ElCentro Record: (a) deconvolved, Haile (1996) and (b) scaled to Hawassa's PGA of 0.11g

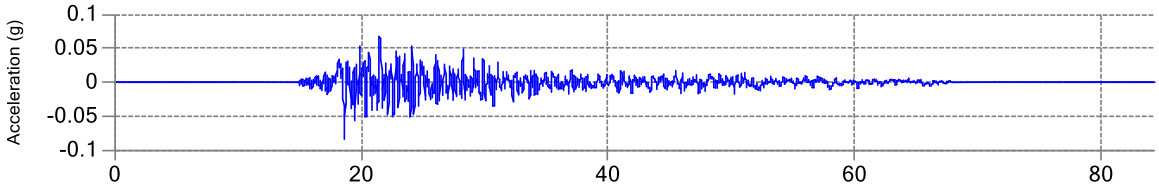

(a)

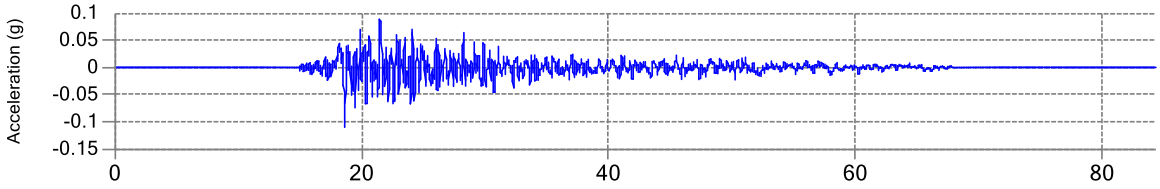

(b)

Figure 4.7 Kern County Earthquake (1952) Taft Record: (a) deconvolved, Haile (1996), and (b) scaled to Hawassa's PGA of 0.11g

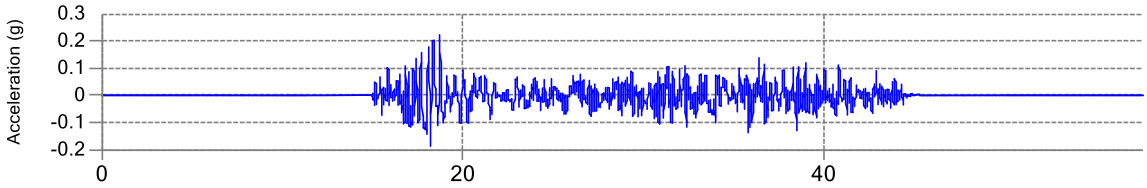

(a)

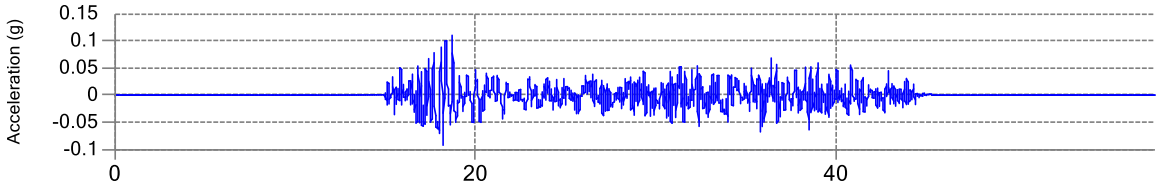

(b)

Figure 4.8 Tokachi-oki Earthquake (1968) Hachinohe Record: (a) deconvolved, Haile (1996) and (b) scaled to Hawassa's PGA of 0.11g

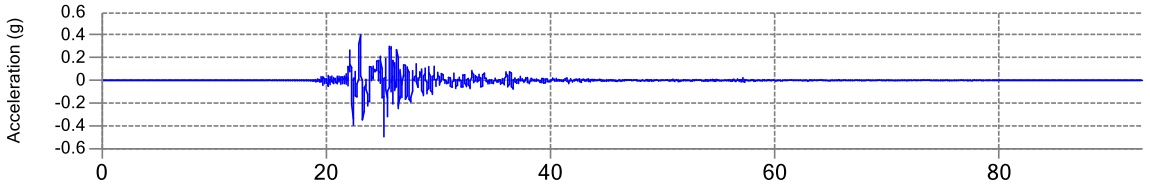

(a)

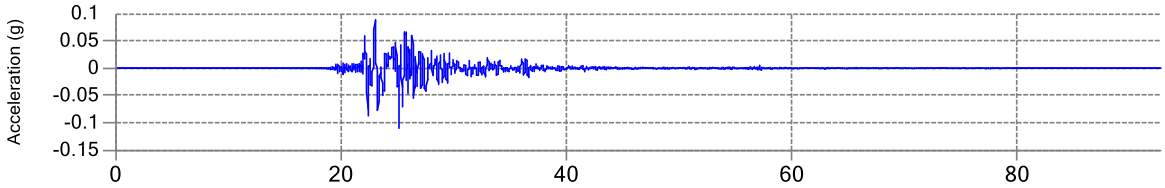

(b)

Figure 4.9 Hyogoken-nanbu Earthquake (1995) Kobe JMA Record: (a) deconvolved, Haile (1996) and (b) scaled to Hawassa's PGA of 0.11g

4.3 Data from Geotechnical Investigation

It cannot be denied that a direct measurement is the most preferred method of determination of shear-wave velocity. In the absence of such measurements, or if it is desired that additional methods confirm the direct measurement, penetration tests may be used as an alternative. These penetration tests, (more specifically and commonly in Ethiopia, Standard Penetration Tests), are properly correlated so as to obtain shear-wave velocity profiles at locations where the investigations have been conducted. It was mentioned before that SPT investigations found in Hawassa seldom reach the desired 30m depth. This called for an additional procedure, statistical extrapolation, be carried out so as to have a complete information. The two procedures (correlation and extrapolation) are discussed in the following subsections.

Available and relevant geotechnical reports are hence collected. The available geotechnical investigations reports are principally conducted for buildings in the city. Understandably, the higher the buildings, the more depth and detailed the investigation is going to be. This is, unfortunately, the reason as to why one finds it impossible to find data relevant to this research

upto a customarily desired depth of 30m. The geotechnical investigation reports that were collected were taken from buildings found in Hawassa, ranging from G+1 upto G+11 and with a maximum depth of investigation of 25m. In fact, the majority of the building sites were investigated using trial pits of maximum depth of 3m. Table 4.4 presents a summary of the noteworthy geotechnical investigation reports that were acquired.

Table 4.4 A summary of relevant geotechincal reports for buildings in Hawassa

Project Name	Consulting Firm (that conducted the investigation)	Number of Storeys	Depth of Investigation (m)
"Hawassa Hotel and Resort"	Ethiopian Construction, Design and Supervision Corporation	B+G+6	15
"Ethiopian Revenue and Customs Authority"	Ethiopian Construction, Design and Supervision Corporation	B+G+6	15.5
W/o Tigist Kassa*	Ethiopian Construction, Design and Supervision Corporation	B+G+7	15
Ato Eskinder Tesfaye*	Ethiopian Construction, Design and Supervision Corporation	B+G+7	15
Nib International Bank	Addis Geosystems P.L.C	2B+G+11	25
Awash International Bank	Addis Geosystems P.L.C	B+M+G+7	13
Hawassa Industrial Park	Ethiopian Construction, Design and Supervision Corporation	-	10
"BGI Brewary Factory"	Ethiopian Construction, Design and Supervision Corporation	-	10

"Hawassa University Administration Buildinig"	Ethiopian Construction, Design and Supervision Corporation	-	15
"SNNPR Manucipality Building"	Ethiopian Construction, Design and Supervision Corporation	-	7.5
"Qualiy and Standards Authority"	Ethiopian Construction, Design and Supervision Corporation	-	4 (test pits)
"Hawassa Stadium"	Ethiopian Construction, Design and Supervision Corporation		20

*indicates clients' names

It can be inferred from the geological discussion mentioned in Chapter 2 that the majority of the city's area is resting on a lake bed. The reports also indicate the presence of rhyolites at shallow depths in the southern part of the city(Figure 4.10, region enclosed with blue lines). Bound by Tabor Mountain on the west and Alamura Mountain on the south, this region dominates the southern part of the city. Other geotechical reports that were compiled for sites at the heart of the city (central and nothern-central areas) show the presence of a thin layer of welded-tuff/ignimbrite at a very shallow depth (<7m). It is worth noting that the majority of the city is lying on this region. Albeit supported by very shallow investigations, the area in north-eastern part of the city is dominated by silty sand deposits that extend down to the investigation depth. In this respect, 30 boreholes conducted as part of the geotechnical investigation program for Hawassa's Industrial park consistently confirm this formation that extends to a depth of 10 m. The three regions are shown in Figure 4.10 . The boreholes can be found in Appendix A.

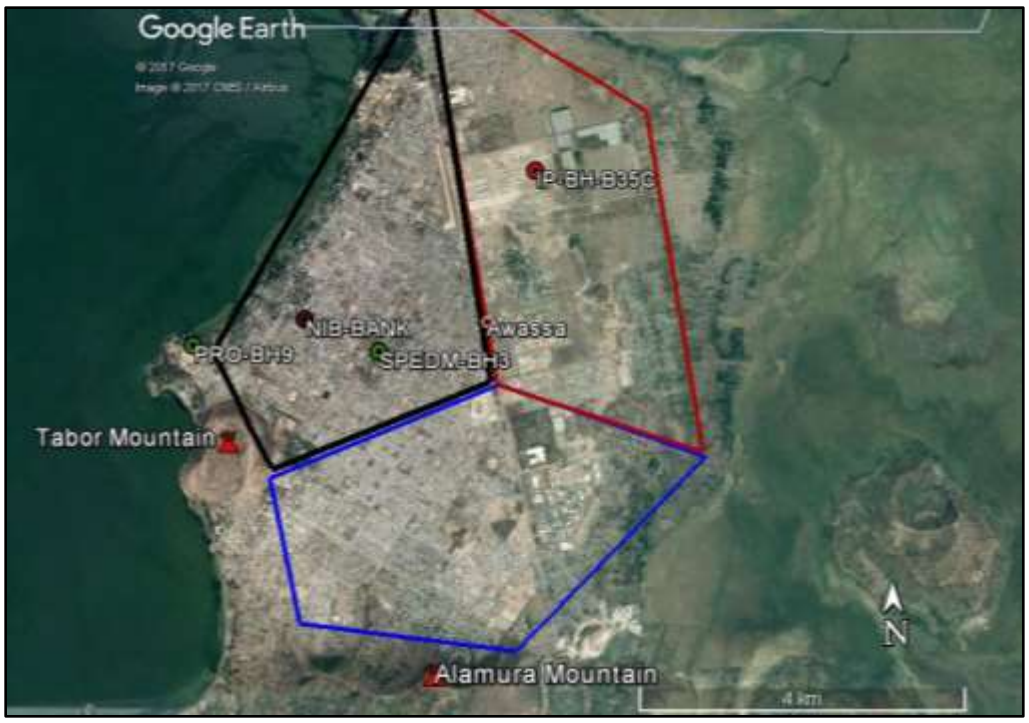

Figure 4.10 Rough demarcation of the city based on geotechnical investigation: the black territory is where the majority of the critical structures located, the red territory is predominantly loose (from shallow investigations) and the blue territory is where strong formation is believed to be available at a very shallow depth, consistent with geological maps

Four geotechnical profiles were selected for analysis as representative of the city's site geology (also shown in Figure 4.10). IP-BHB35C is a borehole taken from the Hawassa's Industrial Park and is a rough representative of the soil in the region bounded by the red polygon. It was mentioned earlier that the majority of the city is found within the black territory. Two profiles, NIB International Bank-BH1 and SPEDM-BH3 were selected from this region. A borehole from Progress International Hotel (PRO-BH9) is selected to represent the southern region due to its proximity to Tabor Mountain.

4.3.1 SPT-V_S Correlation

Before delving deep into the correlation, it is imperative that one applies proper corrections for recorded SPT values found in the investigation reports.

Youd et al. (2001) discussed the different factors that affect SPT results in their study of liquefaction potential and their recommendations have been and still are in use globally. The factors that necessitate correction are overburden pressure, energy ratio, rod length, borehole diameter and sampling method. The corrected SPT hence is given by the following equation.

$$N_{60} = C_N C_E C_R C_B C_S N_m \tag{4.4}$$

where, C_N, C_E, C_R, C_B and C_S are correction coefficients for the previously mentioned factors respectively. Furthermore, the energy efficiency correction is given by Equation 4.5. It is worth noting that it is inappropriate to consider overburden stress correction for shear-wave velocity determination (Wair et al. 2012). It can be seen later that the overburden contribution is separately considered within the correlation equations.

$$C_E = \frac{ER_m}{60\%} \tag{4.5}$$

where, ER_m is the energy efficiency of the machine employed. Youd et al. (2001) proposed a table of values for the other parameters (Appendix C).

Having corrected the SPT values, the next step would be applying a proper correlation tool to obtain the corresponding shear-wave velocities. In their guideline document for the estimation of shear-wave velocity profiles, Wair et al. (2012) made a comprehensive review of previous works (Kanai (1966); Shibata (1970); Ohba & Toriuma (1970); Ohsaki & Iwasaki (1973); Ohta & Goto (1978); Imai & Tonouchi (1982); Seed et al. (1983); Sykora & Stokoe (1983); Lin et al. (1984); Jinan (1987); Lee (1992); Dickenson (1994); Sisman (1995); Iyisan (1996); Jafari et al. (1997); Pitilakis et al. (1999); Kiku et al. (2001); Jafari et al. (2002) and Hasncebi & Ulusay (2007)). The correlations were broadly categorized into three sections: correlations for all soils, correlations for clays and silts, correlations for sands and correlations for gravels. The majority of the correlations were of the form

$$V_s = a \cdot N_{60}^b \cdot \sigma'^c_v \tag{4.6}$$

where a, b and c are coefficients from regression analysis, N_{60} is the corrected SPT value and σ'_v is the effective overburden stress. After analyzing all the aforementioned studies, Wair et al. (2012) provide their recommendations for each category (Table 4.6). In addition to these

recommendations, Otta & Gotto's correlations have also been considered for comparison, due to the fact that they have tried to develop correlations with and without overburden and attempted to develop correlations for all soil categories. Furthermore, their studies provided three separate equations for sands depending on their gradation (Table 4.5). The correlated values of Ohta and Gotto (1978) are used in the subsequent sections.

Table 4.5 SPT-Vs correlations developed by Ohta and Gotto (1978)

Soil Type	Without Overburden	With Overburden
All Soils	$68.4N_{60}^{0.27}$	$66.9N_{60}^{0.21}D^{0.19}$
Clays and Silts	$90.6N_{60}^{0.25}$	$67.5N_{60}^{0.17}D^{0.20}$
Fine Sand	$95.6N_{60}^{0.25}$	$73.3N_{60}^{0.17}D^{0.20}$
Medium Sand	$91.8N_{60}^{0.25}$	$72.0N_{60}^{0.17}D^{0.20}$
Coarse Sand	$94.1N_{60}^{0.25}$	$76.6N_{60}^{0.17}D^{0.20}$

D is measured in m.

Table 4.6 SPT-Vs correlations recommended by Wair et al. (2012)

Soil Type	Shear wave Velocity for Quaternary Soils (m/s)	Age Scaling Factors	
		Holocene	Pleistocene
All Soils	$30N_{60}^{0.215}\cdot\sigma'^{0.275}_{v}$	0.87	1.13
Clays & Silts	$26N_{60}^{0.17}\cdot\sigma'^{0.32}_{v}$	0.88	1.12
Sands	$30N_{60}^{0.23}\cdot\sigma'^{0.23}_{v}$	0.9	1.17
Gravels - Holocene	$53N_{60}^{0.19}\cdot\sigma'^{0.18}_{v}$	----	----
Gravels - Pleistocene	$115N_{60}^{0.17}\cdot\sigma'^{0.12}_{v}$	----	----

σ'_v is measured in kPa.

The corrections and correlations for the four selected profiles are summarized in Table 4.7 (a-d).

Table 4.7 Summary of SPT correction and correlation for: (a) Profile 1 | Progress International Hotel, BH9, (b) Profile 2 | Industrial Park, BH B35C, (c) Profile 3 | Nib International Bank, BH1,and (d) SPEDM, BH3

(a)

Profile 1 | Progress International Hotel, BH9								
Layer depth (m)	Measured SPT (N-70%)	C_E	C_R	C_B	C_S	Corrected $(N)_{60}$	Ohta and Gotto (m/s)	Recommended by Wair et al. (m/s)
0.0-3.3	10	1.17	0.85	1.0	1.0	10	138	118
3.3-6.4	-	-	-	-	-	-	-	-
6.4-7.0	12	1.17	0.95	1.0	1.0	13	167	145
7.0-9.0	23	1.17	1.0	1.0	1.0	27	199	178
9.0-11.0	21	1.17	1.0	1.0	1.0	25	205	180
11.0-15.0	21	1.17	1.0	1.0	1.0	25	218	190

(b)

Profile 2 | Industrial Park, BH B35C								
Layer depth (m)	Measured SPT* (N-70%)	C_E	C_R	C_B	C_S	Corrected $(N)_{60}$	Ohta and Gotto (m/s)	Recommended by Wair et al. (m/s)
0.0-1.5	8	1.17	0.85	1.0	1.0	8	113	86
1.5-3.0	15	1.17	0.85	1.0	1.0	15	145	118
3.0-6.0	25	1.17	0.95	1.0	1.0	28	185	161
6.0-7.5	26	1.17	0.95	1.0	1.0	30	196	172
7.5-10.4	38	1.17	1.0	1.0	1.0	44	221	201

(c)

Profile 3 | Nib International Bank, BH1								
Layer depth (m)	Measured SPT* (N-55%)	C_E	C_R	C_B	C_S	Corrected $(N)_{60}$	Ohta and Gotto (m/s)	Recommended by Wair et al. (m/s)
0.0-0.5	20	0.92	0.85	1.0	1.0	16	146	126
0.5-3.45	20	0.92	0.85	1.0	1.0	16	146	126
3.45-5.0	-	-	-	-	-	-	-	-
5.0-6.4	-	-	-	-	-	-	-	-
6.4-8.45	24	0.92	1.0	1.0	1.0	22	190	158
8.45-10.45	20	0.92	1.0	1.0	1.0	18	192	156
10.45-12.45	23	0.92	1.0	1.0	1.0	21	204	166
12.45-14.45	27	0.92	1.0	1.0	1.0	25	216	177
14.45-16.45	20	0.92	1.0	1.0	1.0	18	203	161
16.45-20.0	-	-	-	-	-	-	-	-

(d)

Profile 4 | SPEDM BH3								
Layer depth (m)	Measured SPT (N-70%)	C_E	C_R	C_B	C_S	Corrected $(N)_{60}$	Ohta and Gotto (m/s)	Recommended by Wair et al. (m/s)
0.0-1.2	6	1.17	0.80	1.0	1.0	6	95	78
1.2-3.0	15	1.17	0.85	1.0	1.0	15	133	127
3.0-4.5	-	-	-	-	-	-	-	-
4.5-7.0	-	-	-	-	-	-	-	-
7.0-10.0	12	1.17	1.0	1.0	1.0	14	182	151

4.3.2 Statistical Extrapolation

Most geotechnical as well as measured data do not extend to the contextual desired depth of 30m. This is especially true in cities like Hawassa, where most structures are medium rise buildings with shallow geotechnical investigation depths. Having this in mind, Boore (2004) suggested a method of extrapolating based on statistical analysis of borehole data in California. The study was based on regression analysis of 135 boreholes in California and correlated $V_{S,30}$ with the time-averaged V_S down to the terminal depth of investigation (V_{Sd}). The time-averaged velocity is computed as

$$V_{Sd} = \frac{\sum_{i=1}^{n} d_i}{\sum_{i=1}^{n} \frac{d_i}{v_{Si}}} \tag{4.7}$$

where $\sum_{i=1}^{n} d_i$ is the depth of measurement. Once V_{Sd} is computed, $V_{,S30}$ is then obtained using the equation

$$\log V_{S,30} = a + b \cdot \log V_{Sd} \tag{4.8}$$

a and b are regression coefficients for which Boore provided a table following his study (Appendix C). Using this computed value of $V_{S,30}$, V_{Sd} at required depths are found and from these values, shear-wave velocities at required depths can be computed.

It is worth noting that Boore's method is much more appropriate for sites with relatively uniform soil conditions as it employs a statistical methodology. This goes well with most of the locations in Hawassa, where significant and abrupt velocity contrasts are few within the 30m. An observation from the geotechnical reports showed the presence of a thin ignimbrite layer of very high stiffness at depths in the region of 6m. This thin layer has not been taken into consideration during the extrapolation work. The extrapolation of the four profiles for which SPT-Vs correlation was made is presented in Table 4.8.

Table 4.8 Extrapolated shear-wave velocities of the four selected geotechnical profiles

Profile 1*		**Profile 2**		**Profile 3**		**Profile 4**	
Depth(m)	Vs (m/s)	Depth(m)	Vs (m/s)	Depth(m)	Vs (m/s)	Depth(m)	Vs (m/s)
0.0-3.3	138	0-1.5	113	0.0-0.5	146	0.0-1.2	95
3.3-6.4	181	1.5-3.0	145	0.5-3.45	146	1.2-3.0	133
6.4-7.0	167	3.0-6.0	185	3.45-5.0	-	3.0-4.5	-
7.0-9.0	199	6.0-7.5	196	5.0-6.4	-	4.5-7.0	-
9.0-11.0	205	7.5-10.0	221	6.4-8.45	190	7.0-10.0	182
11.0-15.0	218	-11	217	8.45-10.45	192	-11	182
-16	228	-12	214	10.45-12.45	204	-12	178
-17	226	-13	213	12.45-14.45	216	-13	175
-18	234	-14	240	14.45-16.45	203	-14	196
-19	244	-15	215	-17	224	-15	178
-20	248*	-16	232	-18	230	-16	190
		-17	230	-19	240	-17	187
		-18	238	-20	244	-18	193
		-19	248	-21	254	-19	203
		-20	252	-22	252	-20	206
		-21	263	-23	265	-21	214
		-22	261	-24	271	-22	212
		-23	274	-25	276	-23	225
		-24	280	-26	283	-24	231
		-25	285	-27	281	-25	235
		-26	292	-28	288	-26	241
		-27	290	-29	283	-27	239
		-28	298	-30	286	-28	243
		-29	293			-29	238
		-30	296			-30	241

*The extrapolation of Profile 1 has been limited to 20m as reports point to the presence of hard rock at that location

4.4 Data from Geophysical Investigation

4.4.1 General Background

Geophysical methods provide non-invasive ways to characterize the earth, much like how medical imaging let us see inside the human body. Although geophysical methods were principally employed so as to characterize deep exploration targets such as mineral and groundwater resources, many sectors (and civil engineering among them) have recently reaped the benefits from them because of the vast advantage that they bring in detecting, classifying and describing shallow subsurface targets (Everett 2013). From among the numerous benefits, of particular interest to this thesis is the methods' ability to address basic questions relevant to near surface tectonics in a bid to assess earthquake-related risks.

Geophysical methods, despite their variation in purpose and instrumentation, follow a certain pattern in their workflow. They all contain a front-end desk work which starts by defining the scientific problem that needs to be solved. Gathering relevant information and initial site reconnaissance can also be included under the front-end work. Carrying out these tasks paves way for deciding the relevant geophysical technique. Also part of this work-phase is acquisition of instrumentation and planning of logistics. The second important phase that all geophysical methods contain is the field work, which mainly revolves around mobilizing and deploying instruments and human resources and collecting data. This phase is followed by the office-work of data reconciliation and processing, and preparation of field report, after which conclusions and recommendations are presented.

Geophysical methods play a crucial role in civil engineering works over recent years due to their time and cost-effective nature of investigation. They offer the chance to overcome some problems associated with the customary ground investigation techniques; achieving their target in a non-destructive testing manner. From among the various geophysical methods, this research employed two of the most popular investigations: Seismic Refraction Method and Electrical Resistivity Method.

4.4.2 Seismic Refraction Survey

As is the case with most geophysical methods, seismic refraction method applies the principles of physics to characterize the earth. The concept is based on the relationship between the time taken for a wave to travel from one location to another in a particular medium, to the medium's stiffness parameter. In response to a certain seismic disturbance, two types of waves are known to be produced: body waves and surface waves. Body waves are termed so because they can travel through the interior of the earth. Body waves are further classified into two as P-waves and S-waves. In the case of P-waves (also termed primary, compressional or longitudinal waves), the direction motion of an individual particle and that of propagation align, whereas in the case of S-waves (secondary, shear or transverse waves), it is perpendicular. Surface waves are, as their name implies, of surface, and travel along the surface of the earth. The two most popular examples of surface waves are Rayleigh waves (retrograde elliptic waves) and Love waves (in which particle displace transverse to the direction of wave propagation on a plane normal to the vertical).

4.4.2.1 Theoretical Formulation

Formulation of body waves expressions through the use of elasticity theory and wave motion equation are discussed in great detail in several textbooks (Everett 2013; Sadd 2013; Telford 1990). This section will be dedicated to the theoretical background of seismic refraction surveying.

Seismic refraction method uses the basic principle of motion to evaluate waves generated from a source. It has an energy source, such as an explosive unit or a hammer, which generates a swarm of waves to receiving units which detect and amplify the energy they receive for purposes of observation. As the test progresses, disturbance from such sources is generated at different known points, thereby generating a time-distance information (Redpath 1973) A simple schematic illustrating a seismic refraction survey is shown in Figure 4.11.

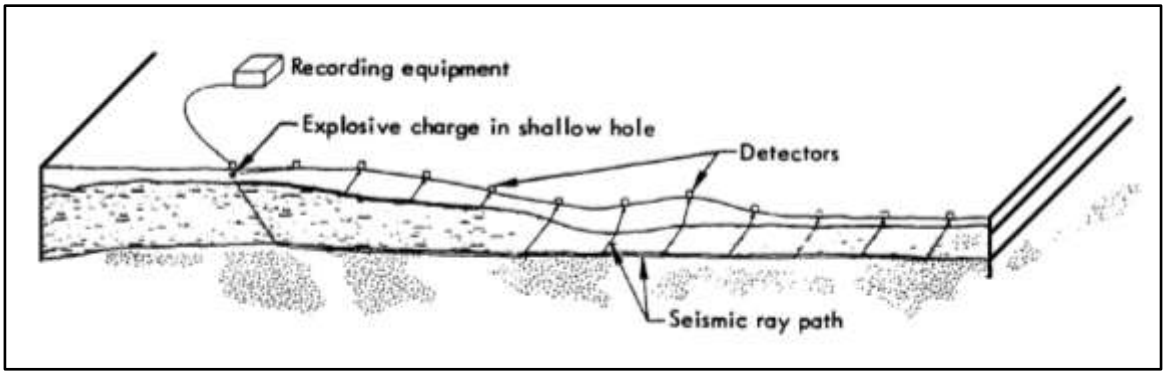

Figure 4.11 Schematic of seismic refraction survey. After Redpath (1973)

Analogous to the situation with light ray propagation through transparent media, a body wave refracts when crossing a boundary separating two materials of varied stiffness. Another part of the wave reflects depending on the stiffness gradient. The refraction principle (Figure 4.12), just as in the case of refraction of light rays, obeys Snell's law.

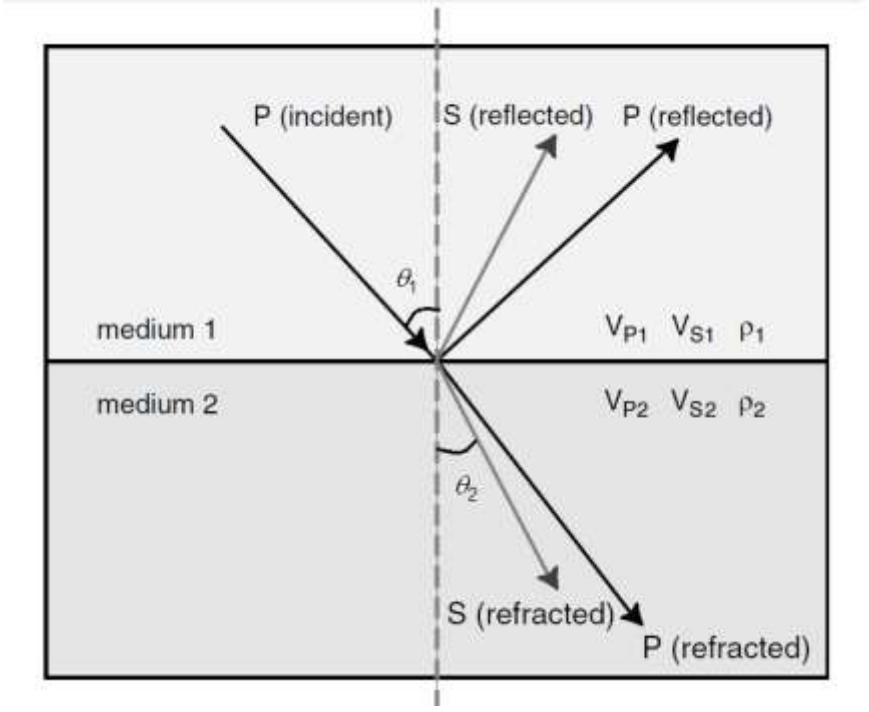

Figure 4.12 Incident and refracted waves propagating through two mediums of different stiffness. After Everett (2013)

Considering an incident wave travelling through a medium of velocity V_1 at an angle θ_1 from the vertical, underlain by a stiffer layer of a higher velocity V_2 making an angle θ_2, Snell's law of refraction relates the parameters as,

$$\frac{\sin\theta_1}{V_1} = \frac{\sin\theta_2}{V_2} \tag{4.9}$$

Energy gets refracted until an angle, called critical angle of incidence, is reached. At angles exceeding the critical angle, waves will be reflected back to the upper medium and refraction does not take place. The critical angle occurs when θ_2 is 90^0; making the critical angle of incidence, α, obtained from Equation 4.9 as $\sin\alpha = V_1/V_2$. Making the reasonable assumption that the critically refracted ray travels along the boundary, subsequent derivations for refraction surveys can be made possible. Critically refracted waves that travel along the boundary generate waves referred to as head waves, which depart from the boundary at the critical angle. Detecting these waves from the surface is hence possible (Redpath 1973).

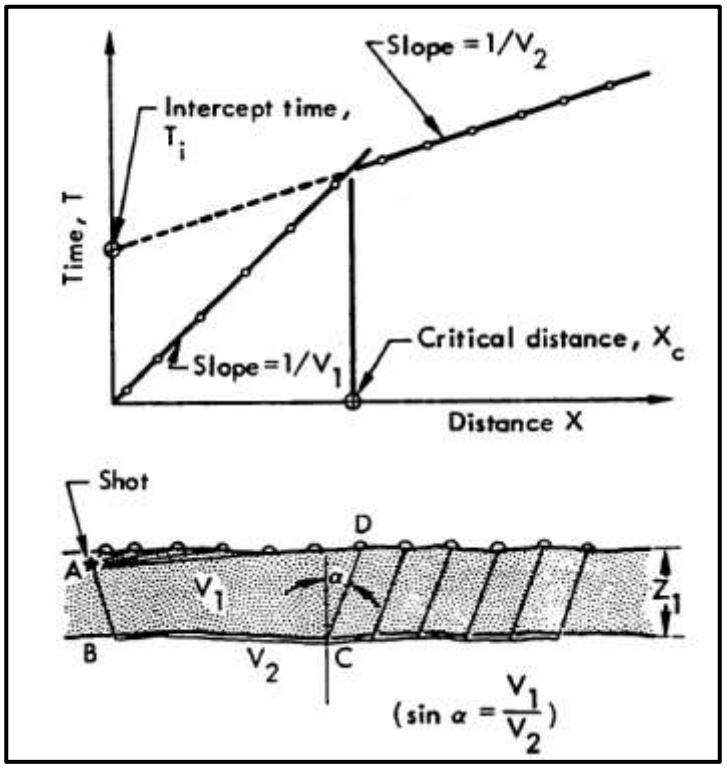

Figure 4.13 A simple, two-layer case with plane, parallel boundaries and corresponding time-distance curve. After Redpath (1973)

For a simple two-layer case of parallel boundaries shown in Figure 4.13, the arrival times of the generated disturbances against shot-detector distance can be plotted. Direct arrivals dictate the first slope of the plot and its reciprocal gives the velocity of the first layer. At distances beyond the critical distance X_C , generated waves find it easier to take a path similar to ABCD as can be seen in the Figure. This path is takes less time, making the plot beyond the critical distance rise with a gentler slope. This slope can be extended to meet the y-axis at a time called intercept time, T_i. The derivations of the equations take into account the following three important assumptions, which are deviated in few actual cases (Redpath 1973).

1. The layers are isotropic, having a consistent wave velocity;
2. ray paths are made up of straight line segments;
3. each layer has a higher velocity than the overlying layer.

Since a seismic refraction survey gives a plot similar to the one depicted in Figure 4.14, and the parameters, V_1, V_2, α and T_i can easily be read/obtained. The thickness Z_1 can be expressed as:

$$Z_1 = \frac{T_i \cdot V_1}{2\cos\alpha} \tag{4.10}$$

Alternatively, Z_1 can also be expressed as

$$Z_1 = \frac{T_i \cdot V_1 \cdot V_2}{2(V_2^2 - V_1^2)^{1/2}} \tag{4.11}$$

These simple solutions can be easily extended to the case of multiple plots using similar derivations (Redpath 1973).

4.4.2.2 Conducting Seismic Refraction Test

A research crew of applied geophysicists and seismologists was setup to conduct the seismic refraction test with the aim of determining wave velocity profile at selected sites in the city. Available and relevant geotechnical as well as geological reports were consulted; patterns were observed and sites were selected. The geotechnical reports indicate the presence of consistent loose formation in the northern and north-western part of Hawassa. The central part of the city was observed to have a relatively thin layer of welded tuff at shallow depth. The city has two

mountains (Mt. Tabor, and Mt. Alamura) in its south eastern and southern parts, respectively. According to geological reports, these regions are expected to have hard strata at shallow depths.

Site reconnaissance was carried out in three phases.

1. Phase I – preliminary visit to the city was made.
2. Phase II – available secondary data were consulted. Potential areas for conducting field tests were identified. The number and the location of the field tests took the following points into consideration.
    - Degree of Representativeness – Using the compilation of secondary data, certain patterns were attempted to be drawn and accordingly, representative locations with those common behaviors were identified.
    - Suitability of the site – Potential sites were selected to be as far away from potential disturbance as possible. In this context disturbance refers to unwanted noise generated by sources other than the excitation induced by the test. These include disturbance due to movements from cars, machineries, and even pedestrians.
    - Spatial Considerations – The amount of space that these tests require is an important consideration and a very important filtering criterion. The sites needed to be long enough to accommodate the full spread of geophysical instruments.
    - Research Interest – The location of the sites were selected having the main objective in mind; which is indicating the potential site amplification of the city. The heart of the city is expected to witness even bigger structures over the city, hence more focus goes here in comparison to the peripheries.
    - Limitations – miscellaneous limitations such as financial and time-related were taken into account. The tests were to be conducted on a limited budget and duration which directly affects the number of tests that were expected to be conducted.
3. Phase III – is the final reconnaissance. The crew had the chance to visit four selected sites before deciding to conduct the tests. Quick plans were drawn on how to sequence the sites and best manage the available space and time.

Selected Sites

Taking the criteria mentioned in the previous section into consideration, four sites (Figure 4.14) were selected to conduct the in-situ tests.

Figure 4.14 Distribution of selected sites for in-situ tests (Google Earth)

1. Site 1 (441634E, 779410N) – A wide field commonly known as "Amora-Gedel" Park (Figure 4.15) with very low disturbance. The site is located next to Mt. Tabor, near the lake and Progress International hotel, which is the first geotechnical log used for analysis.

Figure 4.15 Site 1: Amora Gedel Park Site

2. Site 2 (444835E, 782083N) – This site is located right across the northern fence of the industrial park. The field was left undeveloped as partitioned agricultural land (Figure 4.16), and was wide enough to conduct refraction test with additional geophones.

Figure 4.16 Site 2: Industrial park Site

3. Site 3 (441661E, 779855N) – The third site is located in the compound of Hawassa University, College of Agriculture, on the sport field (Figure 4.17). This is the closest open field that could be found to the geotechnical profile of Nib International Bank.

Figure 4.17 Site 3: Hawassa University, College of Agriculture Site

4. Site 4 (442878E, 779357N) - The fourth site was perhaps the most challenging one in that it was narrowest as well as central to the city, making the site prone to disturbance from city traffic. It is located at a place more commonly referred by the locals as “Meskel Adebabay” (Figure 4.18).

Figure 4.18 Site 4: Meskel Adebabay Site

Materials and procedures

The materials used in the seismic survey are as follows.

1. Hammer and strike plate

The energy source used in the test comes in form of a 10kg hammer (Figure 4.19 (a)) and a metal plate. The hammer has a wrapped electric cable with a switch that runs along its handle as shown in Figure 4.19(b).

(a) (b)

Figure 4.19 (a) Strike plate and (b) Hammer, used as energy source

2. Geophones

Geophones are the detecting units in the refraction survey. Twenty-four channels are commonly deployed with different spacing. The spacing of the geophone spread depends on the desired depth of investigation. Approximately, the length of the spread should be 4-5 times the depth of investigation. Although the desired depth in the context of this research was 30m, geophones were placed at an interval of 4m (Figure 4.20) (23 spacing's of 4 meters = 93 meters of lateral spread) owing to the fact that the energy generated will seldom reach the farthest few geophones. The fact that the soil is very loose was an additional challenge, making it even more difficult to investigate greater depths.

(a) (b)

Figure 4.20 (a) Geophones, and (b) Spreading the geophones at intervals

After deciding on the preferred alignment over which the geophones are to be spread, a measuring tape is laid. For the chosen 4-meter spacing, the first geophone is placed at 2.0m on the tape. The geophones are vertically and tightly inserted. A good tip here is trying wiggle a geophone with a finger, if it does not move, then it is tight enough. The hammer and the plate are placed at the first shot point location (0m on the tape). In Sites 1, 3 and 4, 24 geophones were used with shot locations fixed at 2m, 22m (between geophones 6 and 7), 42m, 50m and 90m. Site 2 was wide enough to use additional geophones: 36 channels, with additional shot locations at 98m, 118m and 138m.

3. Data acquisition unit

The third piece of the seismic refraction equipment ensemble is the seismograph (Figure 4.21) which serves as the data acquisition unit. The electric signals are transcribed into the seismograph which are decoded in an acquisition software installed in the field computing equipment.

Figure 4.21 Seismograph

4. Other equipment

Additional equipment include field computer/laptop which is connected to the seismograph. Once the trigger cable, geophone cable, and battery cable are connected to the seismographs, the system is powered up. The acquisition software is set up, inserting survey mode, geophone intervals and shot locations.

Other equipment (some of which have already been mentioned,) are:

- hand-held GPS apparatus,
- batteries and,
- circuit terminator.

4.4.2.3 Data Processing

The refraction data is processed using SeisImager/2D that consists of two modules: Pickwin and Plotrefra. The recorded seismic files are first loaded into Pickwin, where source and receiver locations, followed by the raw data will be displayed. Alternatives are present for first arrivals to be picked automatically or manually. Considering the aforementioned difficulties in the survey, the first arrivals were manually selected. After taking care of possible deviations and having clear sloping patterns, Plotrefra is launched. Here, a travel-time curve is displayed, where travel

times are modified and or edited should they be found misplaced. This comes down to the experience of the interpreter, who manipulates deviations so as to identify clear changes of slopes. The time-inversion is then computed using flat-surface model, on account of Hawassa's flat topography. As an output, the program will compute a layered model. After each time-inversion is done, an RMS error indicating the quality of least-square inversion is displayed. An error of less than 1.5 msec is generally acceptable (Ntuli 2017). The four profiles recorded an RMS between 1.5 – 2 msec.

4.4.2.4 Output

Models are generated using Plotrefra package of SeisImager/2D for the conducted refraction survey. Profiles of primary-wave velocity are obtained from the survey. The generated tomographic models at the end of the inversion for the four sites are given in Figure 4.22.

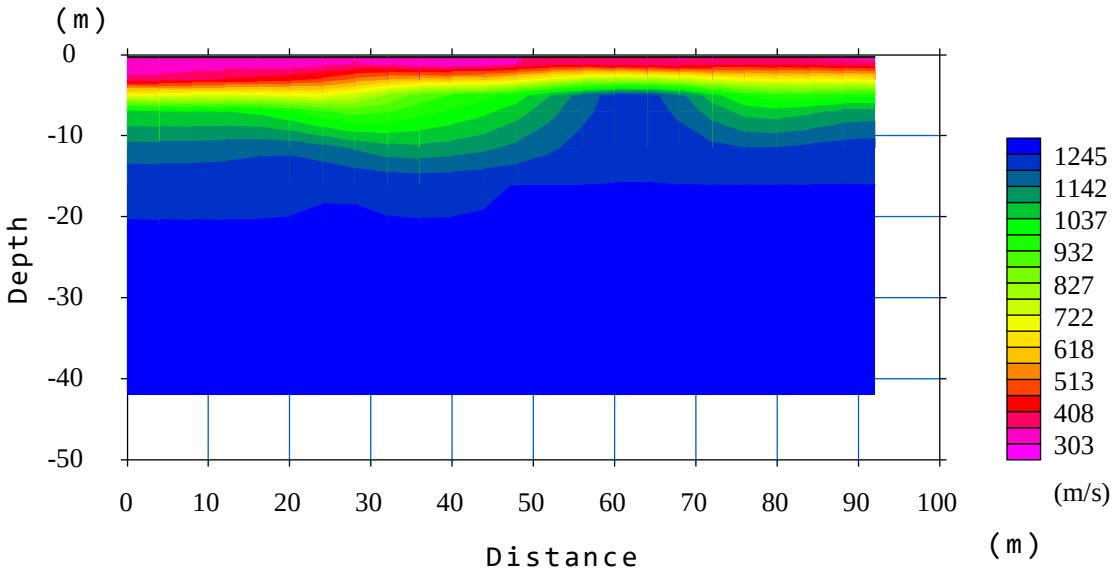

(a)

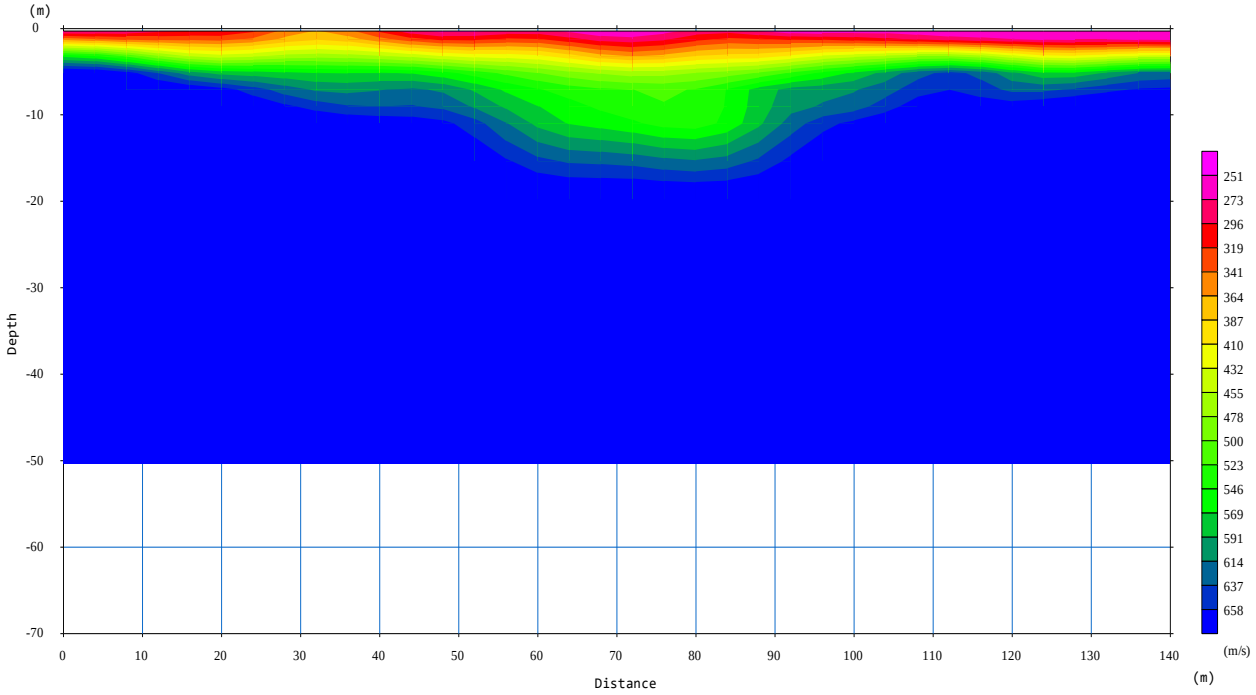
(m)
0
-10
-20
-30
-40
-50
-60
-70
Depth
0
10
20
30
40
50
60
70
80
90
100
110
120
130
140
Distance
(m)
251
273
296
319
341
364
387
410
432
455
478
500
523
546
569
591
614
637
658
(m/s)

(b)

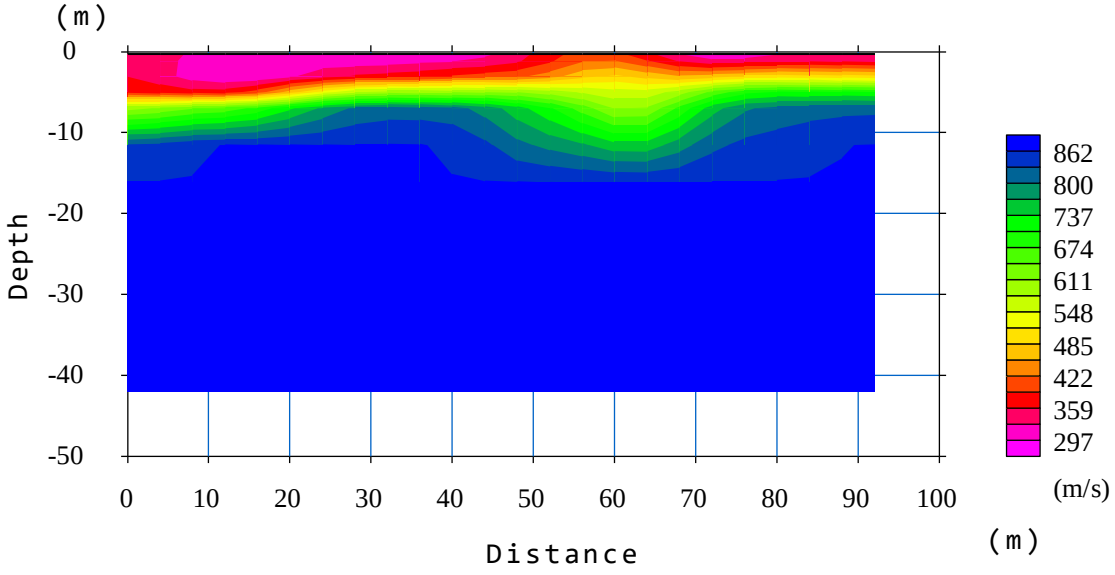
(m)
0
-10
-20
-30
-40
-50
Depth
0
10
20
30
40
50
60
70
80
90
100
Distance
(m)
862
800
737
674
611
548
485
422
359
297
(m/s)

(c)

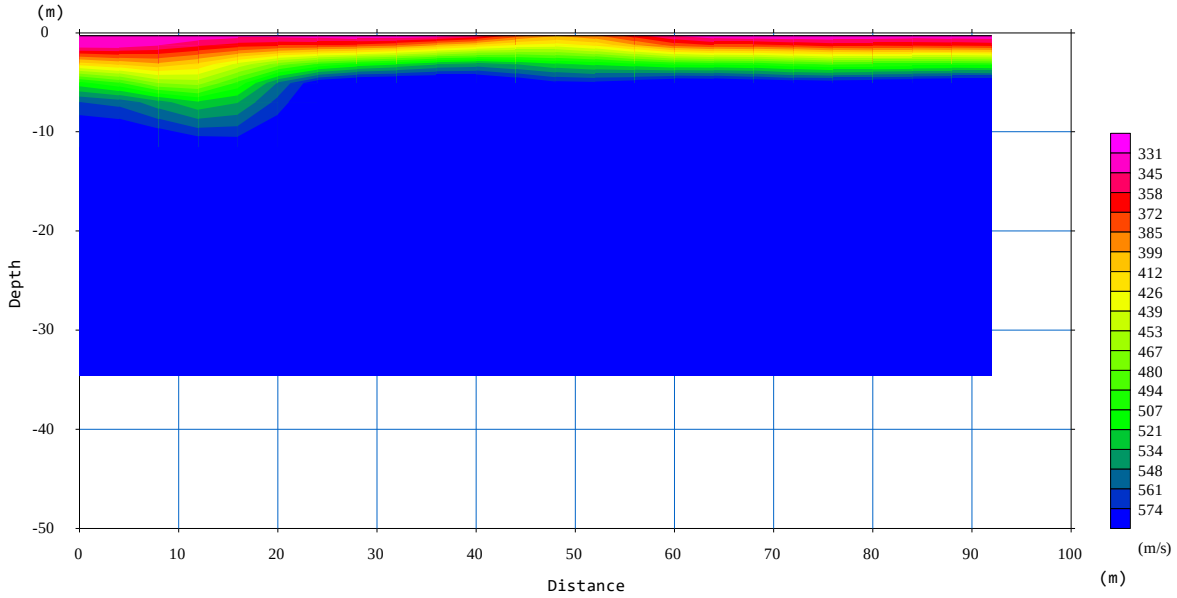

(d)

Figure 4.22 Tomographic plots showing P-wave profile of: (a) Site 1, (b) Site 2, (c) Site 3 and (d) Site 4

4.4.2.5 Vp-Vs Conversion and Extrapolation

It is worth highlighting that the measured parameter in the seismic survey is the primary velocity (P-wave). As shear wave velocity is needed to conduct ground response analysis, the P-wave velocity is easily determined using a standard relation, established in elasticity theory given by

$$\frac{V_P}{V_S} = \sqrt{\frac{2(1-\nu)}{1-2\nu}} \tag{4.12}$$

where ν is the material's Poisson's ratio.

As was discussed earlier, the sites were selected for the in-situ test such that they are as close to the selected geotechnical profiles as possible. This was beneficial in that (1) the measured profiles can be used to cross-check the secondary-data correlation outputs, and (2) the detailed soil investigations in the geotechnical investigation can help gauge seismic survey outputs. It has been observed from the compiled geotechnical reports that, with the exception of the intercalated

weathered tuff, a silty-sand profile was dominant in almost all of the selected investigation sites. In light of this, an acceptable Poisson's ratio of silty-sand was needed to be used.

Several works have been consulted to select an appropriate Poisson's ratio. Poisson's ratio in soils, among other things, is affected by homogeneity. It is a well-established fact that the softer and small the grain of a soil particulate, the higher the Poisson's ratio. Numerous studies have shown that saturated clays can have a Poisson's ratio value of as much as 0.49. In regards to sand, a range of 0.30-0.35 has been suggested by Davidovici (1985) (as cited by Essien et al. 2014), depending on the amount and type of fines. A study by Suwal and Kuwano (2012) on Poisson's ratio evaluation on silty and clayey-sands led to a similar conclusion as can be seen in Figure 4.23.

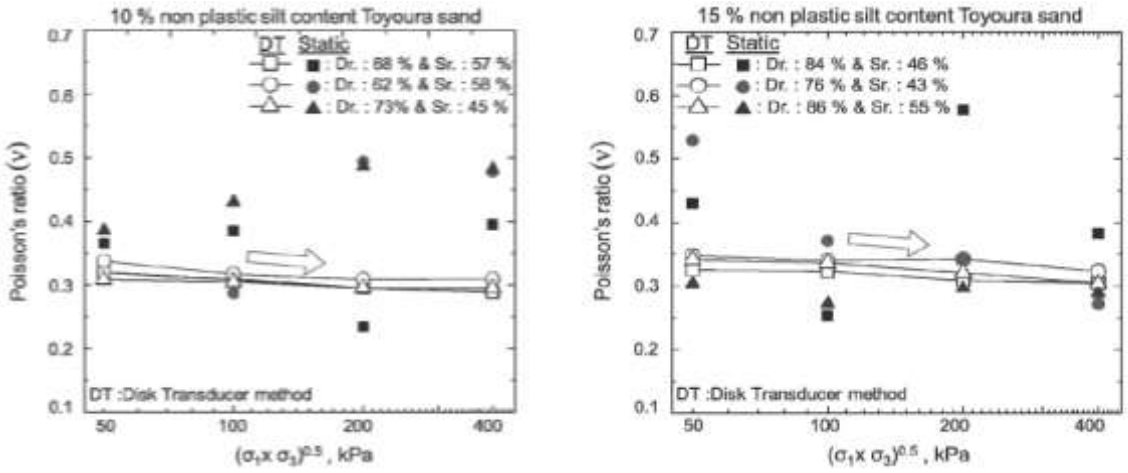

(a) (b)

Figure 4.23 Poisson's ratio for: (a) 10% non-plastic silt content, and (b) 15% non-plastic silt content in Tyoura sand (Suwal and Kuwano 2012)

Expectedly, higher ordinates can be observed for higher silt content, with the majority of the values falling within the aforementioned range. Laboratory investigations from collected geotechnical documents in this research show that the number of fines well exceeds the percentage tested by Suwal and Kuawano (being around 40%), with the vast majority described as silt. Taking a value near the upper limit of Davidovici's 0.3-0.35 would be sensible, considering the high amount of fines relative to the study that was just cited. In consequence, a Poisson's ratio of 0.35 was used in relating primary and secondary wave velocities.

One-dimensional P-wave velocity profiles have been picked up at locations of 0m, 70m, 15m and 15m for sites 1, 2 3 and 4 respectively (Table 4.9). These locations were in such a way that they are the most critical (in that they had loose formations with greater thickness) and detailed (had greater investigation depths). They are extrapolated as per the discussion under Section 4.3.2 and the results are presented in Table 4.10.

Table 4.9 Selected 1-D P-wave profiles and their correlation to S-waves

	Site 1		**Site 2**		**Site 3**		**Site 4**	
Depth (m)	V_P (m/s)	V_S (m/s)	V_P (m/s)	V_S (m/s)	V_P (m/s)	V_S (m/s)	V_P (m/s)	V_S (m/s)
0	-	-	-	-	-	-	-	-
1	290	139	251	121	297	143	331	159
2	290	139	273	131	297	143	345	166
3	290	139	319	153	297	143	372	179
4	408	196	341	164	318	153	399	192
5	408	196	364	175	338	163	412	198
6	670	322	387	186	359	172	439	211
7	670	322	410	197	422	203	453	218
8	827	397	432	208	485	233	480	231
9	827	397	455	219	611	294	521	250
10	827	397	478	230	674	324	548	263
11	1037	498	500	240	737	354	574	276
12	1037	498	500	240	800	384		
13	1087	522	523	251	862	414		
14	1087	522	546	262				
15	1087	522	569	273				
16	1142	549	591	284				
17	1142	549	614	295				
18	1168	561	658	316				
19	1168	561						
20	1168	561						

Table 4.10 Extrapolated shear-wave velocities of the four profiles generated from refraction survey

Profile 1*		**Profile 2**		**Profile 3**		**Profile 4**	
Depth(m)	V_S (m/s)	Depth(m)	V_S (m/s)	Depth(m)	V_S (m/s)	Depth(m)	V_S (m/s)
0-3	139	0-1	121	0-3	143	0-1	159
3-5	196	-2	131	3-4	153	-2	166
5-7	322	-3	153	-5	163	-3	179
7-10	397	-4	167	-6	172	-4	192
10-12	498	-5	175	-7	203	-5	198
12-15	522	-6	186	-8	233	-6	211
15-17	549	-7	197	-9	294	-7	218
17-20	561	-8	208	-10	324	-8	231
		-9	219	-11	354	-9	250
		-10	230	-12	384	-10	263
		10-12	240	-13	414	-11	276
		-13	251	-14	278	-12	254
		-14	262	-15	250	-13	256
		-15	273	-16	270	-14	288
		-16	284	-17	270	-15	258
		-17	295	-18	279	15-17	279
		-18	316	-19	290	-18	289
		-19	267	-20	295	-19	300
		-20	271	-21	307	-20	305
		-21	282	-22	306	-21	318
		-22	281	-23	317	-22	317
		-23	293	-24	324	-23	328
		-24	300	-25	330	-24	335
		-25	305	-26	338	-25	340
		-26	313	-27	336	-26	349
		-27	310	-28	347	-27	347
		-28	320	-29	342	-28	359
		-29	315	-30	346	-29	354
		-30	318			-30	358

*The extrapolation of Profile 1 has been limited to 20m as reports point to the presence of hard rock at that location

4.4.3 Electrical Resistivity

Electrical resistivity is another popular geophysical method that uses the fundamental concept of electricity to characterize the ground from the surface. The fundamental concept is that the method involves injecting electric current into the ground through a pair of electrodes, and measuring the resulting voltage, so as to determine the resistivity. Lateral extent of electrodes is varied depending on one's interest in resistivity variation with depth.

4.4.3.1 Theoretical Background

Electrical resistivity method applies one of physics' most fundamental laws of electricity: Ohm's law. Four electrodes are commonly used while conducting: two current electrodes and two potential electrodes in different arrays. An electric current is injected into the ground through the current electrodes, and the potential difference is measured using the potential electrodes. Ohm's law relates resistance $R[\Omega]$ with voltage V and current I as $R = V / I$. Although the resistance describes the extent of a material's impedance for current flow, it is not a material property. The parameter used to describe this particular aspect of material property is the resistivity $\rho[\Omega m]$, and it is closely related to resistance as $\rho = RA / L$. The inverse of resistivity, electrical conductivity (σ), is a measure of the ability of a material to sustain/conduct electric current flow (Everett 2013). The previously described Ohm's law, which applies to a simple resistive circuit, can extendedly be expressed as

$$\mathbf{E} = \frac{\mathbf{J}}{\sigma} = \rho \mathbf{J} \tag{4.13}$$

where E is the electric field and J is the current density.

To define current density, one has to assume a hypothetical whole-space of uniform resistivity/conductivity as shown in Figure 4.24. If an electric current is injected at an assumed origin, it will spread out in all three dimensions. The current density at a point in the vicinity of the origin is

$$\mathbf{J} = \frac{I \cdot \hat{\mathbf{r}}}{4\pi r^2}, \tag{4.14}$$

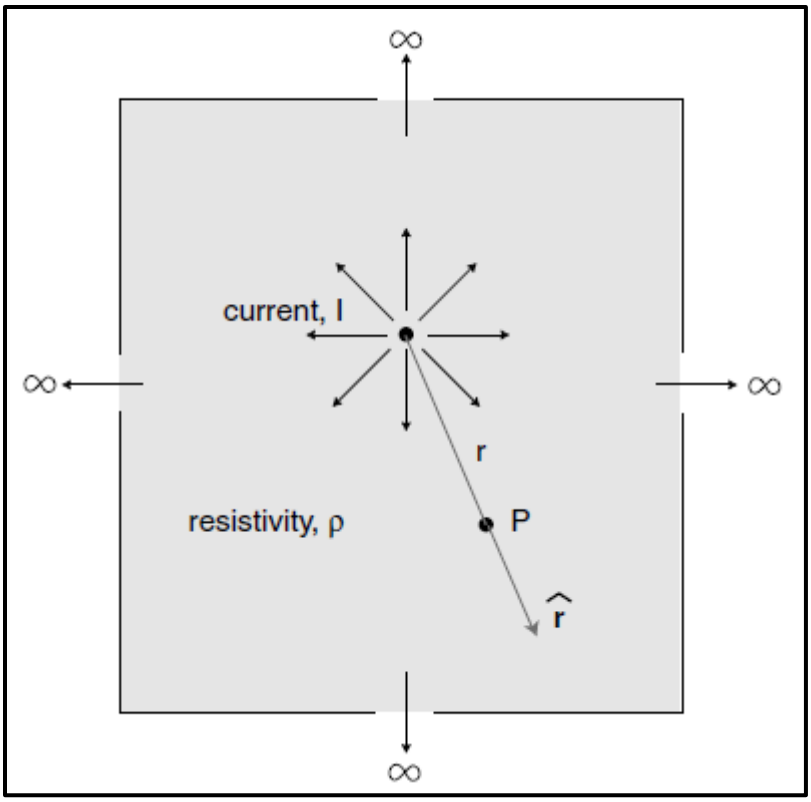

Figure 4.24 Current injection into a wholespace of uniform resistivity, ρ . After Everett (2013)

where the nominator, $I \cdot \hat{\mathbf{r}}$, describes the magnitude and the direction, while the denominator describes the spherical area (Everett 2013).

In this context, the electric field does work (voltage) by moving a charge from infinity to point. This can be expressed by a line integral along the direction $\hat{\mathbf{r}}$ as

$$V = \int_{r}^{\infty} \mathbf{E} \cdot d\mathrm{r} = \int_{r}^{\infty} \frac{I \cdot \rho}{4\pi r^2} dr = \frac{I \cdot \rho}{4\pi r}. \tag{4.15}$$

For electrical resistivity test, the aforementioned whole-space is limited to a half-space, hence every term that involves a spherical area needs to be divided by two.

The array most convenient for depth penetration is the nested Schlumberger array, in which four electrodes are deployed collinearly: current electrodes A and B on the outside and potential electrodes P and Q on the inside.

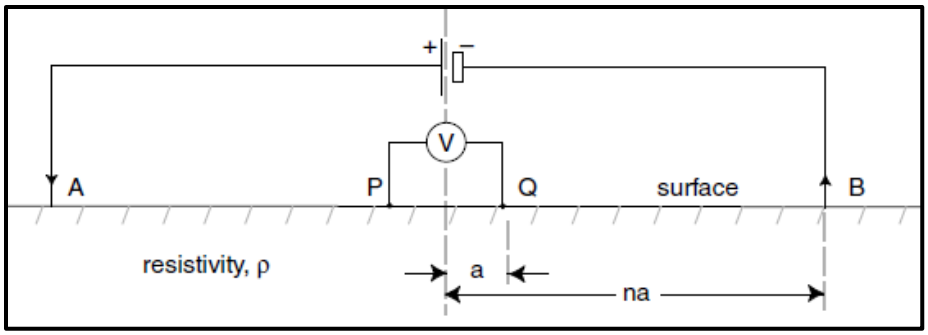

Figure 4.25 Schlumberger configuration

For the Schlumberger configuration, the potential difference across P and Q is

$$V_{PQ} = V_P - V_Q = \frac{I \cdot \rho}{2\pi}\left[\frac{1}{r_{AP}} - \frac{1}{r_{PB}} - \frac{1}{r_{AQ}} + \frac{1}{r_{QB}}\right] \tag{4.16}$$

The resistivity that can be obtained by rearranging this equation is not true resistivity but the apparent one. This is due to the fact that a homogeneous half-space had to be assumed to make the formulations.

Materials and Procedures

Principally, electrical resistivity method involves two devices, a terrameter and electrodes. The resistivity imaging system used in the study is a SARIS terrameter that has an in-built ammeter and a voltmeter.

Figure 4.26 Terrameter

Four electrodes were used, two potential and two current electrodes. Additional materials include electric wires, measuring tapes and hammers for nailing the electrodes.

It was earlier noted that available space had to be one consideration to make in selecting potential sites for refraction survey; and this is particularly critical for electrical sounding, as outer electrode spacing can go as long as 300 meters. The resistivity tests were conducted simultaneously with the refraction survey at the same sites.

Having precautions in mind, as any contact with a live electric circuit could be damaging, the procedure is pretty straightforward. A measuring tape is first laid on the ground from an assumed center. A PQ/2 distance of 0.5m is first fixed and the two potential electrodes connected to the terrameter were hammered into the ground. The first two current electrodes are laid collinearly at an AB/2 distance of 1.5m, and readings are taken. AB/2 distance is extended progressively to 2.1m, 3.0m, 4.2m, 6.0m, 9.0m, 13.5m, 20.0m, 30.0m, 45.0m, 66.0m, 100.0m and 150.0m in both directions and attainable depth range is increased accordingly. As a large ratio of AB/PQ makes a potential drop across PQ too small to be measured, PQ had to be increased to 6.0m at an overlap AB/2 of 20m and 30m.

4.4.3.2 Output

Results are plotted on an apparent resistivity against some geometric factor (such as AB/2) graphs. The recorded data was processed using the software IPI2WIN and the obtained curves are presented in Figure 4.27. Site-2 (Industrial Park site) was convenient enough to make more than one vertical electrical resistivity profile, hence making a 2-D section possible (Appendix A).

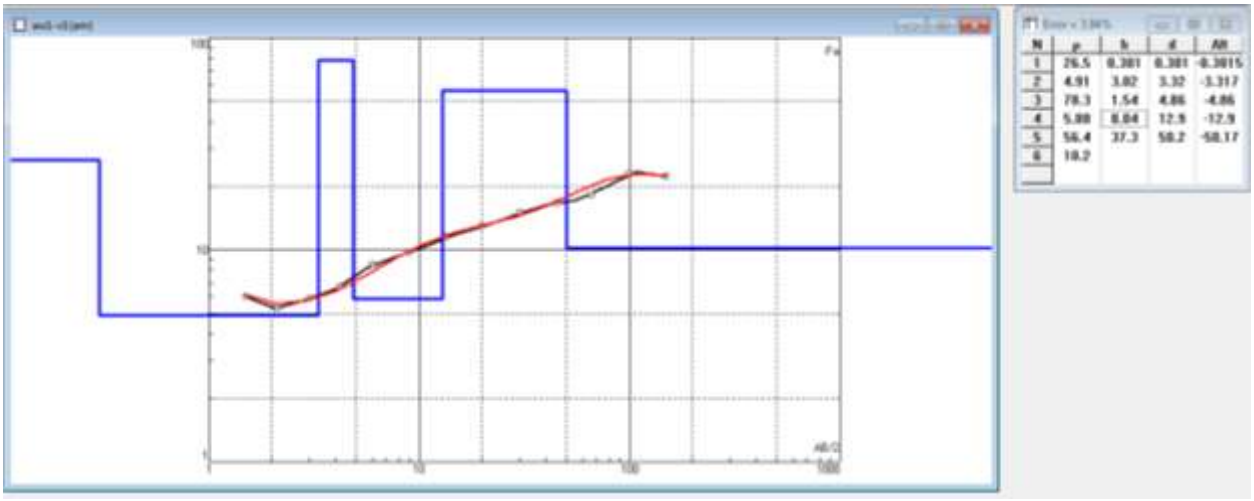
N ρ h d Alt
1 26.5 0.381 0.381 -0.3815
2 4.91 3.82 3.32 -3.317
3 78.3 1.54 4.86 -4.86
4 5.88 8.04 12.5 -12.9
5 56.4 37.3 58.2 -58.17
6 18.2

(a)

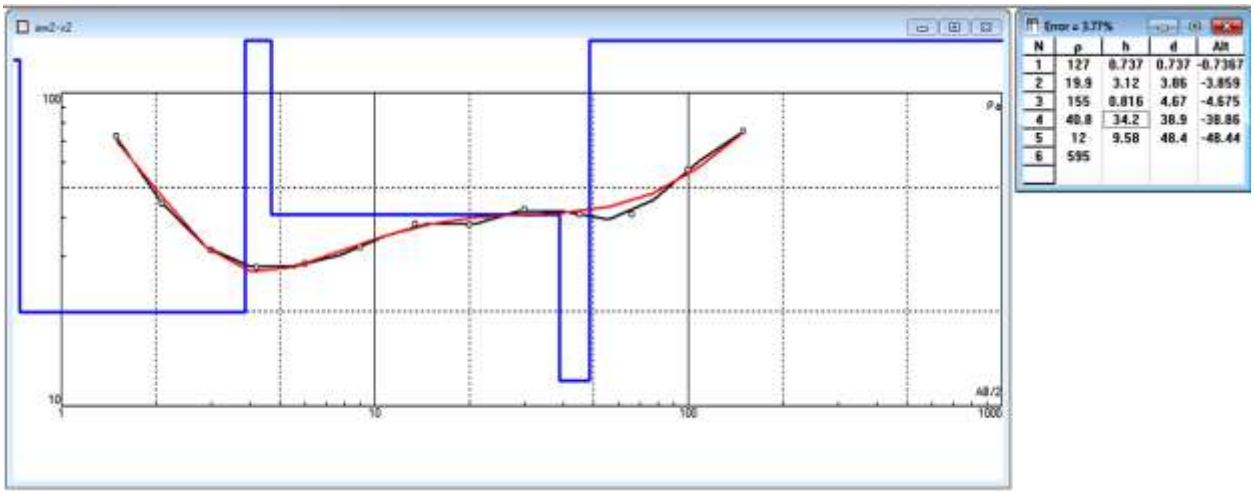
N ρ h d Alt
1 127 0.737 0.737 -0.7367
2 19.9 3.12 3.86 -3.859
3 155 0.816 4.67 -4.675
4 40.8 34.2 38.9 -38.86
5 12 9.58 48.4 -48.44
6 595

(b)

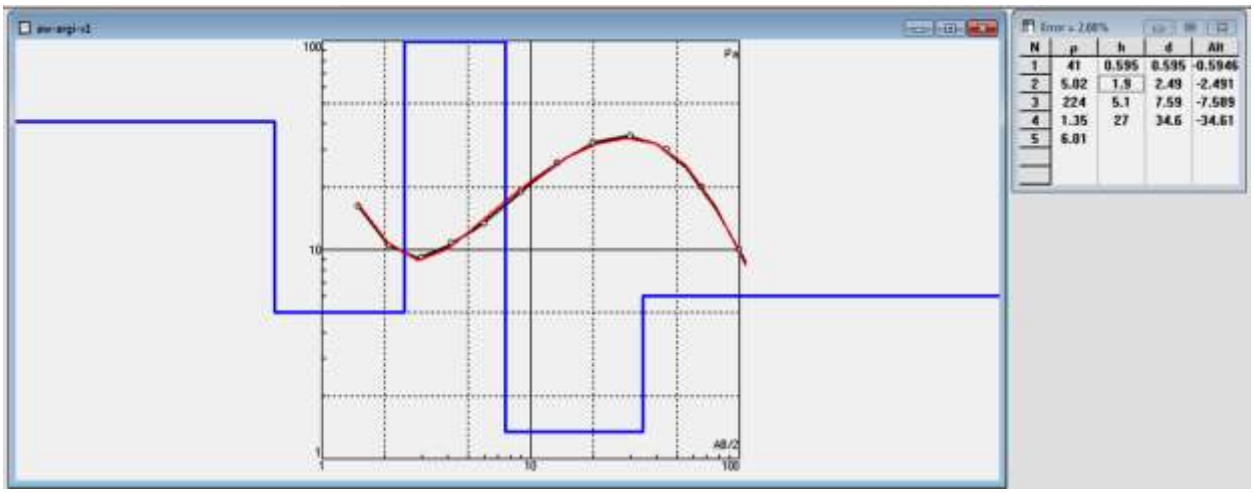

(c)

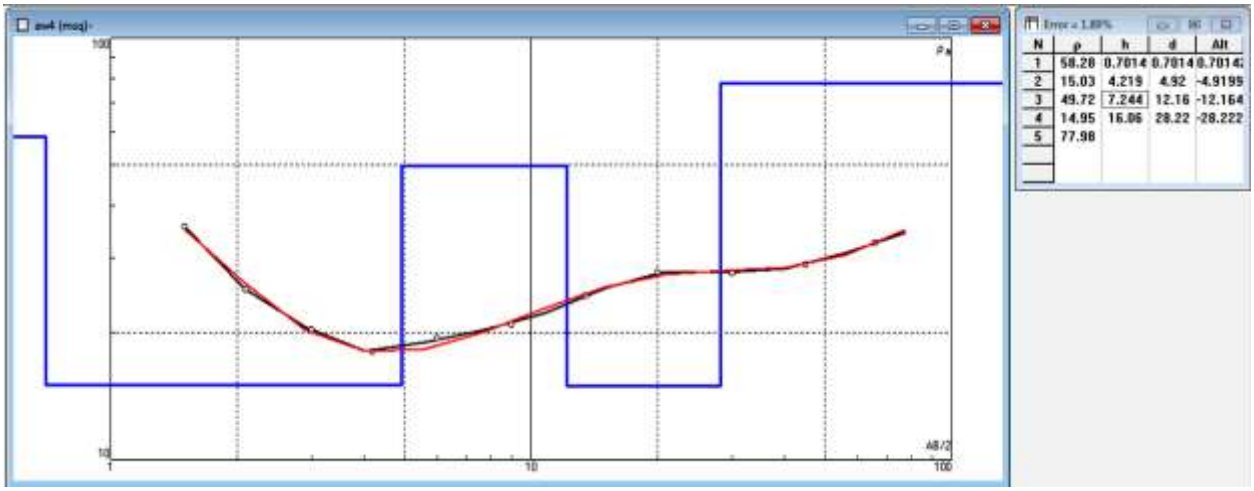

(d)

Figure 4.27 Tomographic plots showing P-wave profile of: (a) Site 1, (b) Site 2 [1 of 2], (c) Site 3 and (d) Site 4

`

CHAPTER FIVE

ANALYSIS AND DISCUSSION

Analyzing the geological and geomorphological setup of an area of interest gives a valuable input for decision as to what type of analysis is appropriate. It is widely accepted that 1D analysis is preferred for flat terrains with nearly uniform and horizontal geological stratification (Kramer 1996). Haile (1996) drew comparisons between the outputs of 1D and 2D GRA. It was observed that at places where topographic settings change abruptly within fair distances, such as valleys, 1D analysis may not be the ideal approach as a site response model. For an assumed trapezoidal valley of a certain depth, basin effects have been found insignificant for a width to depth ratio greater than 4, making 1D approximation of 2D analyses justified. It was pointed out in Chapter 2 that with the exception of the two hills in the south, the vast majority of the city along with the most critical structures rests on a lacustrine deposit of flat terrain. For such consistently flat topography, 1D analysis is found fitting. Furthermore, based on observations of fairly uniform geological formation and anticipated shaking intensity, the equivalent-linear method is employed in this study.

Studies have shown that most of the EQL programs that are currently available employ the approach that is discussed under Section 3.2.2; they use the same basic computational procedure, as demonstrated by analyses software such as DEEPSOIL and STRATA yielding consistent results with the pioneering EQL program SHAKE (Hutabarat 2016; Kottke & Rathje 2009; Schnabel et al. 1972).

DEEPSOIL v 6.1 (Hashash et al. 2016) is selected for this study and acquired with an official permission from the University of Illinois at Urbana-Champaign website.

5.1 Equivalent Linear Analysis Procedure

The Kelvin-Voigt solid shear stress relation in Equation 3.1 can be used for formulating the wave equation:

$$\rho \frac{\partial^2 u}{dt^2} = G \frac{\partial^2 u}{dz^2} + \eta \frac{\partial^3 u}{\partial z^2 \partial t} \tag{5.1}$$

`

where ρ is density and u is the displacement function. The solution u to this one-dimensional wave equation of single wave frequency ω, as a function of depth z and time t is

$$u(z,t) = A\exp[i(\omega t + k^* z)] + B\exp[i(\omega t - k^* z)] \tag{5.2}$$

In the equation, the alternating signs of z for the corresponding amplitude coefficients A and B indicate upward and downward propagating waves; k^* is a complex wave number which is defined in terms of a complex shear-wave velocity as ω / v_S^*, and likewise v_S^* is defined in terms of a complex shear modulus G*, which is a function of damping ratio, D:

$$G^* = G(1 + i2D) \tag{5.3}$$

This formulation for a single layer can be extended to a layered system of different parameters (Figure 5.1). The transfer function between two layers, which is the ratio of amplitudes of corresponding displacement, velocity or acceleration, can be obtained from,

$$TF_{(m,n)}(\omega) = \frac{A_m + B_m}{A_n + B_n} \tag{5.4}$$

where A_m, B_m, A_n and B_n are wave amplitudes at respective layers.

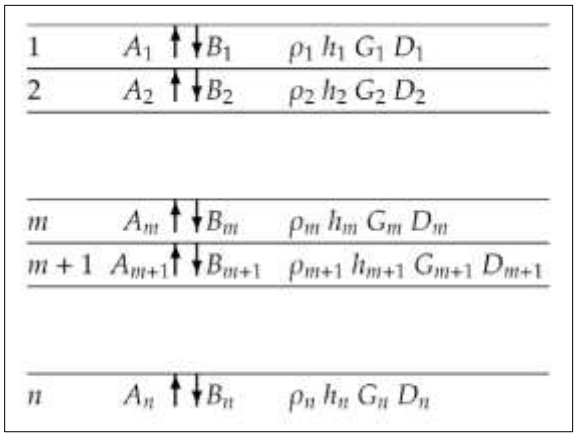

Figure 5.1. Multiple-layered system of different amplitudes, thicknesses, densities, shear moduli and damping ratio. After Kottke & Rathje 2009.

`

In other words, if the transfer function between two layers is obtained, the response at the layer of interest can be found by multiplying the Fourier amplitude spectrum (as operations are done in frequency domain) and the input rock motion.

DEEPSOIL employs the iterative procedure that was discussed in Section 3.2.2 in defining soil properties (shear moduli and damping ratios) much like the pioneering program SHAKE (Hashash et al. 2016). The EQL approach defines modulus reduction and damping factors using discrete points, the curves of which can be found in-built within the software. Depending on the preference of the user, it is alternatively possible to manually define curves. Modulus reduction and damping curves proposed by Seed at al. (1986) were used for the silty-sand dominated formations. At one instance in which clay was encountered, the curve by Vucetic and Dobry (1991) were applied.

5.2 Consideration of Ignimbrite

As was mentioned several times within the discussions in Chapter 4, an ignimbrite horizon was observed at various locations in the city at shallow depths. Geotechnical investigation reports showed the presence of a thin layer (1.4 – 4.0m) of the welded-tuff/ignimbrite at shallow depths (<7m). This thin layer was not apparent in north-eastern parts of the city. The borehole summaries from the selected geotechnical investigation reports (Profiles 1, 3 and 4) presented in Table 4.8 show that there are missing SPT records at certain depths; and these locations are further described qualitatively as formations of ignimbrite.

Seismic refraction survey operates with the assumption that shear-wave velocity increases with depth, and the inversion that was carried out did not detect the presence of these thin welded-tuffs. However, resistivity tests were conducted to supplement refraction surveys, and expectedly, abrupt changes in resistivity were observed at locations where the ignimbrite layers were anticipated. Having taken these indications into consideration, the output from the refraction and resistivity surveys were merged with geotechnical reports in developing their respective models.

`

Choi (2008) proposed a semi-logarithmic relationship between the small-strain shear modulus, $G_{\max}$ and the density, γ_t for welded tuff. The relationship is expressed as:

$$G_{\max} = 13.13 \exp[0.00307\gamma_t] \tag{5.5}$$

where $G_{\max}$ is in MPa, and γ_t is in kg/m^3. In the absence of directly measured values, Choi's relation was used directly to estimate the shear-wave velocity of the welded tuff. Table 5.1 summarizes welded-tuff moduli used to model the profiles of primary and secondary data for analysis.

Table 5.1 Welded-tuff parameters used in soil models from geophysical methods

Profiles	Depth range (thickness)	Shear-wave velocity (m/s)
Profile 1	3.3-6.4m (3.1m)	3231
Profile 3	5.0-6.4m (1.4m)	2617
Profile 4	3-4.5m (1.5m)	2616
	4.5-7.0m (2.5m)	3379

The shear-wave velocities from Choi's recommendation appear exaggerated, as their qualitative descriptions include terms like "weathered, slightly weathered" and even "fractured". Comparing these numbers with recommended shear-wave velocities for intact rocks from building codes (NEHRP >760 m/s, ES EN >800m/s for intact rocks), they do appear larger than what is anticipated. It will be shown later that separate analyses have been run with reduced shear-wave velocities of 800 m/s. In addition, the effect of the ignimbrite on the overall response has also been studied by removing the ignimbrite layer. The overall effect of varying the values was found negligible.

Profile 2, which is believed to represent the north-eastern part of the city, does not exhibit the ignimbrite layer (from geotechnical reports and refraction surveys). Although resistivity output indicates the presence of a stiff formation a depth of approximately 5 m below the surface, it is believed that this could be attributed to a thin highly-dense layer of silty sand among a consistently uniform layer of similar material. This is confirmed by the observation of 30 boreholes drilled for Hawassa's industrial park project in this area, where some SPT profiles indicated higher SPT values at such depths, despite maintaining uniformity. Accordingly, the

`

ignimbrite layer has not been included in analyzing Profile 2 for both of the Industrial Park profiles (geotechnical and geophysical profiles).

5.3 Analysis Results

The shear-wave profiles given in Tables 4.8 and 4.10 are updated with the ignimbrite data in Table 5.1 in the subsequent analyses. Based on these updated V_S profiles, the $V_{S,30}$ is evaluated for each case in accordance with the pertinent code provisions. The average $V_{S,30}$ values for all sites have been found to fall within the range of 215 and 300 m/sec so that the corresponding site class for all profiles is 'D' and 'C', according to NEHRP 2015 and ES EN 1998:2015, respectively. It is to be noted that for the purpose of site classification, a shear-wave velocity of 760 m/sec and 800 m/sec is assigned for all rock layers including the ignimbrite in accordance with the respective codes.

5.3.1 Summary of Profiles

5.3.1.1 Summary of PGA Profiles

A summary of PGA profiles obtained from analyses for the sites modeled from geotechnical investigations and refraction & resistivity surveys are summarized in Figure 5.2 and Figure 5.3, respectively.

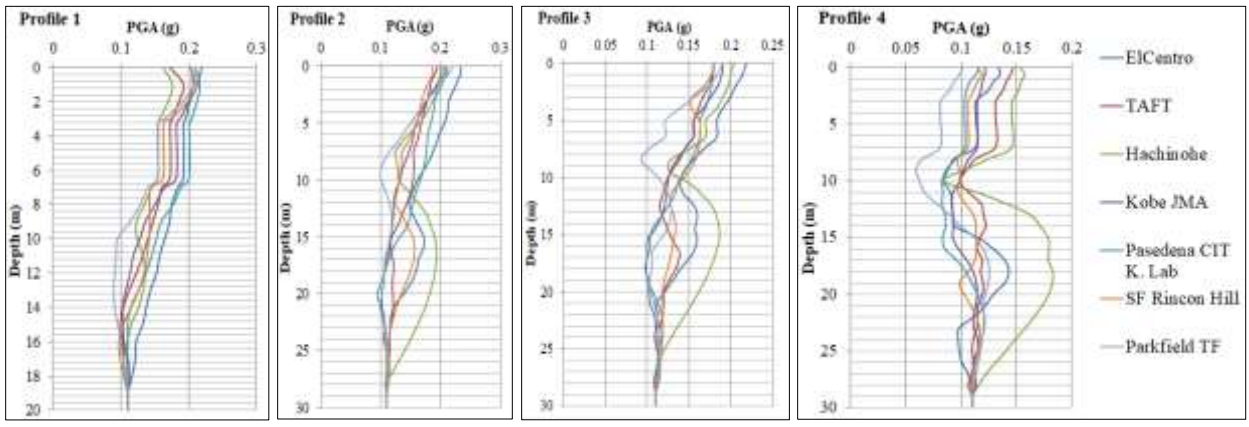

Figure 5.2 PGA profiles of the four sites modeled from geotechnical investigation reports

`

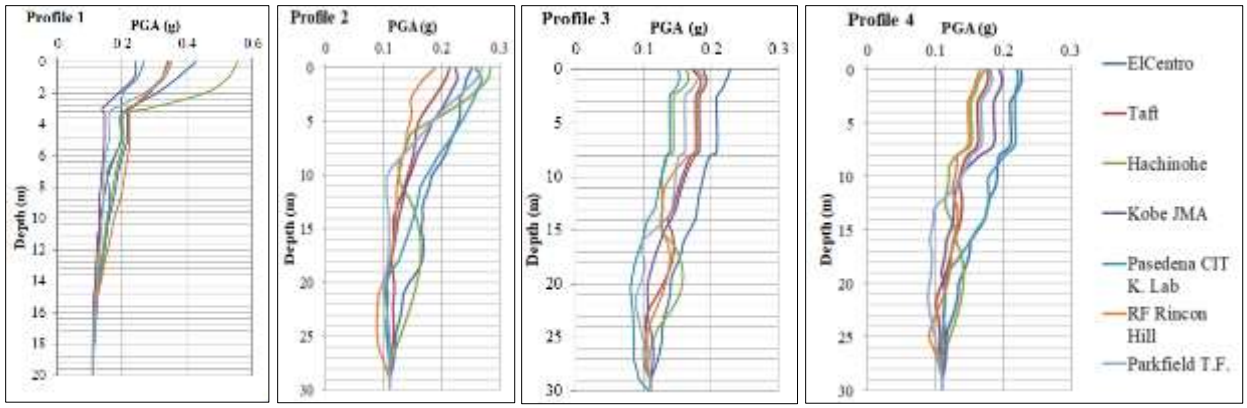

Figure 5.3 PGA profiles of the four sites modeled from refraction and resistivity surveys

It can be observed from the plots that Hawassa's PGA of 0.11g was consistently amplified going upwards, with the majority of the surface PGA's falling within the range 0.15-0.23g. Mentionable extremes are Profile 4 (SPEDM office building site) with a low PGA range of 0.1-0.15g, and Profile 1 from refraction (Amora Gedel Park) with sharp deflections above the depth of 2 meters with PGA's reaching up to around 0.6g.

Average predictions from geotechnical and seismic refractions are more or less consistent, with an exception being the corresponding outputs of Profile 1. While Profile 3 and Profile 2 showed identical PGA ranges from the two surveys, geotechnical survey of Profile 4 generally exhibits lower predictions as compared with those from geophysical survey.

The impact of the ignimbrite can be seen clearly from the plots, with its relatively high shear-wave velocity (and hence, high stiffness) resulting in the PGA remaining constant going through these profiles. Theoretically, the stiffer the material, the more it tends to experience a rigid-body motion. This results in a zero relative displacement between the material's base and its top, while maintaining the acceleration of the base all the way up to its top. This constant PGA can be observed in Profiles 1, 3 and 4 for both geotechnical and geophysical profiles (Figures 5.2 and 5.3).

`

5.3.1.2 Summary of Displacement Profiles

Peak displacement profiles are presented in Figures 5.4 and 5.5 as follows.

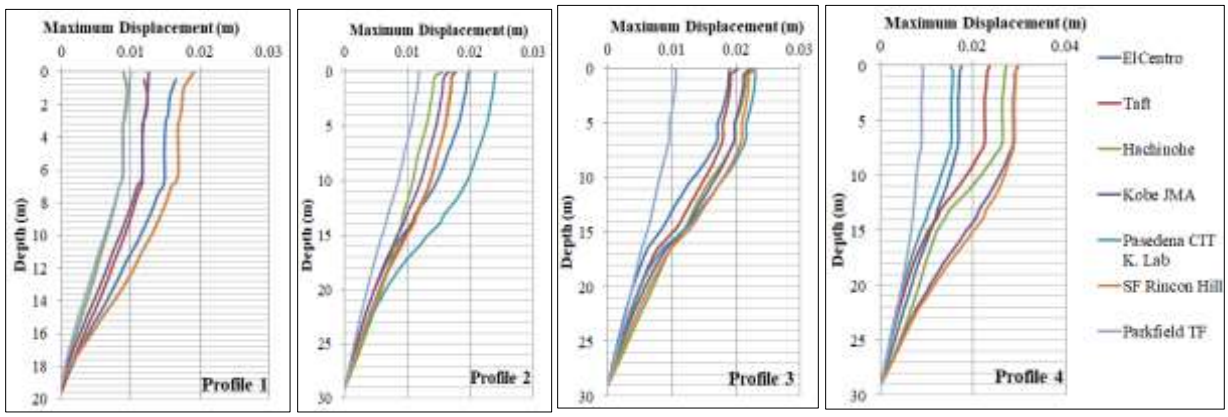

Figure 5.4 Peak displacement profiles of the four sites modeled from geotechnical investigation reports

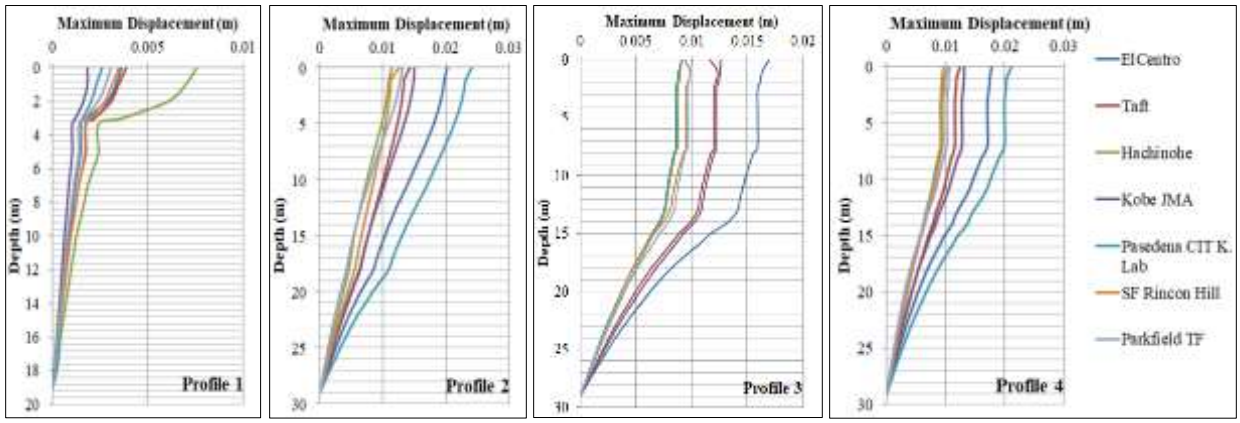

Figure 5.5 Peak Displacement profiles of the four sites modeled from refraction and resistivity surveys

The plots in Figure 5.5 show a maximum peak displacement was predicted at Profile 4 from the geotechnical model, with a peak displacement at the surface close to 3 cm. In the case of Profile 2, where both the geotechnical as well as geophysical surveys have predicted a value of approximately 2.5 cm, also stood out as having relatively large peak displacements. Consistent with the trend observed for the PGA profiles in the previous section, the ignimbrite layer for Profiles 1, 3 and 4 (in both methodologies) indicated no relative displacement as a wave

`

propagates through it. This can be noted from the plot, as in the case for the PGA, the displacement magnitude is constant within those stiff layers.

5.3.1.3 Summary of Strain Profiles

Analyzing the strain profile of a GRA output is very crucial in that it contains a very good indicator regarding the appropriateness and reliability of the method of analysis. It is a well-established fact that non-linear method of analysis is appropriate for strains exceeding a certain strain threshold, with studies showing EQL analysis results to be satisfactory up to a strain threshold in the region of 0.5% (Udaka 1983 as cited by Haile 1996). Other studies (Kaklamanos et al. 2013) also concur with this, concluding that non-linear analysis is necessary beyond a strain level of 0.4%, with a range of shear strain between 0.1-0.4% being labeled "an EQL transition zone". The strain profiles obtained for all sites are presented Figure 5.6.

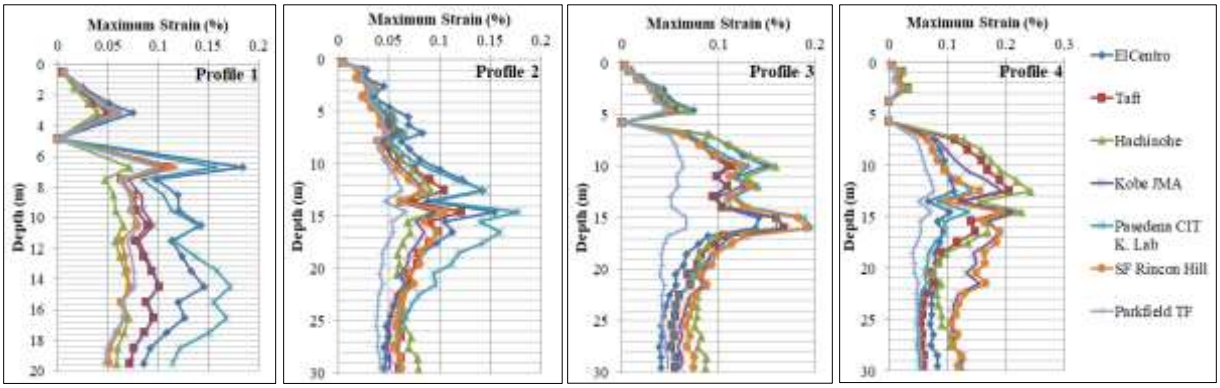

Figure 5.6 Strain profiles of the four sites modeled from geotechnical investigation reports

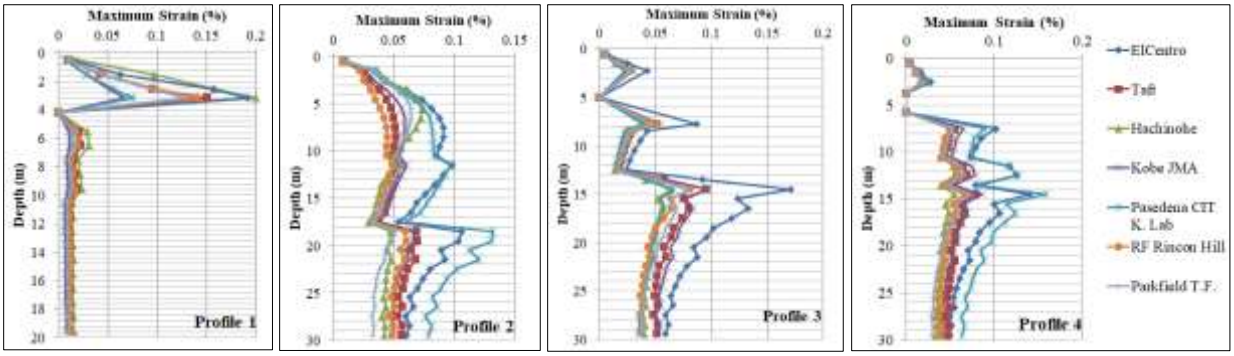

Figure 5.7 Strain profiles of the four sites modeled from refraction and resistivity surveys

`

One can observe from the plots that the majority of the peak strains fall within the range of 0.1-0.2% and seldom (one response out of 56 analyses) exceed the strain level of 0.2%. It was described earlier in this chapter that one of the reasons for selecting EQL analysis was due to the anticipated shaking intensity. Earthquakes expected to occur in the region will not be so strong as to induce large strains that require truly non-linear analysis. The observed strain level supports this hypothesis, with a maximum observed strain of almost 0.2% partly validating the use of the EQL site response model. Another observation from the plots is that the strains are zero at depths where there is ignimbrite, owing to the high stiffness.

5.3.2 Response Spectral Analysis

From the eight geotechnical and geophysical profiles, four have been further pursued having taken investigation depth, level of detail and observable trend into consideration. Profiles 1 and 3 from geotechnical investigation reports and Profiles 2 and 4 from geophysical methods are used for drawing interpretations. A customary structural damping of 5% is employed in all of the subsequent response spectral analyses with reinforced concrete structures being the most widely used in urban construction.

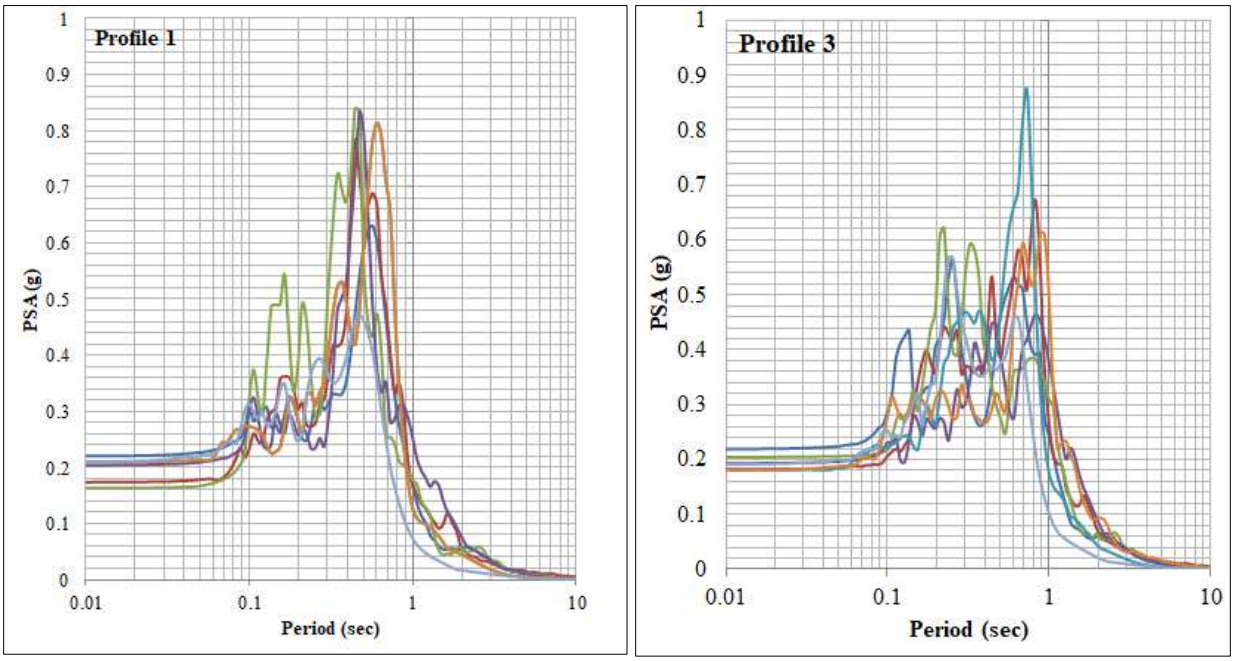

(a)

`

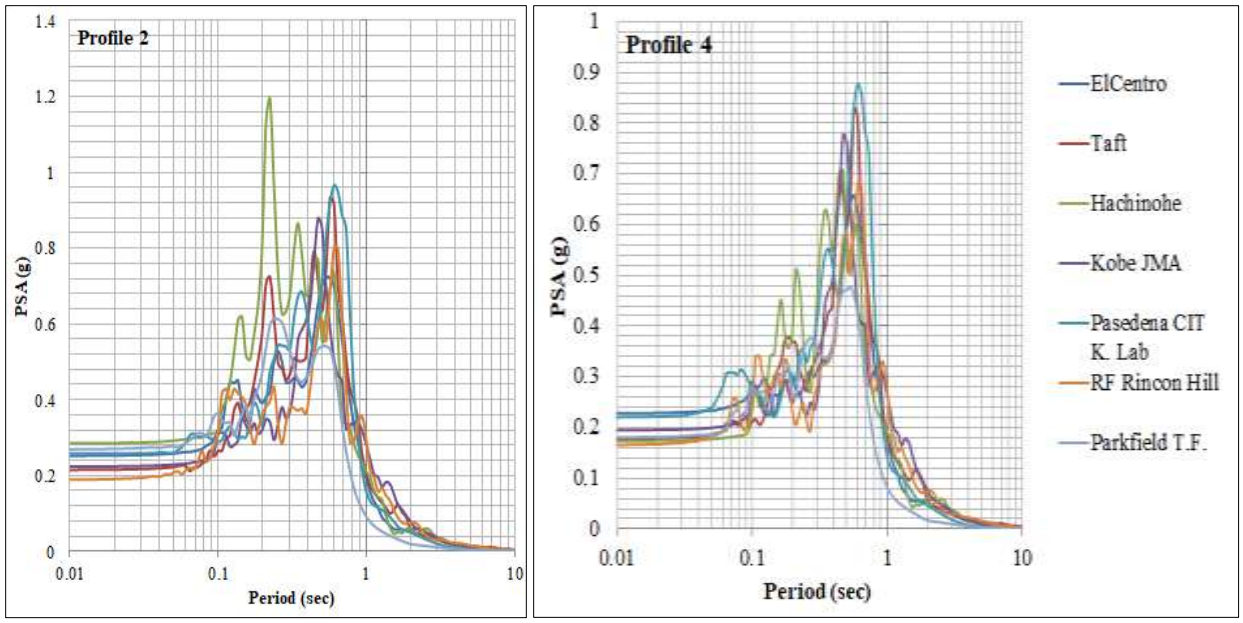

(b)

Figure 5.8 A summary of response spectra at the ground surface for the four selected profiles: (a) Profiles 1 and 3 from geotechnical investigation reports, and (b) Profiles 2 and 4 from refraction and resistivity surveys

Consistent with what was noted on PGA profiles; significant amplification is also observed in the spectral curves. Response spectra of the seven input motions analyzed for Profile 1 showed a predominant period in the range of 0.4 - 0.7 sec, with a spectral acceleration reaching up to around 0.84g at the ground surface (Figure 5.8 (a)). Also, appreciable, but lower peak values for periods within the range of 0.1 to 0.3 sec are noted. Hachinohe record uniquely peaked when run through Profile 2 (Fig. 5.8 (b), exhibiting a PSA of 1.2g at 0.2 sec. The PSA ordinates of the other motions for Profile 2 gradually increase as one goes to the right from 0.3 sec, with overlapping peaks reaching 0.95g at around 0.6 sec. Profile 3 showed a similar trend with Profile 2 whereby spectral values of around 0.5g are observed in the period range of 0.2 - 1 sec. Pasedena CIT K. record uniquely peaked to 0.88g at 0.7sec for this profile. Profile 4, like Profile 1, had multiple motions peaking at around 0.5 - 0.6 sec, with Pasedena CIT K. record and Taft record, having PSA ordinates of 0.88g and 0.82g, respectively, around that period.

Having combined response spectral curves from geotechnical and geophysical modeling, mean spectral curves have been plotted for each Profile as shown in Figure 5.9.

`

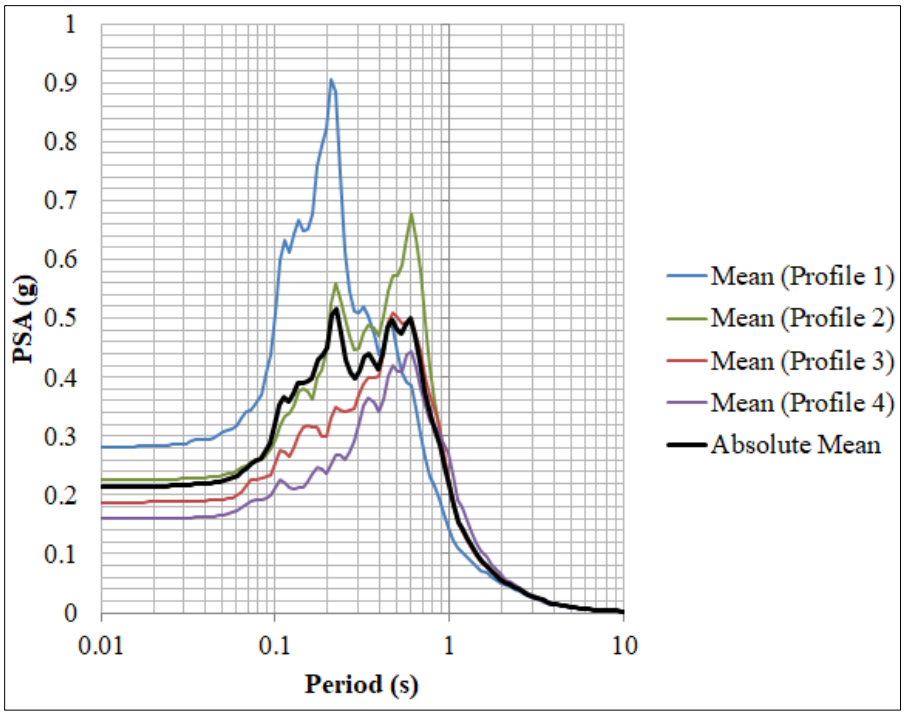

Figure 5.9. Mean response spectra of geotechnical and geophysical output for each Profile

It can be observed from the plot that the PSA values of Profiles 2, 3 and 4 trend in a similar fashion. That of Profile 1, analogous to what has been observed in PGA discussions, peaked uniquely at natural periods close to 0.2 sec. It was observed that some records, particularly Hachinohe record, was observed to consistently peak (albeit with varying extent) at 0.2 sec for the majority of the profiles. Its effect was significantly apparent in the case of Profile 1 (Amora Gedel Park) generated from geophysical methods, whose fundamental site period of 0.23 sec is very much close to the aforementioned period that records such as Hachinohe uniquely amplify. Potential resonance is believed to have taken place especially at the particular period of around 0.2 sec as shown in Figure 5.10.

`

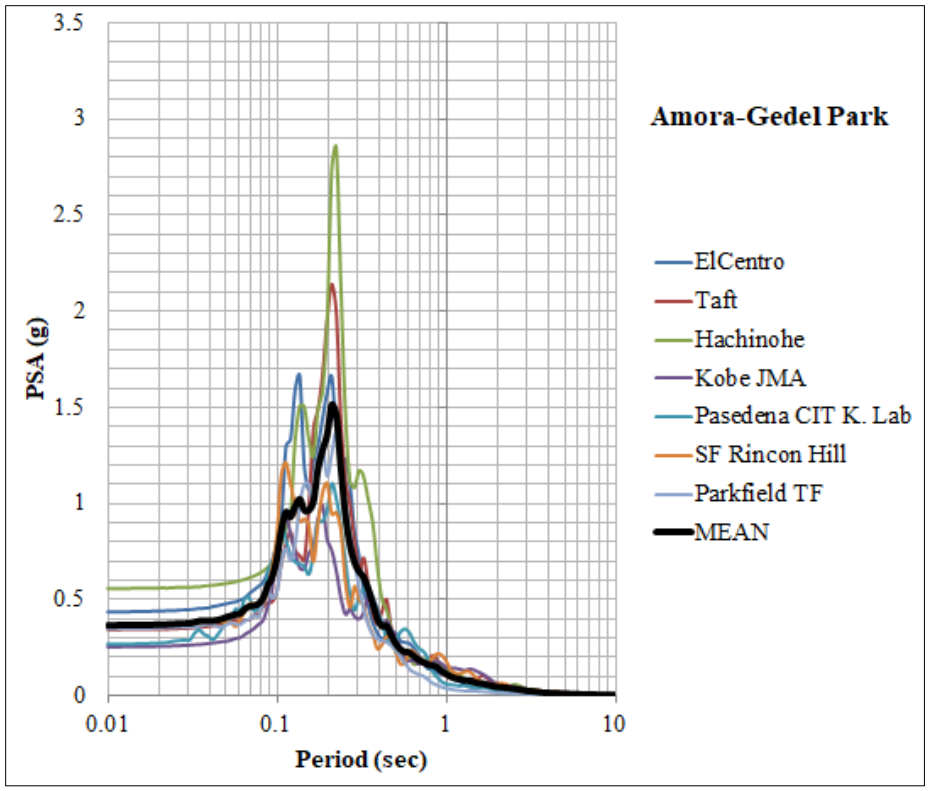

Figure 5.10. Observed resonance at Amora-Gedel Park site

The mean plot of "Amora-Gedel Park" site significantly influenced the mean of Profile 1 as shown in Figure 5.9, where a mean PSA of 0.9g can be observed at a natural period of approximately 0.2 sec. A close inspection of Table 4.10 shows that the majority of the shear-wave velocities of Profile 1 are consistently higher all the way down to a depth of 20m, with velocities nearing rock wave velocities (~550m/s) observed at depths below 15m. This apparently led to the decrease of the site period of the Profile; furthermore, the behavior of the PSA curves in Figure 5.10 uniquely peaks at a particular period (as one would expect from stiffer formations such as rocks) rather than spreading over a range of periods (like in the case of loose soils).

5.3.3 Comparison with Code Specified Design Spectra

5.3.3.1 Site-specific Comparisons

Spectral analysis outputs are compared with the design spectra from ES EN 1998:2015 (identical with Eurocode) and NEHRP 2015 as identified above for the respective site classes. The two

`

design spectral types of Ground Type C of ES EN 1998:2005 and the design spectrum of Site Class D of NEHRP 2015 are used for comparison with the response spectra obtained for the actual ground motions as shown in Figure 5.11.

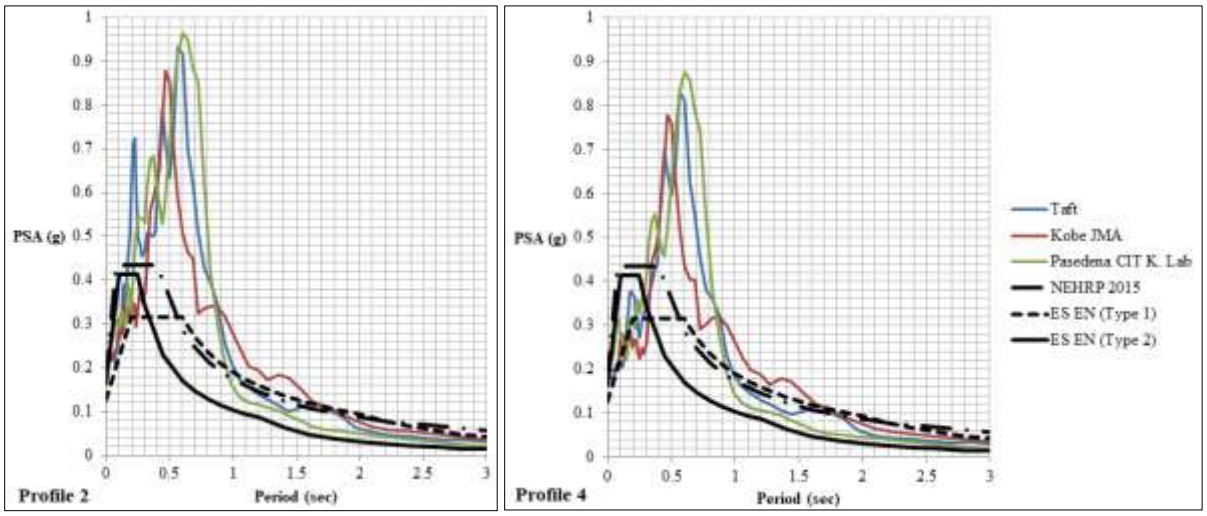

Figure 5.11 Comparison of some analysis outputs against building codes

The results for two site profiles and selected representative ground motions show a clear underestimation of site effect by the design spectra of both codes. Spectral ordinates of Profile 2 exceed the spectral plateaus provided by ES EN 1998:2015 and NEHRP 2015 by a factor of up to 3. In a similar trend, those of Profile 4 exceed the code predictions by a factor of up to 2.75. Whereas NEHRP's and Type 2 of ES EN 1998:2015 design spectral curves give similar maximum values at very short periods, both design spectra peak in a narrow period range significantly to the left of the actual predominant period range identified for the sites. Furthermore, Type 2 design spectrum of ES EN 1998:2015 underestimates the spectral values over the majority of the period range considered.

Beyond the period of 0.6 sec (up to approximately 1.7 sec), Type 1 of ES EN 1998:2015 and NEHRP 2015 give practically identical spectral values that are reasonably comparable with the actual values. Beyond the periods of around 1.7 sec, these two design spectra provide a very good representation of the actual response.

`

5.3.3.2 Absolute Mean Response Spectrum

The absolute mean (referring to the mean PSA of the eight sites analyzed with seven motions) from mean spectra plotted in Figure 5.9 under section 5.3.2 has also been compared with the design spectra from ES EN 1998:2015 and NEHRP 2015, for the respective site classes. The comparison is given in Figure 5.12.

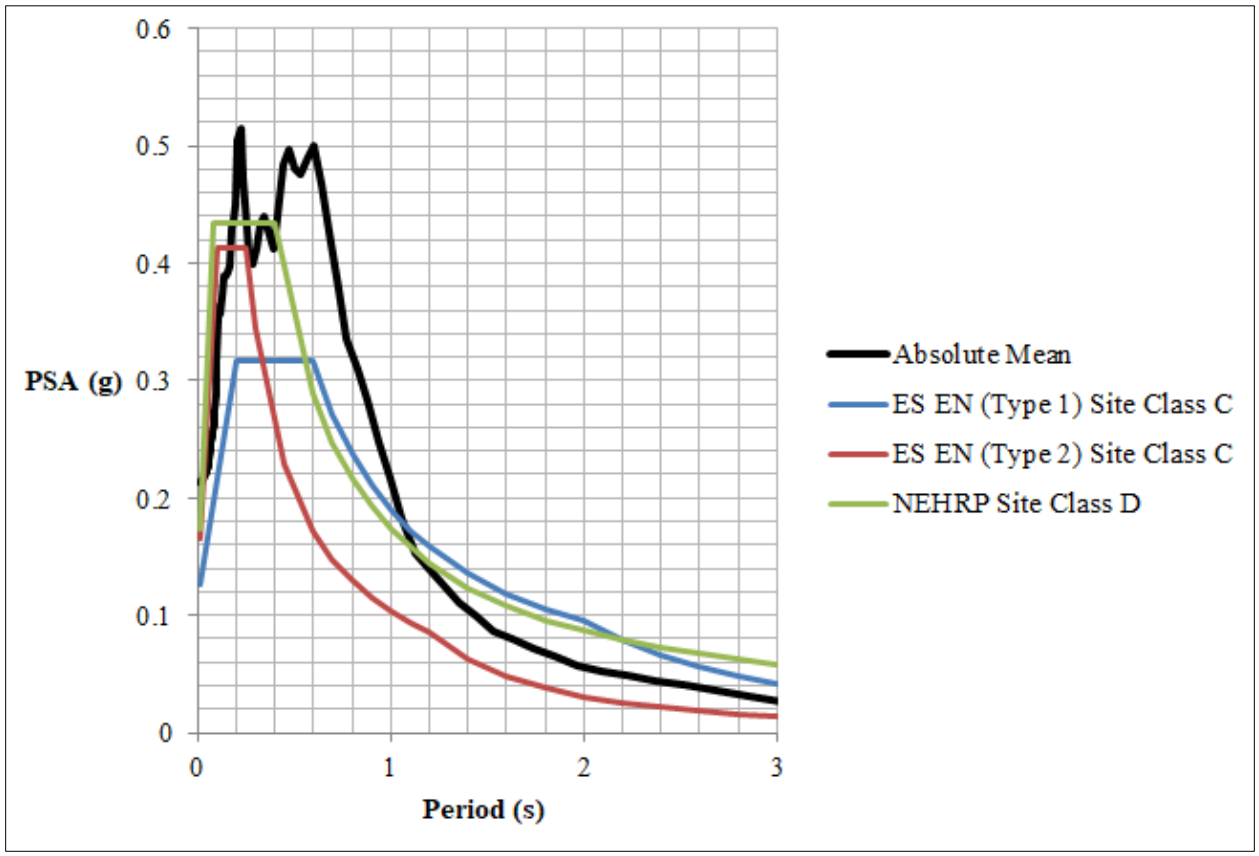

Figure 5.12 Comparison of the absolute mean against design spectra of building codes

The underestimation by both codes can also be clearly seen in the period range of 0.4 – 1.1 sec by all codes. While spectral plateaus of NEHRP 2015 and ES EN 1998:2015 (Type 2) almost align with that of an anticipated PSA plateau of the absolute mean, that of ES EN 1998:2015 (Type 1) appears to have a noticeably lower prediction. It should also be noted that despite having PSA ordinates close to that of the absolute mean, both NEHRP's and ES EN's plateaus are narrow and do not spread as wide as what is predicted by the absolute mean curve, which

`

extends to a period of 0.6 sec. The velocity and displacement spectra of this absolute mean are presented in Figure 5.13.

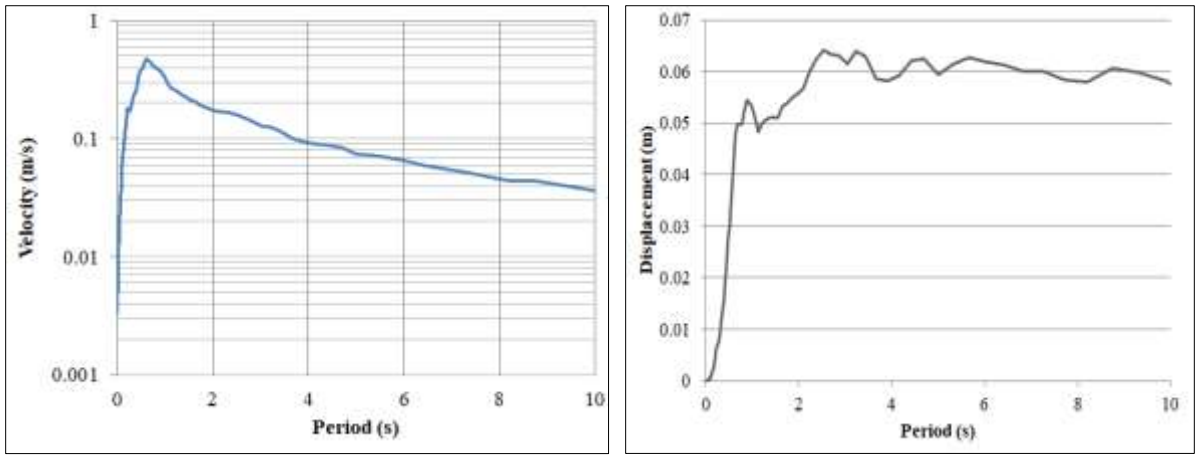

(a) (b)

Figure 5.13 Response of Pseudo-velocity (a), and displacement (b), of the absolute mean

In conclusion, the code-based design spectra by and large do not sufficiently represent the response of the most important range of building types prevalent in the city that are mainly of reinforced concrete and ranging between three and ten stories in height (about 0.3 to 1.0 sec), calling for a site specific design spectrum for Hawassa.

5.3.3.3 Proposed Design Spectrum

In light of the discussion in the previous sub-sections, a design spectrum that closely fits the absolute mean is suggested as follows.

`

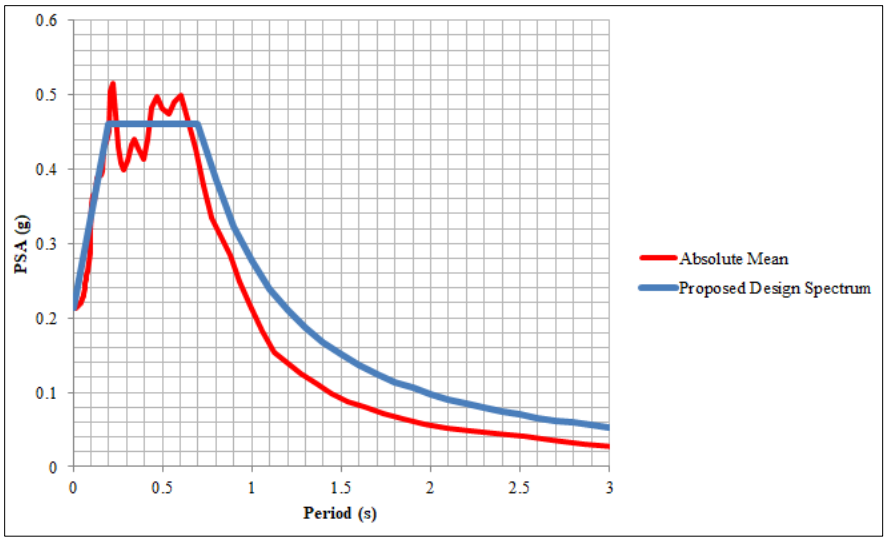

Figure 5.14 Proposed design spectrum fitted to the absolute mean

Comparisons of this proposed design spectrum with the code-based design spectra of ES EN 1998:2015 and NEHRP 2015 for the existing site classes (C and D, respectively) and the more critical site classes (D and E for ES EN 1998:2015 and E for NEHRP 2015), are presented in Figure 5.15.

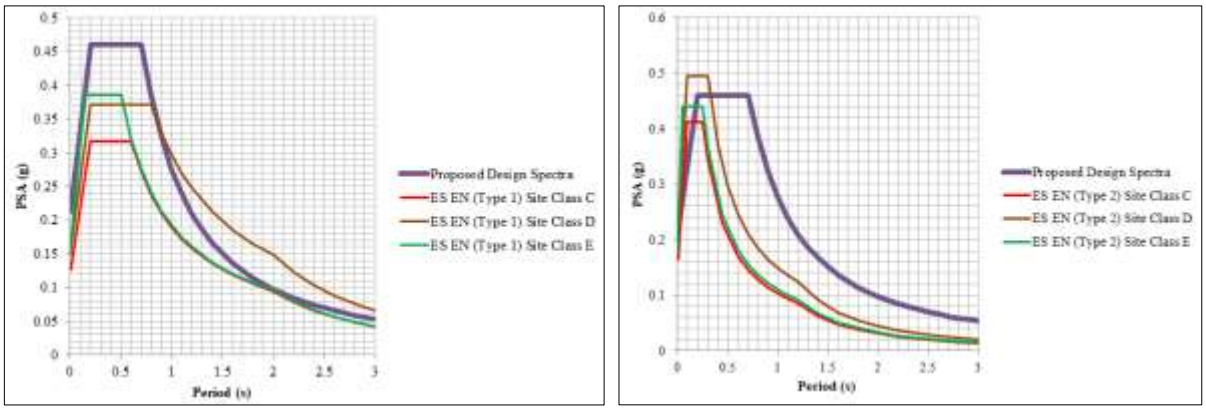

(a)

`

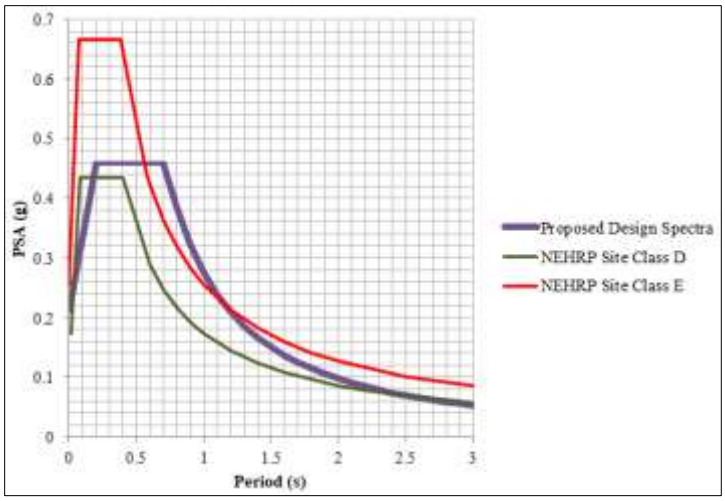

(b)

Figure 5.15 Comparisons between the proposed design spectrum and design spectra of two site classes for ES EN 1998:2015 (a), and NEHRP 2015 (b)

Predicted ordinates of Type 1 site class D for ES EN 1998:2015 can be observed in Figure 5.15 (a) to be much closer to the proposed design spectrum than those of site class C and E. The general behavior of the design spectra that ES EN proposes remains similar, (narrower and higher plateaus for Type 2 and broader but lower plateaus for Type 1). Type 2 spectrum of site class D looks to have slightly exceeded the proposed design spectrum at short periods by some amount, but just as in the case with site class C and E, the plateau is significantly narrower than actually observed. At periods beyond the end of the plateau, the response is significantly underestimated. Type 1 spectrum has a plateau wide enough to cover the anticipated plateau. Yet, the spectral ordinates also remain underestimated for site class D in comparison with the proposed design spectrum until a period of 0.9 sec. Beyond this period, the curve provides adequate prediction for the anticipated response.

Additional observations can also be made as one compares the proposed design spectrum with those of NEHRP 2015. It was remarked in the preceding subsection that NEHRP 2015 predicts a much closer PSA value to the proposed design spectrum until the period of 0.3 sec (which is the period at which the plateau ends). Beyond this period, the response remains underestimated until a period of about 2.4 sec. NEHRP 2015 site class E has a rather exaggerated prediction in short period range and beyond the period of 1.2 sec. However, this site class is unique in that it is

`

defined for soils with undrained shear strength of less than 25 kPa, a value tremendously small in the context of soil description. The two spectra observed to be the closest for the proposed design spectrum are presented in Figure 5.15.

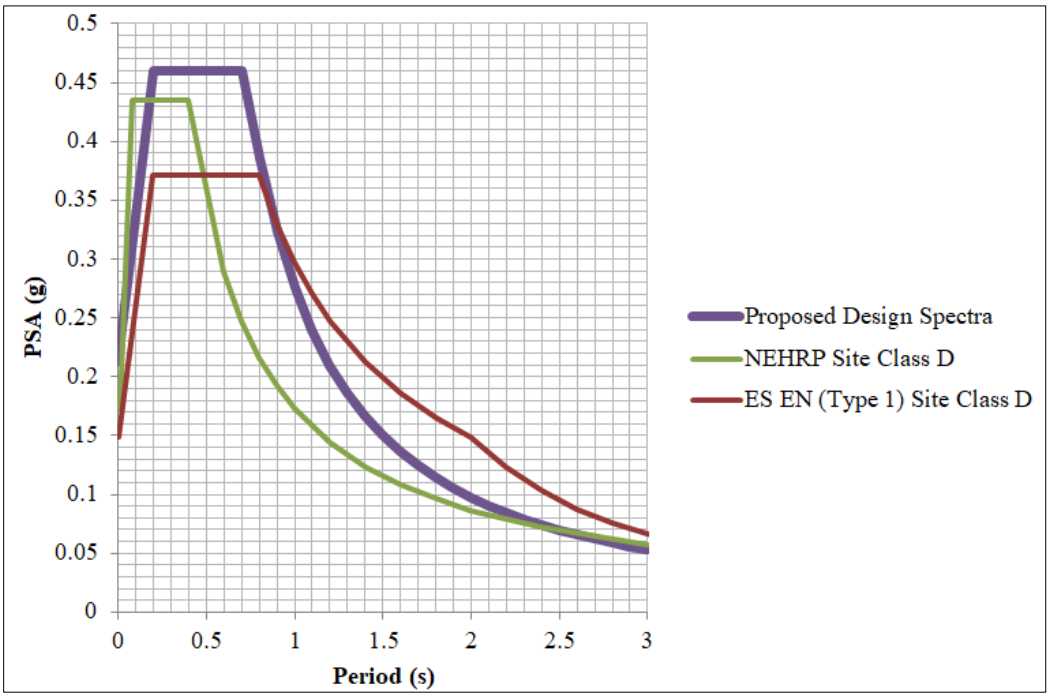

Figure 5.16 Selected design spectra that were found to be closest to the proposed design spectrum

Noting that none of the predictions from the building codes (even those selected to be closest to the proposed design spectrum) satisfactorily match the target, with most of them underestimating and some exaggerating, the design spectrum shown in Figure 5.14 is proposed for the city. It can be expressed using the following relationship.

$$
\begin{aligned}
&0 \le T \le 0.2\,\text{sec}: \; S_e(T) = 0.21 + 1.24T \\
&0.2 \le T \le 0.7\,\text{sec} \; : \; S_e(T) = 0.46 \\
&T > 0.7\,\text{sec}: S_e(T) = \frac{0.276}{T^{1.5}}
\end{aligned}
\tag{5.6}
$$

`

5.3.4 Effect of the Ignimbrite Layer

In order to see the effect of the ignimbrite horizon observed in most places of the city at a shallow depth, the analysis was conducted for Profile 4 with and without this layer. Three ground motion records with more or less consistent spectral behavior - Taft, Kobe JMA and Pasedena CIT K. Lab - were used for comparison. The results are presented in Figure 5.17.

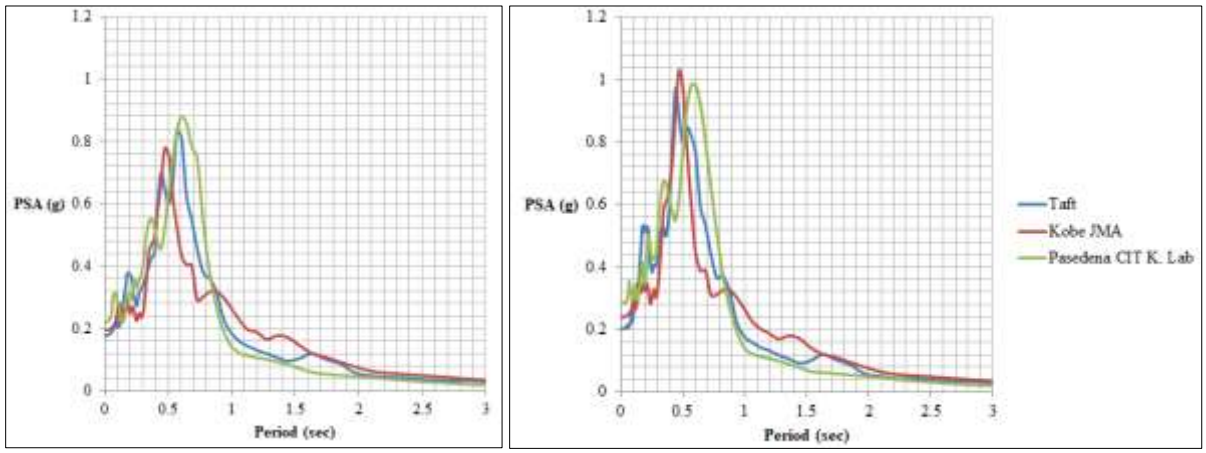

(a) (b)

Figure 5.17 Spectral curves at the ground surface for Profile 4: (a) with ignimbrite, and (b) without ignimbrite

It can be seen from the plots that the ignimbrite layer has the effect of suppressing the spectral values in the significant period range by up to 20%.

Noting that this study used Choi's (2008) recommendation for estimating shear-wave velocity of ignimbrites that assigns shear-wave velocity in the range of 2500-3500 m/sec, which might give the impression of inflated figures, analyses were also run with values reduced down to 800 m/sec. The analyses yielded practically identical results indicating that variation of shear-wave velocity for the ignimbrite within the range of rock wave velocities has little effect on the response.

5.3.5 Effect of Half-space Selection

While analyzing the effect of half-space properties in site response, ground motions can be roughly categorized as "outcropping" and "within" motions. "Outcropping" motions refer to

`

those motions which are recorded on rock outcrops while “within” motions apply to those that are recorded deep inside a borehole. A study by Stewart and Kwok (2008) has shown that analyzing “within” motions using elastic half-space and “outcropping” motions using rigid half-space leads to erroneous results, and that definition of a half-space should be done with care. The difference in output for the same event recorded in these two situations is as a result of the difference in impedance ratio between the layers that a wave propagates. The impedance ratio is a ratio of the product of density and shear-wave velocity between two neighboring layers. At the surface, (in the case of “outcropping” motions), the impedance ratio is 0 as one cannot talk about impedance for seismic wave propagation above the ground. The impedance ratio is different from zero for those cases where waves are assumed to propagate from one formation to another. This fact alone indicates that the two motion cases should be treated differently in GRA.

Two categories of motions were applied in this study; three motions downloaded from PEER database (Pasedena CIT K. Lab record, Rincon Hill record and Parkfield record) and four deconvolved motions (ElCentro record, Taft record, Hachinohe record and Kobe JMA record). The deconvolution process has already removed site effects and reduced the earthquake motions back to the state where they can be treated as bedrock motions in the latter group. These motions can hence be treated safely as “within motions” and analysis was conducted considering them as such. As for the PEER motions, no information is available regarding the station location and there is a possibility that they were recorded on rock outcrop. Having this in mind, the former three motions were used for further analysis to compare the effect of employing an elastic half-space of standard hard rock (NEHRP 2015) in the analysis at Profile 4. The output presented in Figure 5.18 shows that a spectral different of as much as 18% is observed at the predominant period with the one analyzed with an elastic half-space, showing some level of radiation damping, thus reduction in spectral ordinates.

`

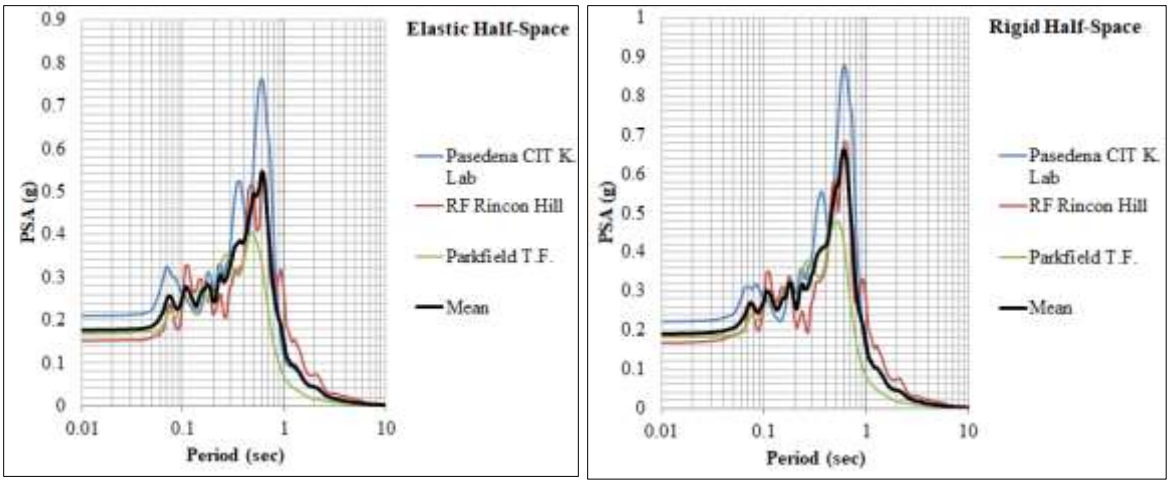

(a)

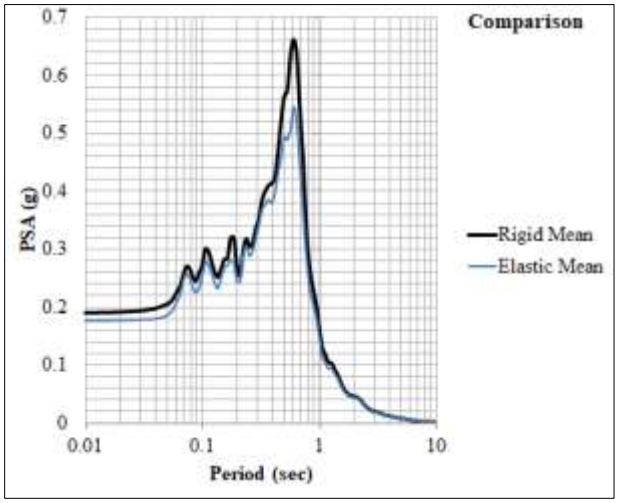

(b)

Figure 5.18 Comparison of: (a) analysis performed on Profile 4 done for elastic and rigid half-space, and (b) the mean spectral ordinates

CHAPTER SIX

CONCLUSIONS AND RECOMMENDATIONS

6.1 Conclusions

A one-dimensional, equivalent-linear site response study is conducted at representative sites in Hawassa city. The following conclusions are made.

- Geophysical investigations and compiled geotechnical and geological reports indicate that Hawassa is a city resting on lacustrine deposit. A thin ignimbrite horizon of varying thickness was encountered at shallow depths (around 3 meters) of most sites. The average $V_{S,30}$ values have been found to fall within the range of 215 and 300m/sec; hence the corresponding site class for all profiles is 'C' and 'D', according to ES EN 1998:2015 and NEHRP 2015, respectively.
- Ground motions are greatly influenced by local site soils across the selected locations for analysis. Analysis outputs show that PGA almost doubled at the surface. Furthermore, up to 60% increase in spectral ordinates is observed in the short and intermediate period ranges as compared to predictions of the recent local code design spectrum.
- The EQL site response model that was employed in the analysis is justified as the maximum predicted strain levels seldom exceeded 0.2%, which are much lower than the 0.4-0.5% strain threshold that necessitates non-linear method of analysis according to recent studies.
- The design spectra of ES EN 1998:2015 and NEHRP 2015 for the respective site classes (C and D, respectively) have been found to seriously underestimate the potential of the sites to amplify the input motion. Having merged response spectral analysis outputs from 56 cases, a mean spectral curve and a fitting proposed design spectrum have been produced.
- From among the sites, 'Amora Gedel Park' was observed to be unique in that rock was encountered at shallow depth (at around 20m). Furthermore, the way soil stiffness increases is also different as compared with the other sites. Separate spectra

generated for this site showed significant amplification at shorter periods than observed at other sites. This indicates that site-specific studies for sensitive structures are justified.

- The thin ignimbrite horizon encountered at shallow depths has only a modest role in reducing the responses at the surface and at depths within and above the layer. The layer's shear-wave velocities were initially estimated from literature. Further analyses were also carried out, having reduced the shear-wave velocity to a reference bedrock velocity of 800m/sec. The analyses yielded practically identical results, indicating that variation of shear-wave velocity for the ignimbrite within the range of rock wave velocities has little effect on the response.
- Considering the possibility of the motions downloaded from PEER to be outcropping motions, analyses on a typical profile was conducted having modeled the half-space as elastic. Response spectra were found to be affected by up to 18% at the predominant period (owing to some radiation damping), while having little effect elsewhere. This indicates that the overall effect of radiation damping into the rock represented as elastic half-space is minimal.

6.2 Recommendations

While the results obtained from this study provide strong indication that the majority of the upper geological formation of Hawassa City has the potential to amplify earthquake ground motions to a significant degree much larger than even provided by recent codes, it is also important to note that the geotechnical input data have some limitations in terms of quantity, quality and depth of investigation. This indicates that a carefully planned comprehensive study might be worth contemplating.

REFERENCES

Acocella, V., Korme, T., Salvini, F., and Funiciello, R. (2002). "Elliptic calderas in the Ethiopian Rift: control of pre-existing structures." *Journal of Volcanology and Geothermal Research*, 119, 189-203

Bommer, J. J., Stafford, P. J., and Alarcon, J. E. (2009). "Empirical equations for the prediction of significant, bracketed and uniform duration of earthquake ground motion." *Bulletin of the Seismological Society of America*, 99(6), 3217-3233.

Boore, D.M. (2004). "Estimating $V_S(30)$ (or NEHRP Site Classes) from shallow velocity models (depths <30m)." *Bull. Seismo. Am.*, 94(2), 591-597.

Borcherdt, R.D. (1970). "Effects of local geology on ground motion near San Francisco Bay." *Bulletin of the Seismological Society of America*, 60, 29-61.

Borcherdt, R.D. (1996). "Effect of site conditions on strong ground shaking in the San Francisco Bay during the 1989 Loma Prieta Earthquake." *Eleventh World Conference on Earthquake Engineering*, 2028.

BSSC (Building Seismic Safety Council). (2015) *2015 Edition NEHRP recommended Seismic Provisions for New Buildings and Other Structures*, FEMA P-1050-1 (Provisions and Commentary), Washington, D.C.

Darendeli, M. B. (2001). "Development of a new family of normalized modulus reduction and material damping curves." Ph.D. dissertation, University of Texas at Austin, Austin, TX.

Davidovici, V. (1985). "Génie parasismique." *École Nationale des Ponts et Chaussées*, Paris, 1105.

Essien, U.E., Akankpo, A.O. and Igboekwe, M.U. (2014). "Poisson's Ratio of Surface Soils and Shallow Sediments Determined from Seismic Compressional and Shear Wave Velocities." *International Journal of Geosciences*, 5, 1540-1546.

Ethiopian News Agency (2016). "Hawassa hit by 4.3 Magnitude Earthquake." <http://www.ena.gov.et/en/index.php/environment/item/696-hawassa-hit-by-4-3-magnitude-earthquake> (Oct. 6, 2016).

Everett, M.E. (2013). *Near-Surface Applied Geophysics.* Cambridge University Press. Cambridge, UK.

Fantahun, A. (2016), "Magnitude 4.3 Earthquake Strikes Hawassa." *Ethiopia Observer*, <http://www.ethiopiaobserver.com/2016/01/earthquake-strikes-awassa/> (Sep. 9, 2016).

Giardini, D. and Basham, P. (1993). "The Global Seismic Hazard Assessment Program (GSHAP)." *Annali di Geofisica*, 36(3), 3-13.

Giardini, D., Grünthal, G., Shedlock, K. M. and Zhang, P. (1999). "The GSHAP Global Seismic Hazard Map." *Annali di Geofisica*, 42(6), 1225-1228.

Gouin, P. (1979). *Earthquake history of Ethiopia and the horn of Africa*. IDRC. Ottawa, Ontario.

Haile, M. (1996). "Critical assessment of site effect parameters for strong ground motion prediction." Ph.D. dissertation, Tokyo Institute of Technology, Tokyo.

Hardin, B.O. and Drenvich, V.P. (1972). "Shear Modulus and Damping in Soils: Design Equations and Curves." *Journal of Soil Mechanics and Foundation Engineering Div.,* ASCE, 98(7), 667-692.

Hashash, Y.M.A., Philips, C. and Groholski, D. (2010). "Recent advances in non-linear site response analysis." Fifth International Conference on Recent *Advances in Geotechnical Earthquake Engineering and Soil Dynamics*, OSP 4.

Hashash, Y.M.A., Musgrove, M.I., Harmon, J.A., Groholski, D.R., Phillips, C.A., and Park, D. (2016) "DEEPSOIL 6.1, User Manual." Urbana, IL, Board of Trustees of University of Illinois at Urbana Champaign.

Hutabarat, D. (2016). "Evaluation of One-Dimensional Seismic Site Response Analyses at Small to Large Strain Levels." MSc. Thesis, University of Washington, Seattle, WA.

Idriss, I. M. (1990). "Response of Soft Soil Sites during Earthquakes." *Proceedings*, H. Bolton Seed Memorial Symposium, 2, 273-289.

Ishibashi, I. and Zhang, X. (1993). "Unified Dynamic Shear Moduli and Damping Ratios of Sand and Clay." *Soils and Foundations,* 33(1), 182-191.

JICA (Japan International Cooperation Agency) (2012). *The study on groundwater resources assessment in the rift valley lakes basin in the Federal Democratic Republic of Ethiopia*. Kokusai Kogyo Co., Ltd.

Kaklamanos, J., Bradley, B.A., Thompson, E. M., and Blaise, L.G. (2013). "Critical parameters affecting bias and variability in site-response analyses using Kik-net downhole array data." *Bull. Seismol. Soc. Am.,* 103(3), 1733-1749.

Kebede, F. and van Eck, T. (1997). "Probabilistic seismic hazard assessment for the Horn of Africa based on seismotectonic regionalization." *Tectonophysics*, 270, 221-237.

Kottke, A.R. and Rathje, E.M. (2009). "Technical Manual for Strata." *Pacific Earthquake Research Center,* University of California at Berkeley.

Kramer, S. L. (1996). *Geotechnical Earthquake Engineering*. Prentice-Hall. Upper Saddle River.

Lanzo, G., Pagliaroli, A. and Scasserra, G. (2015). "Selection of ground motion time histories for the nonlinear analysis of earth dams." *Geotechnical Engineering for Infrastructure and Development,* 2031-2036.

Malek, J. (2014). "Seismic hazard of Southern Ethiopia." *Institute of Rock Structure and Mechanics,* Academy of Sciences of the Czech Republic, Prague.

Midzi, V., Dumisani, J.H., Chapola, L.S., Kebede, F., Atakan, K., Lombe, D.K., Turyomurugyendo, G. and Tugume, F.A. (1999). "Seismic hazard assessment in Eastern and Southern Africa." *Annali di Geofisica,* 42(6), 1067-1083.

Ministry of Construction. (2015) *Design of Structures for Earthquake Resistance, Ethiopian Standards based on Euro Norms* (ES EN 1998:2015), Addis Ababa.

Ministry of Works and Urban Development. (1995) *Design of Structures for Earthquake Resistance*, Ethiopian Building Code Standard (EBCS 8), Addis Ababa.

Nida, D. and Bizuye, Y. (2014) *Geological Hazards and Engineering Geology Maps of Hosaina NB 37-2: Explanatory Notes.* Czech Geological Survey, Klarov 3, 118 21 Prague 1, Czech Republic.

Nozu, A. (2003). "What was made clear by strong earthquake motion observation." *Found. Eng. Equip. Mon,* 31(5), 42–46 (in Japanese).

Ntuli, G. (2017). *Processing Refraction Seismic Data Step-By-Step Instructions.* Technical Note.

Ohta, Y., and Goto, N. (1978). "Empirical shear wave velocity equations in terms of characteristic soil indexes." *Earthq. Eng. Struct. Dyn.*, 6, 167–187.

Phanikanth, V.S. and Choudhury, D. (2011). "Equivalent-Linear Seismic Ground Response Analysis of Some Typical Sites in Mumbai." *Geotech. Geol. Eng.*, 29, 1109-1126.

Redpath, B.B. (1973). *Technical Report E-73-4: Seismic Refraction Exploration for Engineering Site Investigations.* U.S Army Engineer Waterway Experiment Station. Livermore, CA.

Sadd, M.H. (2009). *Elasticity: Theory, Applications, and Numerics.* Elsevier Inc. UK.

Schnabel, P.B., Lysmer, J. and Seed, H.B. (1972). "SHAKE: A computer program for earthquake response analysis of horizontally layered sites." Report No. EERC 72-12, Earthquake Research Center, University of California, Berkeley, California.

Seed, H.B. and Idriss, I.M. (1970). "Soil Moduli and Damping Factors for Dynamic Response Analyses." *Report No. EERC-70-10,* Earthquake Engineering Research Center, University of California, Berkeley, CA.

Seed, H.B., Wong, R.T., Idriss, I.M. and Tokimatsu, K. (1986). "Moduli and Damping Factors for Dynamic Analyses of Cohesionless Soils." *Journal of the Soil Mechanics and Foundations Division,* ASCE, 112(11), 1016-1032.

Stewart, J.P. and Kwok, A.O.L. (2008). "Nonlinear Seismic Ground Response Analysis: Code Usage Protocols and Verification against Vertical Array Data." *Geotechnical Earthquake Engineering and Soil Dynamics IV,* ASCE, GSP 181.

Stewart, J.P., Afshari, K. and Hashash, Y.M.A. (2014). "Guidelines for Performing Hazard-Consistent One-Dimensional Ground Response Analysis for Ground Motion Prediction." *Pacific Earthquake Engineering Research Center,* University of California at Berkeley.

Srbulov, M. (2008). *Geotechnical Earthquake Engineering: Simplified Analysis with Case Studies and Examples.* Springer. U.K.

Suwal, L.P. and Kuwano, R. (2012). “Poisson’s Ratio Evaluation on Silty and Clayey Sands on Laboratory Specimens by Flat Disk Shaped Piezo-ceramic Transducer.” *Bulletin of ERS,* Institute of Industrial Science, 45, University of Tokyo.

Telford, W.M., Geldart, L.P., and Sheriff, R.E. (1990). *Applied Geophysics,* Cambridge University Press, Cambridge, UK.

Udaka, T. (1983). “SuperFLUSH user’s manual”, Theoretical background, EETI (2), California.

Vucetic, M. and Dobry, R. (1991). “Effect of Soil Plasticity on Cyclic Response.” ASCE, *Journal of Geotechnical Engineering*, 117(1), 89-107.

Wair. B.R., DeJong, J.T. and Shantz, T. (2012). “Guidelines for Estimation of Shear Wave Velocity Profiles.” *Pacific Earthquake Research Center,* University of California at Berkeley.

Williams, F.M. (2016). *Understanding Ethiopia: Geology and Scenery.* Springer. Switzerland.

Worku, A. (2011). “Recent developments in the definition of design earthquake ground motions calling for a revision of the current Ethiopian seismic code – EBCS 8:1995.” *Zede - Journal of EEA*, 28, 1-15.

Worku, A. (2014). “The status of basic design ground motion provisions in seismic design codes of sub-Saharan African countries, a critical review.” *Journal of the S. African Institution of Civil Eng.,*56(1), 40-53.

Yoshida, N. (2015). *Seismic Ground Response Analysis.* Springer. Dordrecht.

Youd, T.L., Idriss, I.M., Andrus, R.D., Arango, I., Castro, G., Christian, J.T., Dobry, R., Finn, W.D.L., Harder, L.F., Hynes, M.E., Ishihara, K., Koester, J.P., Liao, S.S.C., Marcuson, W.F., Martin, G.R., Mitchell, J.K., Moriwaki, Y., Power, M.S., Robertson, P.K., Seed, R.B. and Stokoe K.H. (2001). “Liquefaction Resistance of Soils: Summary Report from the 1996 NCEER and 1998 NCEER/NSF Workshops on Evaluation of Liquefaciton Resistance of Soils.” *Journal of Geotechnical and Geoenvironmental Engineering.* 817-833.

APPENDIX

Appendix A
Geotechnical Investigation reports
Progress International Hotel, BH9
Hawassa Industrial Park, BH B35C
Nib International Bank, BH1
SPEDM BH3

Appendix B

Downloaded Motions from PEER

RSN	Scale Factor	5-95% Duration (sec)	Earthquake Name	Year	Station Name	Magnitude	V_{S30}(m/s)
680	0.9479	6.2	"Whittier Narrows-01"	1987	"Pasadena – CIT Kresge Lab"	5.99	969.07
797	0.9416	14.2	"Loma Prieta"	1989	"SF – Rincon Hill"	6.93	873.1
4083	0.5737*	8.8	"Parkfield-02_CA"	2004	"PARKFIELD – Turkey Flat #1 (0M)"	6.0	906.96

Whittier Narrows-01, Pasadena – CIT K. Lab Record

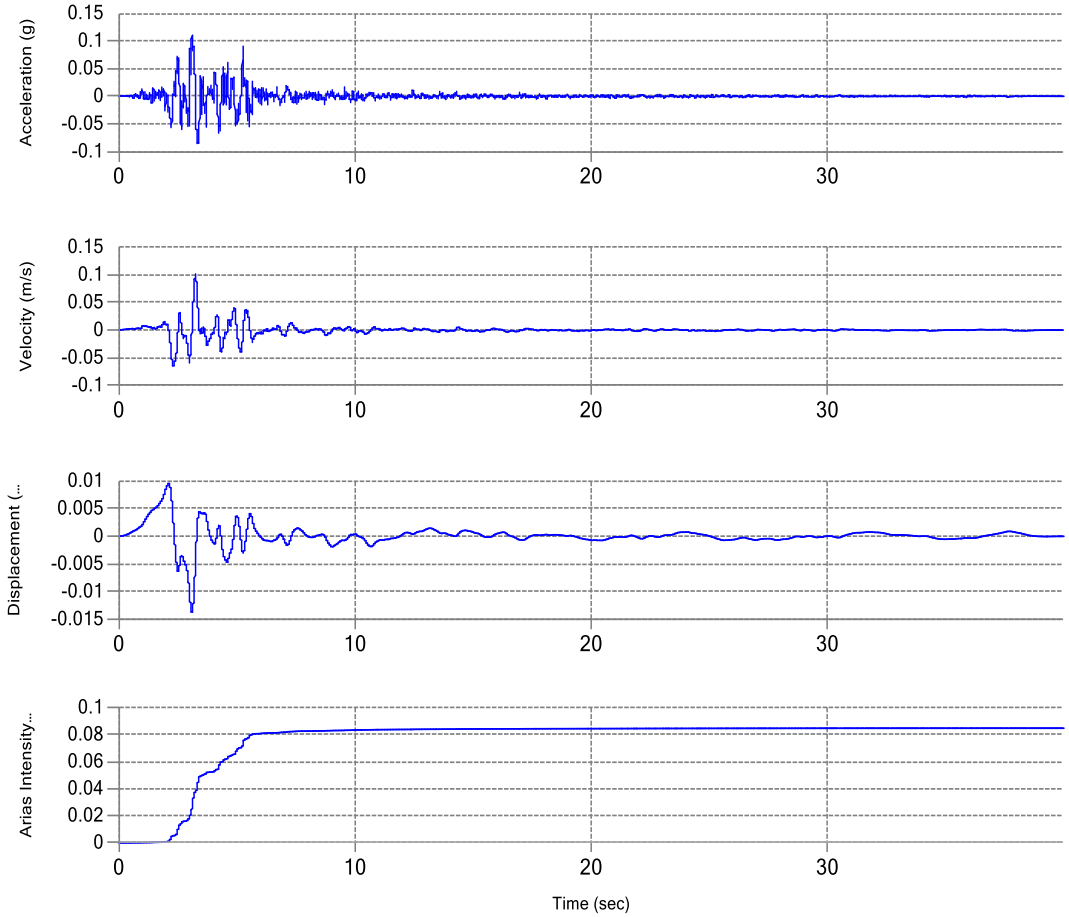

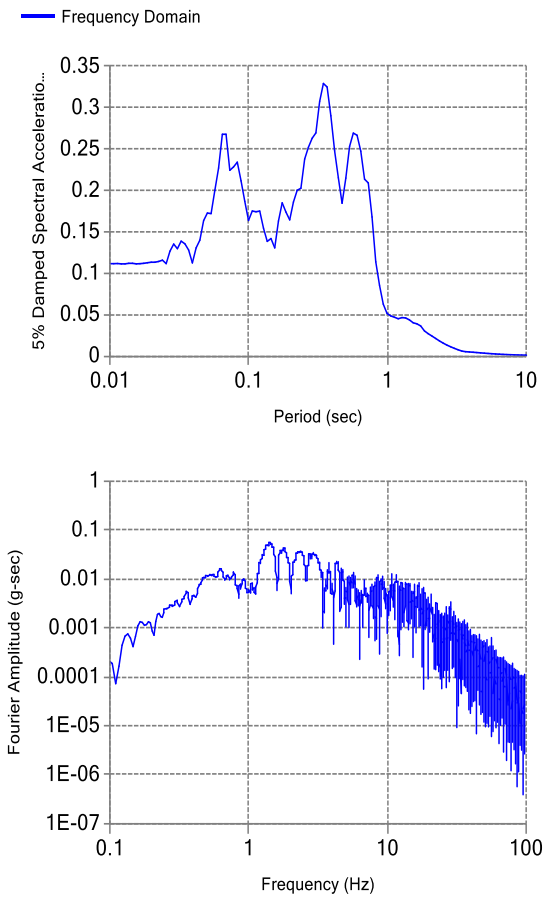

Loma Prieta, SF- Rincon Hill Record

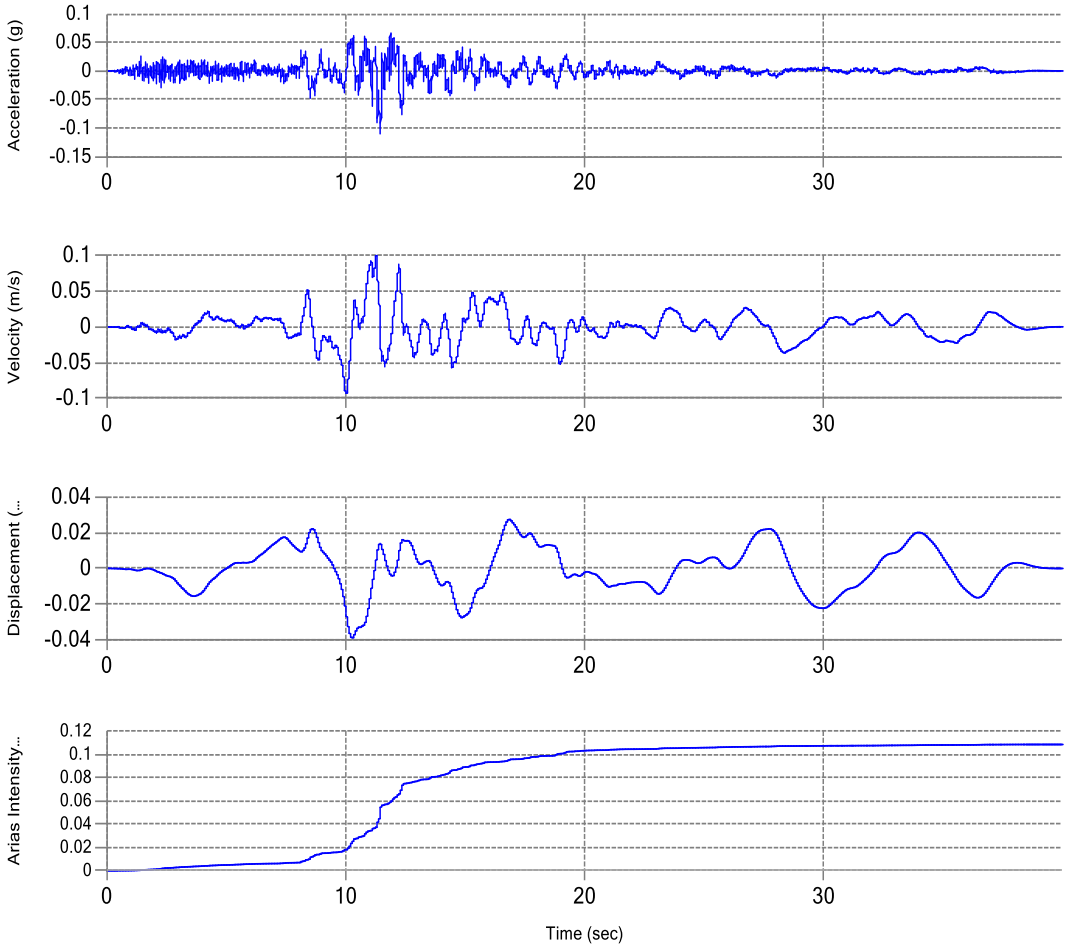

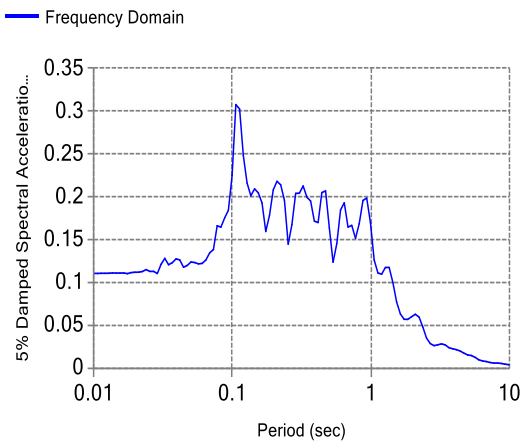

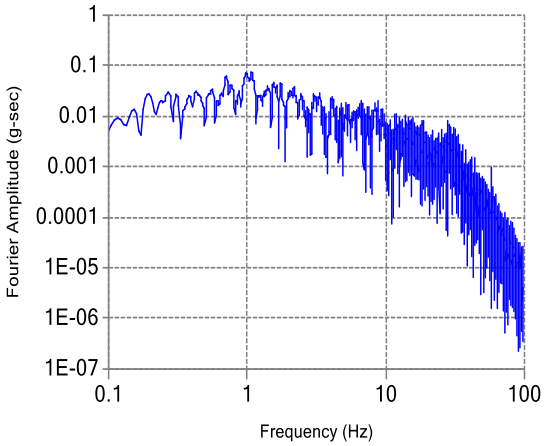

Parkfield 02_CA, PARKFIELD – Turkey Flat #1 (OM) Record

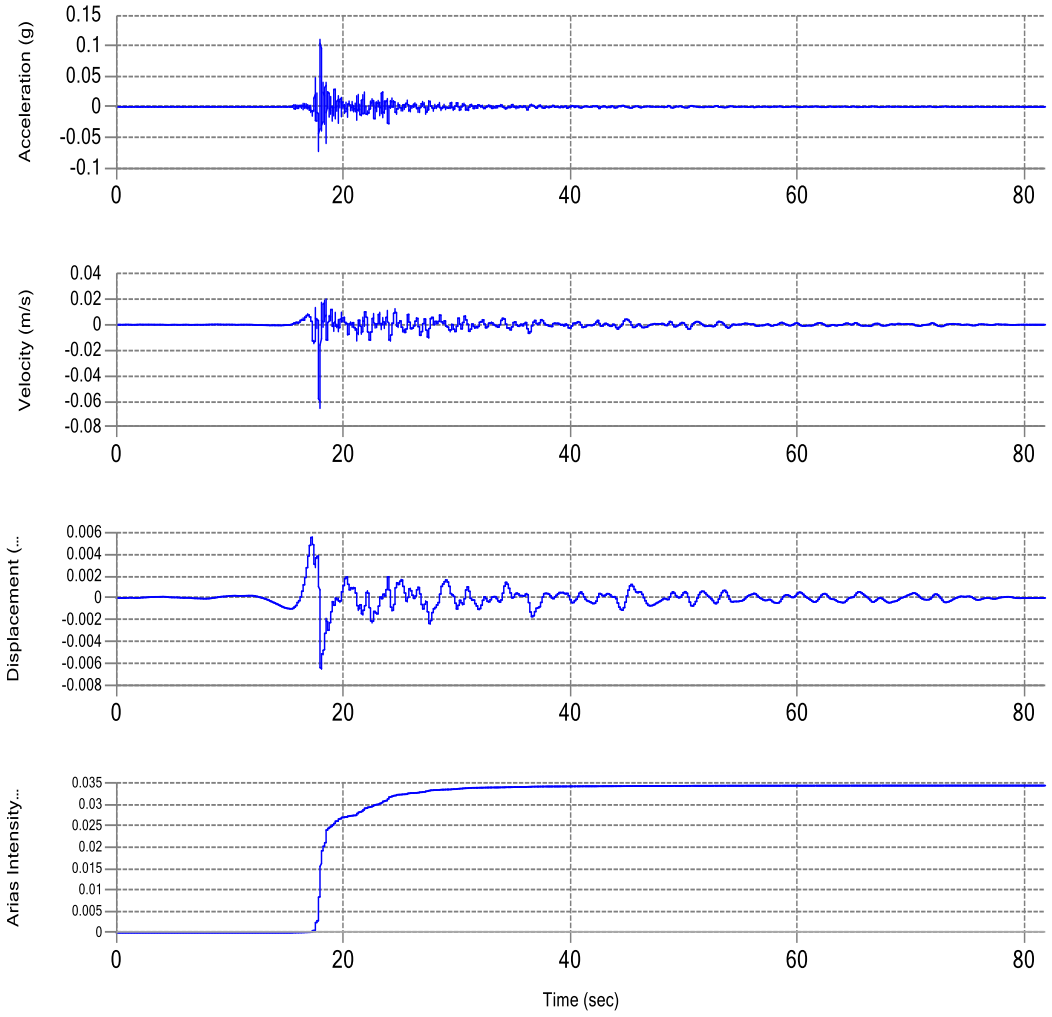

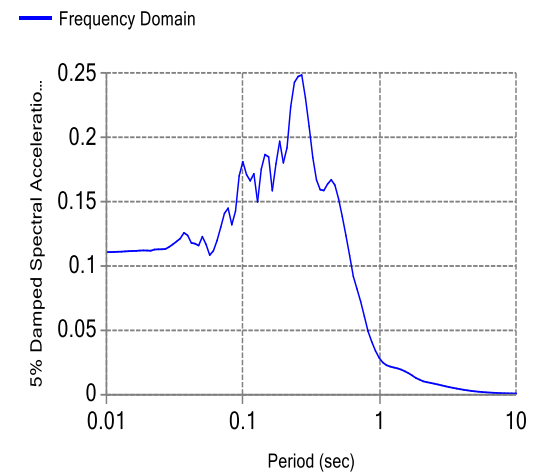

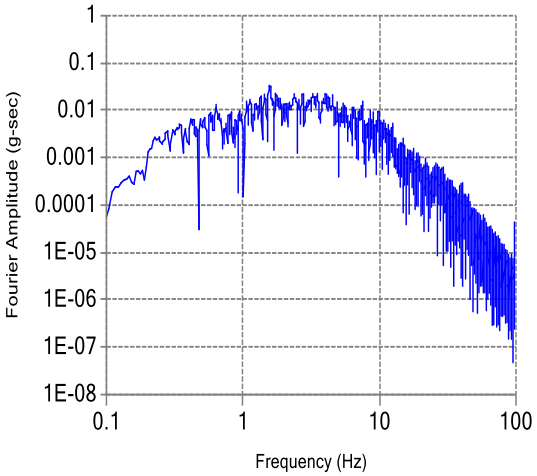

Appendix C

Corrections to SPT (Modified from Skempton 1986) as Listed by Robertson and Write (1998) (Youd et al. 2001)

Factor	Equipment Variable	Term	Correction
Overburden Pressure	___	C_N	$(P_a / \sigma'_v)^{0.5}$
Overburden Pressure	___	C_N	$C_N \leq 1.7$
Energy ratio	Donut hammer	C_E	0.5-1.0
Energy ratio	Safety hammer	C_E	0.7-1.2
Energy Ratio	Automatic-trip Donut-type hammer	C_E	0.8-1.3
Borehole Diameter	65-115mm	C_B	1.0
Borehole Diameter	150mm	C_B	1.05
Borehole Diameter	200mm	C_B	1.15
Rod Length	<3m	C_R	0.75
Rod Length	3-4m	C_R	0.8
Rod Length	4-6m	C_R	0.85
Rod Length	6-10m	C_R	0.95
Rod Length	10-30m	C_R	1.0
Sampling Method	Standard Sampler	C_S	1.0
Sampling Method	Sampler without liners	C_S	1.1-1.3

Boore (2004) regression coefficients

Depth (m)	Regression Coefficients	
	a	b
10	0.042062	1.0292
11	0.022140	1.0341
12	0.012571	1.0352
13	0.014186	1.0318
14	0.012300	1.0290
15	0.013795	1.0263
16	0.013893	1.0237
17	0.019565	1.0190
18	0.024879	1.0144
19	0.025614	1.0117
20	0.025439	1.0095
21	0.025311	1.0072
22	0.026900	1.0044
23	0.022207	1.0042
24	0.016891	1.0043
25	0.011483	1.0045
26	0.006565	1.0045
27	0.002519	1.0043
28	0.000773	1.0031
29	0.000431	1.0015